Spinal Fracture Treatment: Finite Element Analysis Of Different Fixation Techniques

BY

NICCOLÒ GALDINI

B.S. , Politecnico di Milano, Milan, Italy, 2015

THESIS

Submitted as partial fulfillment of the requirements

for the degree of Master of Science in Bioengineering

in the Graduate College of the

University of Illinois at Chicago, 2020

Chicago, Illinois

Defense Committee:

Farid Amirouche, Chair and Advisor

Sabri Cetinkunt

Tomaso Maria Tobia Villa, Politecnico di Milano

ACKNOWLEDGEMENTS

First and foremost, I would like to express my sincere gratitude to Professor Farid Amirouche for helping me discover the field of spine implants and for the continuous support during the thesis, both academically and financially. Having this unique opportunity to work in the prestigious UIC Biomechanics Research Laboratory has been an experience that I will never forget.

Moreover, I want to thank Professor Tomaso Villa for his advices and support throughout this thesis.

Many thanks to all the students in the UIC Biomechanics Research Laboratory and particularly to Siddhant Thakur, Niranjan Gadkari and Amir Beltagi who have helped me throughout this journey.

Finally, my utmost gratitude goes to my family, my parents and my sister in particular, for their moral and practical support during my entire scholastic career and to Claudia who has brought the best out of me in these five years with her.

I want to thank all the friends who I had the pleasure to meet in this experience at UIC, in particular Filippo, Caterina and Ludovica.

NG

TABLE OF CONTENTS

LIST OF TABLES

LIST OF FIGURES

FIGURE……………………………………………………………………………………….………PAGE

LIST OF ABBREVIATIONS

E	Elastic Modulus
CT	Computer Tomography
DICOM	Digital Imaging and Communications in Medicine
HU	Hounsfield Unit

SUMMARY

The spondylolysis is usually associated with the fracture occurring in the pars interarticularis of the neural arch of the vertebra. It is considered to be caused by the hyperextension or excessive rotation movement due to sports injuries and it is suspected to cause back pain to 50 % of the young athletes [1]. If not treated, the fracture could worsen and develop into spondylolisthesis in 51-80% of all cases [2]. When non-surgical conservative treatments are not successful, clinical intervention may be the solution. Our work aims to compare, through a finite element analysis, the surgical techniques representing the state of the art, such as Buck technique and the evolution of the Morscher technique, with a new design combining both methods to reduce the fracture as proposed by new developments in the Biomechanics Research Laboratory.

The objective of this thesis is to investigate the current fixation techniques of pars fracture and propose an alternative solution. The thesis work follows the preliminary concepts, the anatomy of the spine and pars fracture treatment surgically in Chapter 1. This is followed by the model creation in chapter 2 to give a rationale for the fracture location and depth. What constitutes our methodology is mainly described in chapter 3 which will involve the creation of the fracture and the simulation of the intact, fractured vertebra and the two main techniques chosen to fix the defect in the state of the art. Chapter 4 will discuss the two new designs proposed by the Biomechanics Research Laboratory and their respective simulations comparing them with the past simulations performed. Chapter 5 will conclude the thesis making general considerations on the two designs and understanding their effectiveness under the hypothesis and limitations of the model compared with the other techniques.

CHAPTER 1

1. INTRODUCTION TO THE SPINE AND THE SPONDYLOLYSIS FRACTURE

In this chapter, we will review the basic principles of the anatomy of the spine and introduce the spondylolysis, its causes and symptoms of this fracture for either the non-surgical intervention or surgical treatments.

1.0 Anatomy of the spine

The spine is composed of 33/34 vertebrae, as shown in Figure 1, there are 7 cervical vertebrae, 12 thoracic, 5 lumbar, 5 sacral and 4/5 coccyx depending on the classification. The spine plays a complex role in the musculoskeletal human function and it is designed to protect the spinal cord, which has the role of transmitting the electrical signals from the cortex to the body. The afferent nerves bring the signals to the spinal cord while the efferent one brings the signal from the spine to the rest of the body. The nerves can depart from the spinal cord through the intervertebral foramina, holes that allow the nerves to go through and reach the limbs and the rest of the body.

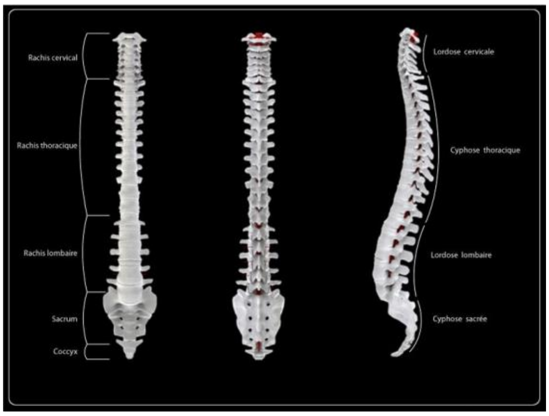

Figure 1: Spine anatomy and vertebrae classification – Credits [https://commons.wikimedia.org/wiki/File:Spine_Anatomy_Kisco.JPG] From Wikipedia

The spine is also essential for the body movement and the bearing of the head, upper limbs and thorax weights. As aforementioned, the functional unit of the spine is represented by the vertebra, which is composed of two different parts: the vertebral body and the vertebral arch. The former has a cylindrical shape with different dimensions with respect to the position along the spine (being thicker and wider as we proceed from the cervical to the lumbar tract) and it is always positioned in the anterior side of the spine. On the other hand, positioned posteriorly, the vertebral arch is composed of three bony structures called processes (two lateral transverse processes and one central spinous). In order for the vertebrae to articulate together, four articular processes are necessary, two for the vertebra below and two for the upper vertebra. To avoid friction hyaline cartilage is present on the articular surfaces. The Figure below illustrates the junction and facet joints to provide a better understanding of the vertebra structure:

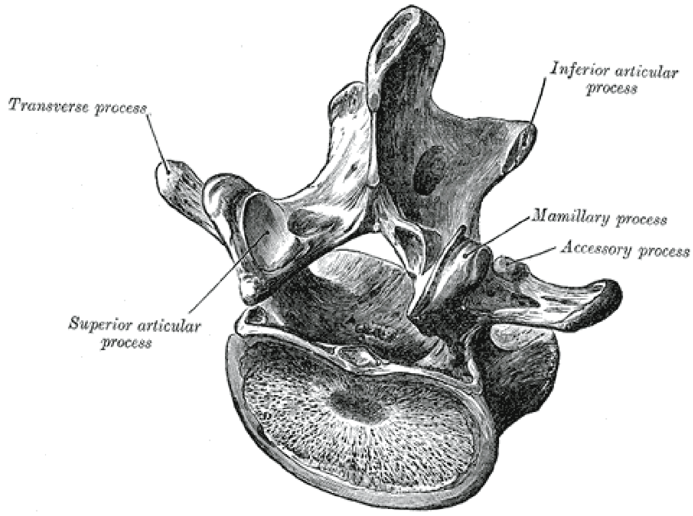

Figure 2: Anatomy of the vertebra. Credits [https://de.m.wikipedia.org/wiki/Datei:Gray93.png] From Wikipedia

Two consequent vertebrae are connected by the intervertebral disc, a fibrocartilaginous structure used for load bearing, absorption and vertebrae movement. The disc itself is composed of two parts: the annulus and the nucleus. The first, positioned in the outer ring of the intervertebral disc, is organized in layers of type I and type II collagen lamellae to form a cross-like structure. The nucleus occupies the inner part of the intervertebral disc. This element is composed mainly by water (around 70-90% [3]) and plays a major role in the load absorption. The nucleus part of the disc distributes the pressure uniformly avoiding abnormal concentrations that could eventually damage the integrity of the disc. When the load acting on the spine exceeds a certain limit, the nucleus can tear and extrude posteriorly compressing the nerves, this pathology is called disc herniation. Along the spine, we can identify two different curves: kyphosis (convex) and lordosis (concave) in the thoracic and cervical, lumbar part respectively. The different shape of these curves is due to the different height of the intervertebral disc alongside the spine: in the cervical and lumbar part, the disc is higher in the anterior part while in the thoracic in the posterior part. These two curves represent the physiological behaviour of the spine until they exceed a certain degree of curvature, then lordosis and kyphosis are considered as pathological conditions.

Concerning the ligaments of the spine, we should understand the fundamental role that these parts play in the spine. The main ligaments of the spine are the following: anterior longitudinal ligament, posterior longitudinal ligament, ligamentum flavum, intertransverse ligament, supraspinous ligament, interspinous ligament and the ligaments at the facets. In order to model the crack properly and understand the exact location, we will create a model composed by two vertebrae, L4 and L5, with the intervertebral disc and the main ligaments involved in the physiological movements of the spine. Hence, understanding the nature of these ligaments and their role is important since we can create a more precise model that is more similar to the real anatomy. Concerning the role of the aforementioned ligaments, the anterior longitudinal ligament runs along the anterior part of the vertebral body from the inferior basilar portion of the occipital bone to the sacrum. Its main function is clearly to limit the extension of the spine and it can break or damage if stretched upon a certain extent. The posterior longitudinal ligament can be identified as the specular structure of the anterior longitudinal ligament, hence it runs parallel to the anterior ligament and it is found on the back of the vertebral body. Being opposite to the anterior ligament, its main role is to limit flexion. The ligament flavum connects the laminae of adjacent vertebrae, starting from the cervical part till the lumbar part of the spine. In the article written by *Rathore et* *al* [4], it is clear that the main role of this ligament is to limit flexion. The intertransverse ligaments connect each transverse process of one vertebra to the other process of the vertebra below. These ligaments have the main role of limiting the lateral flexion of the spine. In the study conducted by *Mahato et al*[5], they dissected human cadavers in order to assess the fiber orientation of the aforementioned ligaments. Concerning the interspinous and the supraspinous ligaments, their main position is the central spinous process and their main role is to limit the flexion. The interspinous process, as the name suggests, can be found in the space between two consecutive spinous processes. The inclination of the fibers can be different regarding the level of the spine we are more interested in. Being focused on the lumbar segment, the interspinous ligaments are found to be almost in a vertical position [5]. The supraspinous ligament connects the tip of the spinous process to the spinous process of the vertebra below. In a study conducted on a porcine model, *Gillespie et al* [6] found that the interspinous and the supraspinous ligament were the most important involved in flexion limiting. In the following Figure, we are presenting all the aforementioned ligaments:

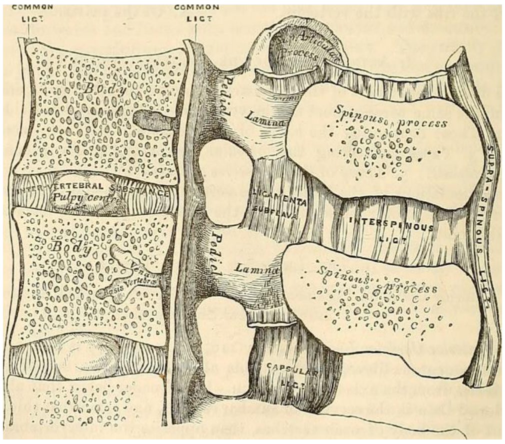

Figure 3: Ligaments of the spine, Credits [https://www.flickr.com/photos/internetarchivebookimages/14742330446/] From flickr

1.1 Spondylolysis fracture

Spondylolysis represents the fracture involving the rupture of the pars interarticularis of the neural arch as seen in Figure 4 below. The level at which the fracture happens could vary, but most of all the spondylolysis cases occur at the fifth lumbar (L5) vertebra (around 85-95% of the total cases[7]) and 5-15% at the L4 level. This is the main rationale for the modelling of the vertebrae at that specific level. Since almost the entirety of the cases happens at the L5, all the computational analysis will be performed on the L5 segment. In the extension and flexion movements, the stresses are concentrated in the neural arch, hence there is a higher probability of stress and further propagation of the fracture at this level. Another important factor that could lead to the fracture is the thickness of the lamina at this location, which is considerably low compared to the rest. The role of ligaments is to limit the movements that could generate an abnormal distribution of stresses and hence damage the spine. As reported in the article by *McTimoney et al*[1] the frequency of the fracture in the global population is around 6% and it is estimated that around 50% of the adolescent low back pain could be due to this particular fracture, hence its treatment could represent a major contribution to a huge problem around the global population. The spondylolysis fracture could be classified in five main categories according to *Wiltse et al* [8]: Type I: dysplastic, due to congenital abnormalities, Type II: isthmic, lesion in the pars interarticularis, Type III: degenerative, due to the degeneration of the intervertebral disc, Type IV: traumatic, due to acute fractures in areas other than the pars, Type V: pathological, due to bone diseases and tumours. Another significant factor that gives spondylolysis considerable importance among the low back fracture is that in 50- 81% of people suffering spondylolysis could ultimately face the creation of a more serious condition: spondylolisthesis [2]. This clinical condition involves the slippage of the vertebra upper vertebra on the lower one, in most cases this happens at the L5-S1 segment. Even though this project does not involve the treatment of the spondylolisthesis specifically, it is important to understand how an early diagnosis of the spondylolysis fracture and its consequent surgical fixation could avoid worse complication that could lead to permanent damage for the patient.

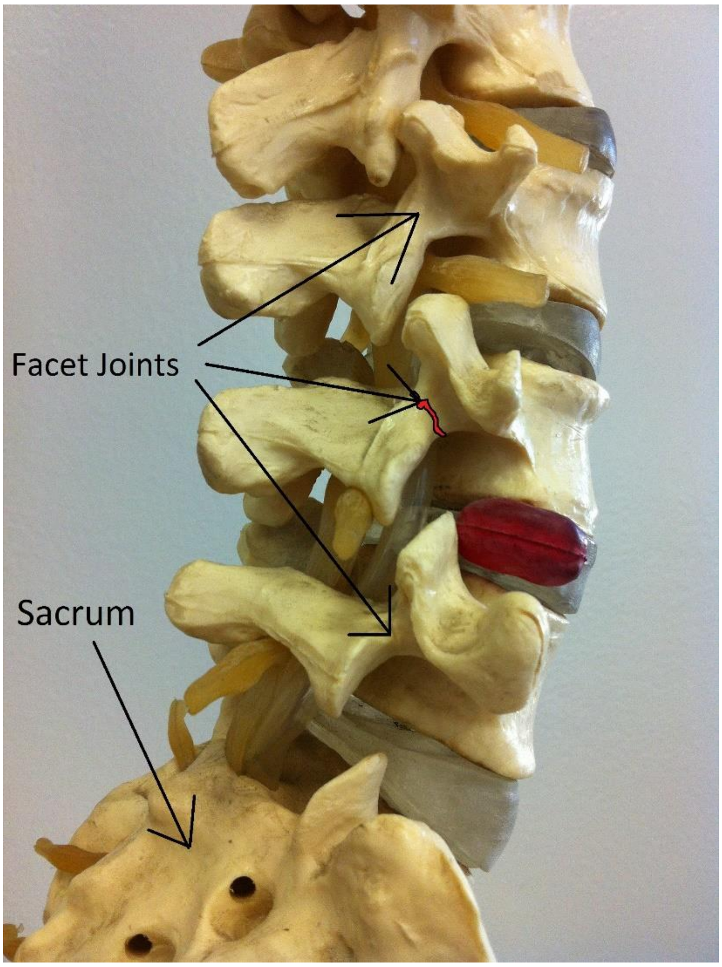

Figure 4: Pars interarticularis fracture location in the vertebra. Credits [https://commons.wikimedia.org/wiki/File:Spondylolysis.jpg] From Wikipedia

1.1.1 Causes and symptoms

The major causes attributed to this kind of fracture is associated with certain kind of activities that generate unusual stress, in terms of direction and magnitude, on the spine. Sports like football, baseball, soccer, gymnastic and weight lifting could involve excessive extension and torsion of the spine that could eventually lead to a damage of the pars interarticularis, fracturing it[1], [9]. There is also evidence that the predisposition of certain subjects to developing the fracture could rely on genetic factors [9]. It is still unclear how this genetic predisposition could express and could eventually lead, with excessive torsion or stress, to fracture. It is thought that the genetic predisposition could make the isthmus part of the vertebra more susceptible to fracture under certain types of stress distribution (such as lumbar hyperextension or excessive rotation). Some researchers have also analysed the hereditary predisposition of first-generation relatives of people affected by this fracture and saw that there is a significant incidence and relation[10], [11]. The fracture at the initial stages could be asymptomatic, but eventually low back pain, starting from the buttock and then spreading in the leg. Indeed, an activity more intense than the normal routine could start the pain[12], [13]. Another symptom of this pathology could be muscle tightness of the hamstrings[14] and other muscles such as quadriceps and triceps surae.

1.1.2 Diagnosis

Concerning the diagnosis of this fracture, imaging techniques such as X-Ray, MRI, CT and even SPECT[15] are usually employed. Before going deeper into the explanation of these techniques and their application in the spondylolysis fracture, it is worth to mention the Stork test. This test is used by physicians to quickly assess the presence of a possible spondylolysis with a simple and efficient exercise[16]. The patient is asked to flex the hip muscles, lifting one leg, and generating a hyperextension of the spine. The test is considered positive if the patients experience pain or discomfort at the level of the suspected spondylolysis. Nevertheless, the test could give the physician just a hint on a possible spondylolysis and hence a more accurate analysis using radiographic images or other images source have to be performed. Plain radiographs are always performed to assess the presence of the fracture and see spine changes, usually performing an analysis on the sagittal and lateral views[17]. Oblique views are performed to assess and evaluate vertebral stability[18] and *Lisbon et al*[19] have found that 19% of the spondylolysis identified were captured only in the oblique views. If a lucency is visible in the plain radiograph in the neural arch, pars fracture is present. The so-called “ collar of the Scottie dog “ visualization is used on the oblique view radiographs to describe and identify the neural arch region fracture in a straightforward manner [13], [17], [18]. For clarity, the Scottie dog is shown in Figure 5, if it has a "collar" it means that there is a fracture in the neural arch and we probably are in the presence of spondylolysis. In order to understand the mitigation of the fracture from multiples angles and see all the extent of a possible degeneration, plain radiographs may not be enough to assess the presence of the fracture while other imaging techniques were[13]. Therefore, other imaging techniques such as CT, SPECT and MRI[20]–[24] are used for a better viewing of the fracture due to their higher sensitivity.

1.1.3 Non-Surgical Treatments

The initial treatment of the pars interarticularis fracture is always non-surgical as several patients set better using conservative treatments. There are several procedures to treat pars fracture non-surgically[25], [26]. First, the patient is asked to avoid any contact sport or activity that could worsen the back pain or the fracture; for some cases of early-stage defects, this is enough to completely remove the pain. It is not uncommon that the physician prescribes nonsteroidal anti-inflammatory drugs to reduce swelling and alleviate the pain. Physiotherapy can be approached to reduce the pain and release the stiffness and tightness of the hamstrings and the lower back muscles and to reinforce other muscles, such as the transversus abdominis and the lumbar multifidus, that play a considerable role in the spine stabilization maintenance. In a recent study by *O'Sullivan et al*[27], it has been shown that a specific exercise treatment could reduce the pain of the subjects till the next 30 month of follow-up. The exercises involved the co-activation of the transversus abdominis and the lumbar multifidus to strengthen those muscle who could help in spine stabilization when the patient suffers from spondylolysis and back inflammation. The group of patients doing the reinforcing exercises was compared with the ones in the control group (standard treatment without these particular exercises involved). Another effective way to limit the fracture from worsening is the use of Braces like the Boston Brace model. The braces are designed to stabilize the fracture and limit the movement of the spine in a predetermined position. The Boston brace limits the position of the spine in a flexed arrangement, allowing a decrease in the stresses in the interested zone (i.e. low back)[28]. Overall, all the braces have similar function mobilizing the position of the spine and constraint the movements in a determined range of motion, depending on the pathology that we are interested in fixing. A significant study on the beneficial effects of the bracing has been reported in the literature by *Steiner et al*[29] although limited by a small size. We should understand that all the non-surgical treatments are not conceived as a definitive treatment for cases of spondylolysis that are already degenerated in severe spondylolisthesis or complete and irreversible damage of the neural arch.

1.2 Surgical Treatments

When non-surgical treatments are not considered sufficient in terms of pain management and fracture stabilization, surgical solutions must be considered. The current literature has presented two main surgical procedures to approach this particular fracture: spinal fusion and laminectomy. Before introducing the two techniques, it is important to mention that 9-15% of the patients with spondylolysis undergo surgery[7]. The surgical procedures outlined are commonly used for spondylolysis purpose but are both well known standardized procedures for most of the classical spine surgery.

Spinal fusion consists in the union of two vertebrae in a “single” piece. It is performed when the associated pain in the lower back region could be generated by the relative movement of two vertebrae or due to the ageing of the intervertebral disc that could be torn or damaged irreversibly. Hence, there is always the removal of the intervertebral disc that acts as a link between the two vertebrae. This is usually substituted with two different options using a bone graft or a cage implant. If the surgeon decides to unify the two vertebrae with the bone graft, this could be taken from the iliac crest of the patient if we are considering an autologous bone graft. This procedure of small bone removal is done within the same surgical procedure of the spinal fusion, therefore requiring more time to perform the total operation and adding another incision to the patient. The overall operation is meant to limit the range of motion of the two vertebrae, removing the possibility of relative displacement or rotation in any plane.

The surgeon can approach the operation from the front, the back and the side of the patient, removing the intervertebral disc first. Successively the two vertebrae are fused with the auxiliary of screws and rods/plates to avoid the slippage that could be generated by the pars defect. In the article written by *Gibson et al* [30] we can understand how spinal fusion allows the eliminate the compression caused by the pars defect and allow the total fixation at that level.

Considering the other solution, laminectomy, this is mostly chosen when the pars fracture pinches the nerves. Hence the most efficient way the surgeon could tackle this fracture is to remove the part of the vertebra that includes the fracture, decompressing the nerves. The procedure will be similar compared to the one mentioned previously, but the intervertebral disc will remain and no plates/screws/rods are required (Figure 7 below for more details). This type of surgical procedure requires more bone removal compared to spinal fusion, but no implant is required. Sometimes the surgeon would perform a laminectomy combined with a spinal fusion to ensure that the spine remains stabilised and that the part interested with the fracture will be removed. Of course, this option requires more time to be performed, hence more risks are associated, and the implant instrumentation will be inserted with less bone available for the surgeon.

1.3 Surgical Techniques for Spondylolysis

Even though it may seem that these techniques may be well known and convenient, there are several limitations associated with them. The laminectomy involves the cutting of the osteoligamentous construction which has been demonstrated being a fundamental component for the axial rotation and flexio-extesnion[31]. Therefore, the removal of this component would harm the stability of the spine. It has also been reported that only 64% of the total laminectomy is completed successfully [32]. Considering the spinal fusion, it is clear that the motion of the fused vertebra is drastically reduced in all directions, leading do a decrease in the range of motion of the global spine.

Therefore, surgeons have tried to look for alternatives solutions to repair directly the fracture avoiding its recurrence. The first technique that we are going to analyse is Buck’s technique that consists of the positioning of a screw directly across the pars interarticularis fracture[33]. The screw is made out of titanium and it is positioned across the fracture with the help of bone graft to guarantee a better fixation and osteointegration[34]. The second approach is the use of wires to fix the fracture which was first introduced by Scott and Nicol in 1986, this technique consists of a wire loop around the transverse process and tightened around the central spinous process[35], [36]. The wiring arrangement has varied throughout the years but the main goal of this technique is to avoid the movement of the pars fracture in any way and allow the healing process between the two parts of the fracture. Morscher introduced the screw-rod-hook technique in 1984 and then it has seen different variations throughout the following years. An updated version of this procedure, the surgeon inserts a screw through the pedicle and a hook system is anchored to the lower articular process to fix rigidly the interesting part of the neural arch where the fracture is located[37]. A rod connects the screw and the hook, guaranteeing the compression for the pars interarticularis. Gillet and Petit introduced their fixing version in 1999 using a similar system similar to the aforementioned one. The surgeon inserts two screws in the pedicles of the vertebra and then connect a V-shaped metal rod to the screws, passing around the central spinous process, in this way the process the neural arch is compressed and the fracture can't move[38].

Mohammed et al[39] have done a brilliant study and comparison of these techniques to better understand the disadvantages of the aforementioned techiques. We know that the Buck technique is difficult to be performed by the surgeon and the right positioning of the screw is vital for the success of the global operation, it reported that also the screw loosening or breaking could lead to a failure of the implant[40]. Regarding Scott procedure, one issue of the surgeon is to cut some muscles around the interesting area to allow the wiring process and hence blood loss could be higher compared to the other methods[40]. Most importantly, in this study, they have found that the major problem is the wire breaking that will then force the surgeon to make a revision surgery[41]. The screw-rod-hook technique will inevitably involve a more complex system and the surgeon could not perform the positioning with the right angle. If the right positioning of the system is not achieved, the fracture won't heal properly. Furthermore, it has been reported that the screw-rod-hook system is too big if two consecutive spondylolysis treatments have to be performed (e.g. L4 and L5 segments)[42].

CHAPTER 2

CT BASED VERTEBRA MODEL

2.1 Understanding of fractures in bone

This chapter focus on understanding the basics of fracture in bone at the biological level. The field of bone fracture is well established in terms of literature and understanding of how fractures develop and propagate. It was usually thought that a good predictor of fracture risk was the bone mass density, as reported by *Maximilien et al*[43]. We know that bone toughens in the presence of a crack to avoid crack propagation, the toughening process consists of the dissipation of energy, avoiding the crack to spread further. There are two main toughening mechanisms that the bone uses to resist crack propagation: intrinsic and extrinsic toughening. The position concerning the crack tip where these mechanisms act is different: ahead of the crack tip and behind of the crack tip for the intrinsic and extrinsic respectively. Both involve a mechanism that acts at the micro level to toughen the bone. The intrinsic mechanism is more involved in limiting crack initiation and growth while the extrinsic mechanism uses crack bridging and deflection to stop the crack to proceed further in the increasing[43], [44]. Considering the nature of the bone we can subdivide it in cortical and trabecular bone. The latter is formed by an arrangement of trabeculae where space in between them there is space filled by bone matrix. The cortical bone is formed by structures called osteons composed by the blood vessels and surrounded by a system of circumferential lamellae.

The intrinsic toughening mechanism involves a set of sub mechanisms at the micro-level. First, the collagen molecules change their spatial structure, stretching and unwinding due to the breaking of hydrogen bonds[43]. This collagen sliding leads to an increase of the plasticity of the bone to resist the crack propagation and initiation creating a zone with higher plasticity[45]. The plasticity process targets mostly the mineralized collagen fibrils which change their conformation due to mechanism like fibrillary sliding, caused mainly by elastic deformation that causes a stretch in the fibrils.

The extrinsic mechanism involves the micro-cracks propagation along the cement lines that are the areas that are more likely to be the start of the crack propagation because the resistance offered to contrast the propagation of these cracks is the least[46], [47]. These lines are localized in the bone as a separation between the osteon from the bone matrix[43]. Usually, the main direction of propagation of these micro-cracks would correspond to the longitudinal and the most common location is near the macro cracks. The most important external bone toughening mechanisms are considered to be crack deflection and crack bridging, that are due to the presence of microcracks[48].

If we analyse the crack deflection mechanism, we can observe the presence of transverse micro-cracks concerning the major crack direction, already said that to be usually longitudinal to the main axis of the bone. These cracks of minor length compared to the main one play a fundamental role in the mechanism of extrinsic toughening because they diminish the local stress field as they decrease the sharpness of the crack[43], [46]. This change in the principal direction of the crack changes the stresses at the crack tip, reducing them. Therefore, a higher force is needed to increase the length of the principal crack.

Analysing the other extrinsic mechanism of toughening, the crack bridging, it acts differently compared to the aforementioned crack deflection. It works in the longitudinal direction with respect to the main crack. The uncracked regions in the longitudinal direction of the crack path bridge and sustain the load that could have increased the propagation of the crack. We should also remember that another important component in the extrinsic crack shielding is the collagen fibrils[46].

2.2 Fracture Modelling and Computational Approach

The thesis contribution starts with modelling and analysis of a single vertebra. In this chapter, we are going to discuss the steps leading to the creation of the vertebra model using Mimics Medical 22.0 starting from the CT scans of a 68 years old white female cadaver specimen.

The first task is to create the vertebra model starting from CT of the patient. We purposely chose to model the L5 segment for the fact that usually, the crack happens at this level (see chapter 1.1 for more information). We first model the L5 segment considering only the bone and no other structures not present from CT scans. Mimics is the abbreviation for Materialise Interactive Medical Image Control System, an image processing software created by Materialise NV, Belgium. Starting from the 2D images, Mimics is able to create a 3D model that could be then processed and imported in other software for further analysis. In our project, the model is first created in Mimics, imported into SolidWorks 2019 Academic version (Dassault Systèmes, Concord, MA) for fracture creation, and finally into Ansys 19.2 Academic Version (Canonsburg, PA) for the static analysis and simulation. The images are created through the segmentation process starting from DICOM (Digital Imaging and Communications in Medicine) data from the CT, Magnetic Resonance Imaging, X-ray, Ultrasound and other images form. The DICOM format is the standardised format for storing and transmitting medical images. After opening the set of DICOM images in the software, three main views are presented with respect to three main planes: sagittal, frontal and transverse. The User could navigate through each slide in each plane and see all the images.

Figure 5: Mimics views

The first task to complete is to create a mask, this part is crucial to differentiate between bone and the other tissue type. The threshold procedure is used to set the value, expressed in Hounsfield unit (HU), from which bone will be differentiated from the following structures. The HU unit is defined as a transformation of the attenuation coefficient μ weighted in the air and water attenuation coefficient value. The attenuation coefficient μ is introduced to indicate how easily the beams pass through the object, a high value of μ means that the material attenuates the arriving beams higher than a material with smaller μ. The attenuation coefficient is expressed in m^{-1}. The formula expressing the linear relation is the following:

$$HU = 1000 \times \frac{\mu - \mu_{water}}{\mu_{water} - \mu_{air}}$$

Where μ_{water} and μ_{air} are the attenuation coefficient for water and air respectively. We chose to decrease the default range of HU and set the range from 110 to 3071 HU. This represents a more conservative choice since with a lower HU threshold we will include also other parts that will be easily polished and corrected, but nothing will be missed. Then the L5 vertebra is isolated from the rest of the spine thanks to the “Split Mask” tool in the Segment section. Hence, a process of trial and error is needed to polish the structure and make it similar to the anatomical model, the greyscale is used to understand where there is bone (white pixels) and where there is air (black pixels). Therefore, using the “Multiple Slice Edit” tool, we can add or remove material to the region of interest in our selected mask to model the vertebra completely. We are finally able to generate the part and generate a 3D model shown in the following Figure:

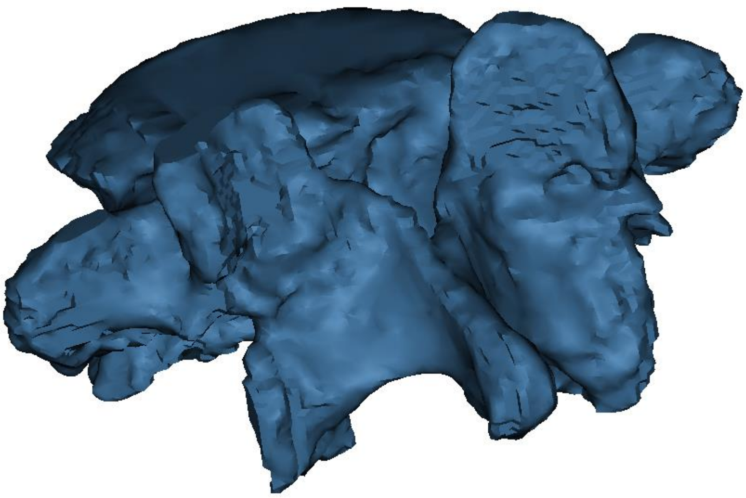

Figure 6: L5 vertebra model in Mimics before smoothing and wrapping operation

As we can observe, the model presents rough surfaces that could generate problems in computational modelling such that they could be computationally heavy and cumbersome. Hence the structure will have to be as precise as possible to avoid the problem with the further passages involved in the creation of the final 3D model. Once the polishing procedure is completed we Wrapp the model created to fill the eventual holes that are present. The user must be aware that a higher value of detail would distort the real model created with material not normally present and the model won’t be precise. Then the last part before importing everything in 3Matics is to Smooth the model with a smooth factor of 0.7 and a number of iterations equal to 3. These values are chosen mainly due to a trial and error process that tries to limit the smooth factor to avoid distorted or too smoothed models. The final model obtained is shown in the following Figure:

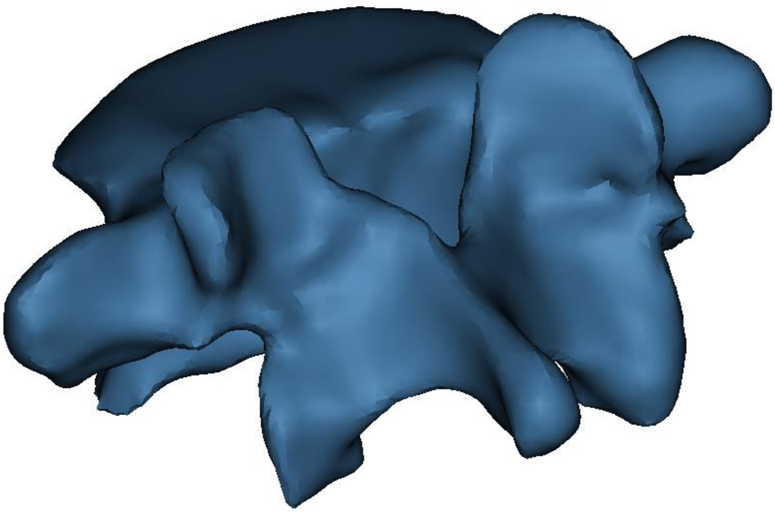

Figure 7: L5 vertebra model in Mimics after smoothing and wrapping operation

The same process was performed for the L4 segment, hence obtaining the two levels in the exact position of the CT scan of the patient. The next Figure shows what the final model would look like:

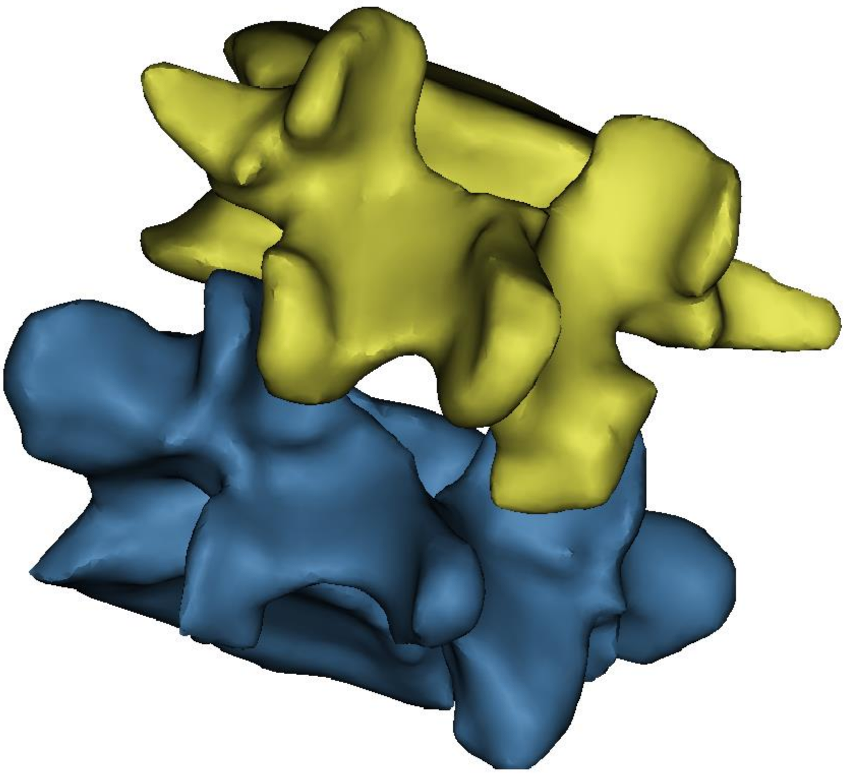

Figure 8: L4-L5 final vertebra model

As discussed previously, taking into account the fact that we took the images from CT scans, all the ligaments and the intervertebral disc of the patient could not be model using the Mimics mask and process outlined for the vertebral model. Hence, a different strategy should be used to model them and we decided to create the ligaments and the intervertebral disc in the SolidWorks. With an MRI scan, we could have been able to model the ligaments and the intervertebral disc properly thanks to the intrinsic difference between the two methods.

This model created will be imported in Geomagic Design X (Delscan, Rochester Hills, MI), a reverse engineering tool that will allow us to convert the model in SolidWorks. The various implant design will be assembled with the vertebra to obtain the final model before the simulation. Subsequently, they will be imported into Ansys to be tested and used as a starting point for all the various design techniques. First, both L4-L5 assembly will be used for understanding the area where the stresses concentrate the most and then we are going to use just L5 vertebra to perform all the surgical techniques and the crack.

Therefore, we imported the model in *stl* format into Geomagic Design X to further create the CAD model in SolidWorks. Geomagic Design $X^{™}$ is a reverse engineering software that converts 3D scan data into high-quality feature-based CAD models. The *stl* format defines the surface geometry of a 3D design, differently from the CAD file, it is defined by triangles and their respective normal and it is more commonly used in 3D printing and additive manufacturing. There are two different forms of this file, ASCII or binary where the second occupies less memory space.

Back to Geomagic, from the Autosurface tool, selecting organic mesh and the autosurface model, it exports directly the model into SolidWorks. From the model imported in *stl* format, it creates a set of surfaces. The next step is to unify these surfaces into one using the “Knit” tool in SolidWorks that allows us to make all the surfaces into one and create a solid from the surfaces. In this way, we can directly work with the CAD model created and eventually export it, after making all the changings we are interested in, into Ansys.

2.3 Ligaments and intervertebral disc modelling

Now that both vertebrae are modelled in SolidWorks environment, we have to model all the remaining structures and their corresponding anatomical parts. The parts that will be created are the following: intervertebral disc, supraspinous ligaments, interspinous ligaments and intertransverse ligaments. Each of the aforementioned components will be modelled singularly and the final result will be assembled in one assembly module. Once this is done, we can import them in Ansys. The facets ligament cannot be modelled because the distance within the facets is zero once we smooth and we wrap our Mimics model, hence we should take into account this limitation into the creation of our L4-L5 model. This L4-L5 segment model will be used to show that the stresses concentrate in the pars interarticularis of the neural arch. This, coupled with the low thickness and the repetition of stresses, will eventually cause the fracture. This model won't be used to make the finite element analysis in the next chapter since the boundary and loading conditions are different and made for a specific testing purpose on a single vertebra

First, we enter the Assembly module where we can import both L4 and L5 segment in their relative position and start modelling the intervertebral disc. We first create a 3D sketch where we seeded points to create the boundary of the intervertebral disc respectively on the lower surface of the L4 vertebral body and the upper surface of the L5 vertebral body. Using the spline command we unified all the points and we create a "net" that will allow us to form a surface starting from the profile we have created. After creating the two "nets" we have to fill the surfaces with the tool Surface Fill. Thanks to this tool we will be able to define two different surfaces that will perfectly resemble the shape of the real surfaces of the vertebrae. Then, using the Boundary surface and creating a connection line to set the direction, we were able to create one closed surface in between the two vertebral body. As done previously, we had to create a solid out of these surfaces and the only way to do was to knit all the three surfaces. Now the two vertebrae are separated by the intervertebral body as shown in the following Figure:

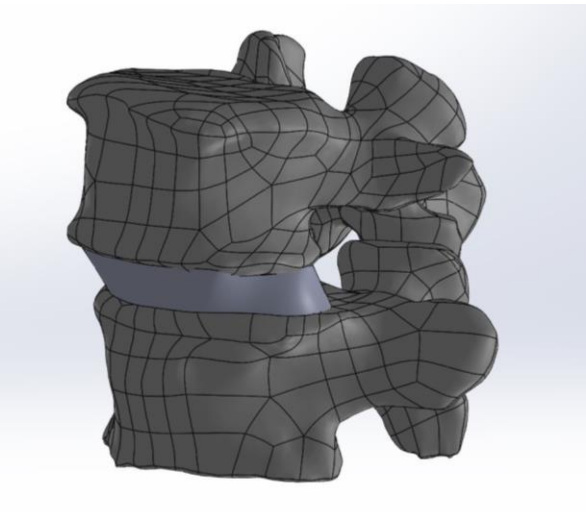

Figure 9: L4-L5 with intervertebral disc.

In order to understand the ligament modelling, we referred to previously published work to get the dimensions and positioning of all the remaining ligaments[4]–[6], [49]–[51]. Concerning the modelling approach, no changes were applied in SolidWorks modelling. The supraspinous and intertransverse ligaments were modelled with a quasi-circular cross-section, but due to the spline interpolation of the points at the extremes, we can’t consider it as perfectly constant. Starting from the supraspinous ligament, we modelled it as a rod and we were not able to create the smoothness of the surface in the real anatomy of the human spine. We need also to take into account that we did not model the interspinous ligament as single ligaments in series, but we chose to make a part that would recreate the fusion of all the ligaments together. We know that the relative distance between the interspinous fibers composing the ligament is negligible comparing to the vertebra dimension, hence we decide to create a uniform solid body that would replicate the fusion of all the fibers. All the measurements about the cross-section dimensions were taken from multiple published papers[5], [49], [52], [53]. The models of the single ligaments were created in different parts of the assembly because we needed to import the assembly file and give the material properties separately for bones, ligaments and intervertebral disc. In the following Figures we wanted to show the coronal and frontal view of the SolidWorks model of L4 and L5 including all the ligaments previously mentioned and the intervertebral disc:

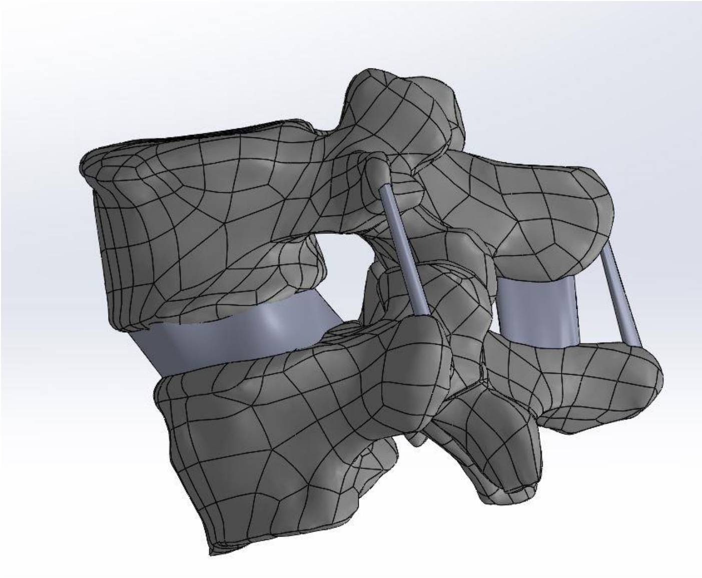

Figure 10: L4-L5 Final spinal segment model including ligaments and intervertebral disc (coronal view)

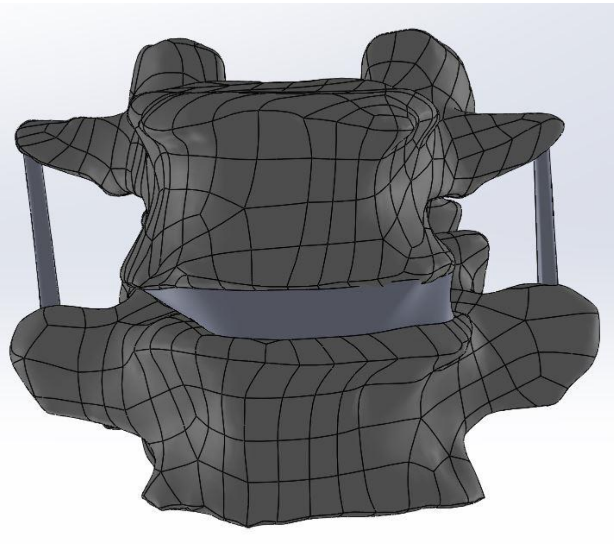

Figure 11: L4-L5 Final spinal segment model including ligaments and intervertebral disc (frontal view)

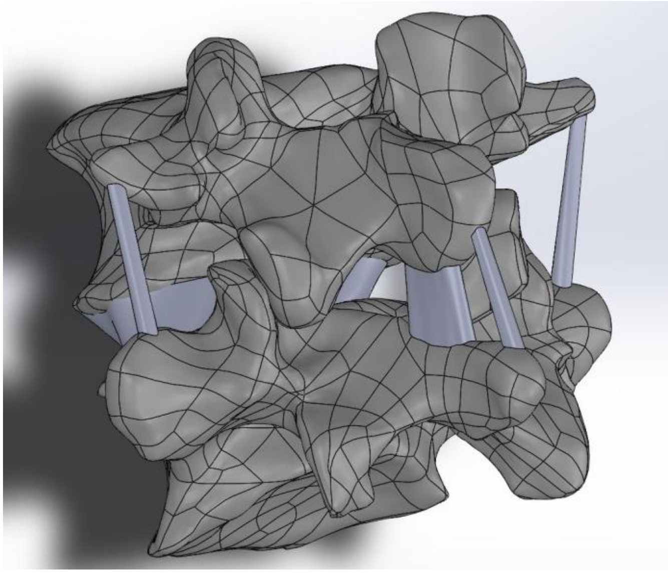

Figure 12: L4-L5 Final spinal segment model including ligaments and intervertebral disc (back view)

2.4 Ansys analysis without crack creation

The general idea of our simulation will be the following: we will simulate an axial compression and flexion moment to replicate a common movement performed during the spine simulations. Before doing that, we have to understand how to treat the material properties of ligaments, intervertebral disc and bone. To understand this fundamental aspect, we looked for papers in order to model each part. First, we have to declare that the ligaments were treated as isotropic elastic parts for sake of simplicity even though they do not behave elastically, but viscoelastic. Secondly, we did not model the Annulus and the Nucleus part of the intervertebral disc separately because it could have created problem in the mesh and we decided to average the Young Modulus of these two different parts with isotropic properties. The vertebrae will be treated as all composed by cortical bone since we are interested in the results in the neural arch that is mainly composed by this type of bone and not cancellous bone. These are all assumptions that will affect our result and should have to be taken into account in the discussion that will follow later. We reviewed different papers trying to understand the proper values to assign to each ligament part [49], [54]–[56] and we decided to assign the material properties base on the paper of *Tyndyk et al* [56]. Hence the ligaments' Young Modulus (all modelled with the same Poisson Ratio of 0.3) are the following:

Intertransverse ligament 54.4 MPa

Supraspinous ligament 34.1 MPa

Interspinous ligament 16.9 MPa

Concerning the intervertebral disc the mean value between Annulus and nucleus was considered (with a Poisson Ratio of 0.4):

Intervertebral disc: 3 MPa

Concerning the material properties of the bone, we decided to set a value of 12 GPa as used in several articles in the literature, whilst on the Poisson Ratio we decided a more commonly used 0.3.

The simulation will be made without the crack presence since we expect to understand the stresses distribution in a normal vertebra and check that they concentrate in pars interarticularis.

2.5 Finite Element Analysis of fracture simulation: understanding where to create the fracture

In order to create the fracture, we needed to create a small gap that shows a separation in the SolidWorks model. We know from the theoretical background previously explained that the fracture will be inserted in the pars interarticularis. In order to prove that the stress concentration is higher in this region, we performed a quick analysis of our complete L4-L5 model just created in SolidWorks. The analysis performed is done in the Static Structural module within Ansys

Workbench environment. We decided to apply a compression load of 500N along the z-component and a moment of 5 N*m along the x-component both applied on the top surface of L4. These loading conditions are commonly used in literature with different values of axial forces and moment. The main rationale used is the following: considering an average weight of 180 pounds (around 81 kg, if you cut the body at the L4 level, we are considering that in a static position the weight is 2/3 of the total body weight taken into consideration. Hence the weight on the vertebra is around 50kg and, therefore, a force of 500N is applied at the L5 level. We also know that this weight increases once a simple motor task (such as running or walking at a different speed) is performed. In order to justify the moment condition we can say that, on average, the centre of mass of the body is 1 cm away from the centre where the force is applied. Hence a force of 500N multiplied by 1 cm leads to our 5 N*m. This moment can range a lot depending on the distance of the centre of mass or the increase of load.

The lower surface of the L5 body was fixed as an encastre without allowing for translation or rotation. The materials were set with the previous characteristics for each component in terms of Elastic Modulus and Poisson's ratio. As a connection property between the surfaces (in total 11 regions: two for each ligament and intervertebral disc and one on the facets between vertebra L4 and L5) we choose bond because no sliding or separation between faces or edges is allowed between the elements. The final model has 9741 tetrahedron elements and 20101 nodes.

The von Mises stresses, which is the main parameter we are interested in, were represented in the next Figure:

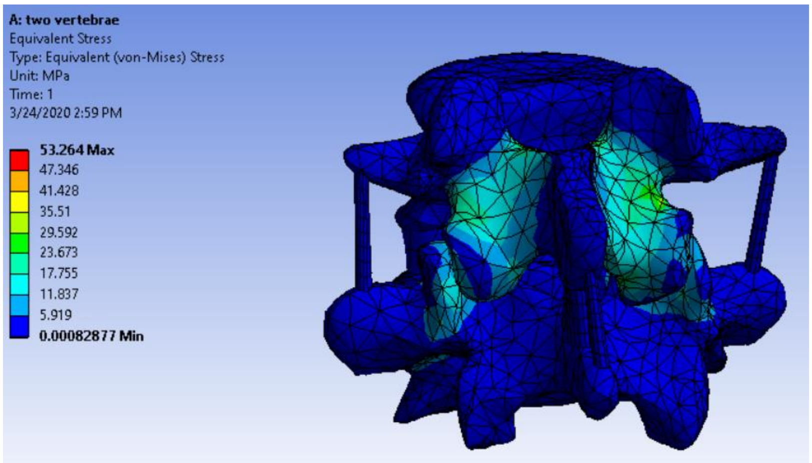

Figure 13: Ansys simulation for two vertebrae under a compressive load of 500N and a flexion moment of 5 N*m

As clearly showed by the previous image, the pars interarticularis is the part of the neural undergoing the major amount of stresses and this confirms what we previously mentioned.

Hence we need to implement the fracture in SolidWorks environment. The location is now uniquely defined and the width of the fracture should be as small as possible, hence we decided to make the fracture 0.5 mm considering that the width is not defined in the literature and can range from 0.1 up to 1 mm[57], [58]

2.6 Fracture creation and simulation

The fracture analysis and creation are performed in the L5 vertebra model previously created. The fracture will be created by the combination of the L5 vertebra and the solid that we are going to describe further. We start creating a plane using three points chosen in the vertebra: two on the corresponding facets and one on the spinous process. This plane will be important in order to sketch the profile of the crack that we are interested in. Thus, we sketch two different lines separated by 0.5 mm that will represent the width of our fracture. We subsequently extrude these two lines in order to completely pass through the vertebra. The next step in to create another plane, parallel to the previous one, and create two lines (in an opposite direction compared to the lines used to extrude). We then have to create the two surfaces that will complete our extruded rectangle, hence we create using the Surface Fill these two surfaces and knit all the four surfaces of interest to create a solid body. Finally, we can combine the L5 vertebra and the extruded rectangle in order to subtract the rectangle from our vertebral part and obtain the final result shown in the following Figure:

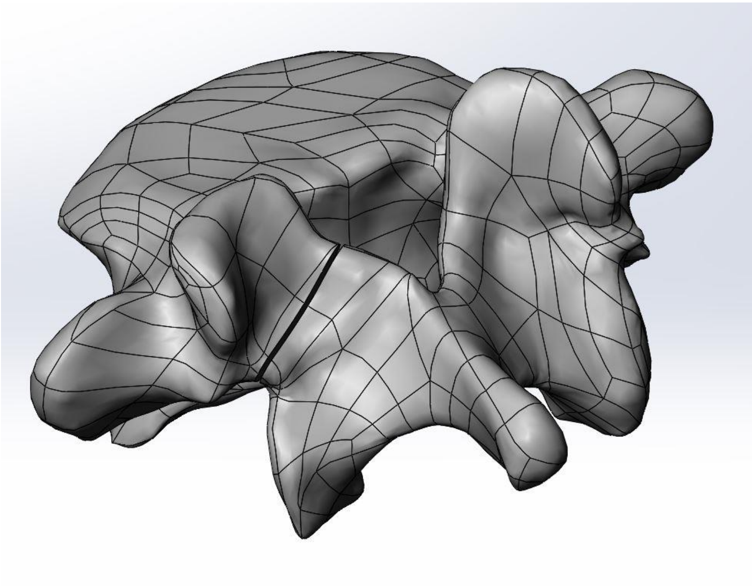

Figure 14: Pars fracture creation on L5

This vertebra will form our starting point for the study and analysis of the proposed implants. The proposed fracture shape represents an approximation of the realistic fracture, but we think that this approximation to our model is negligible since the difference in shape is not expected to influence the results of the simulations. An important factor in our analysis is to position the crack where we found the higher stresses in the neural arch and where all the literature indicate the fracture usually occurs. One should ask why positioning the crack on one side and not on both sides, the reason for this choice is that we are trying to model the pars fracture that characterises the spondylolysis, if we consider a bilateral spondylolysis, we would have described a different pathology: spondylolisthesis. This pathology occurs especially when both pars are fractured and slippage between the L4 and L5 would occur. Since we decide to focus on one vertebra since our purpose is not to study spondylolisthesis, we decided to make the pars defect in one side. In the context of creating a real fracture, an additional question arises concerning the depth. Why making it through the whole vertebra and not, for example, a few millimetres below the surface? The answer is that the surgical operation of the pars, and hence the utilization of an implant, is done only when the pars is completely fractured (doesn't matter which side), not when there is a stress fracture barely visible on the plain radiographs. Hence, a total fracture must be performed on our model to understand the real behaviour of the spondylolysis fracture. Lastly, the side on which the pars defect is present is not relevant since there is not a prevalence in the literature that the defect would occur on the left or right side of the arch.

The next and final step before moving to the next chapter is to make simulations on the intact and fractured L5 vertebra only and see the changings on the stress distribution. We imported the single L5 vertebra on Ansys Workbench in the Static Structural module with the same material properties for the vertebra as shown before in previous examples. We wanted to find a way to fix the vertebra uniquely to avoid slippage or movement as if the two upper and lower surfaces of the vertebral body were fixed with a clamp. This would simulate a testing procedure which can be easily replicated in a laboratory with appropriate machines. We have assigned the following boundary conditions as shown in the following Figures where we can see that both the upper and lower surface is fixed with no rotation or displacement allowed:

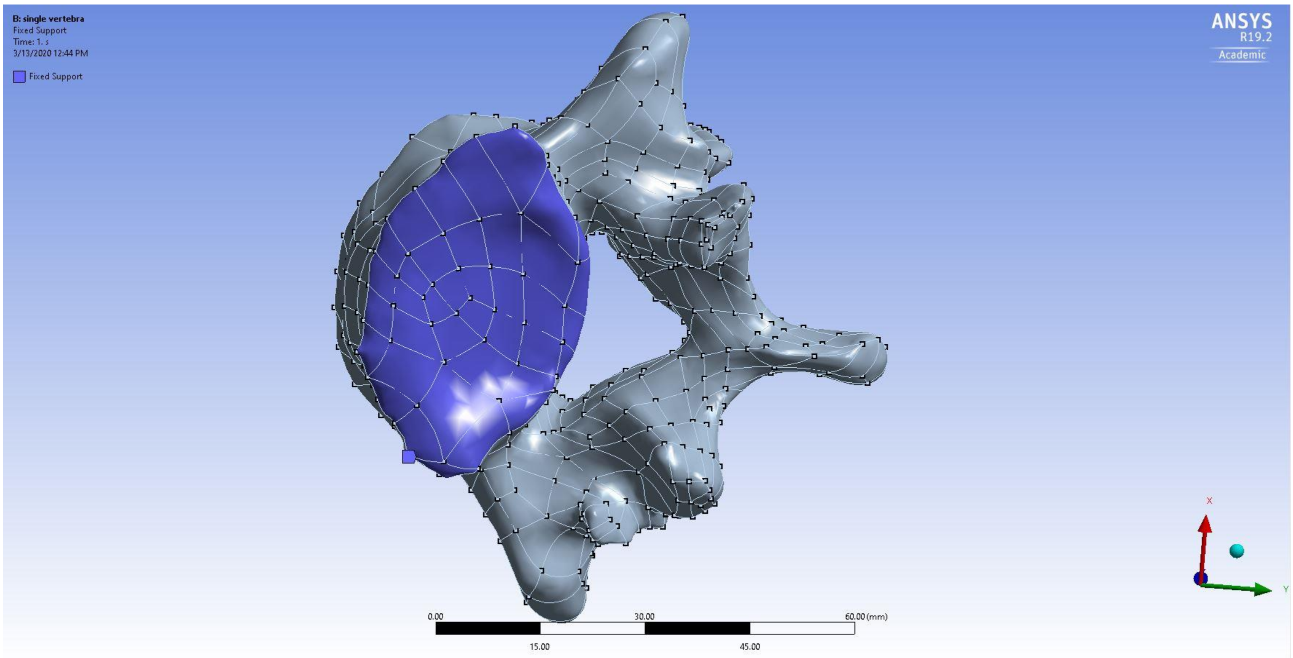

Figure 15: Intact L5 boundary conditions (bottom view)

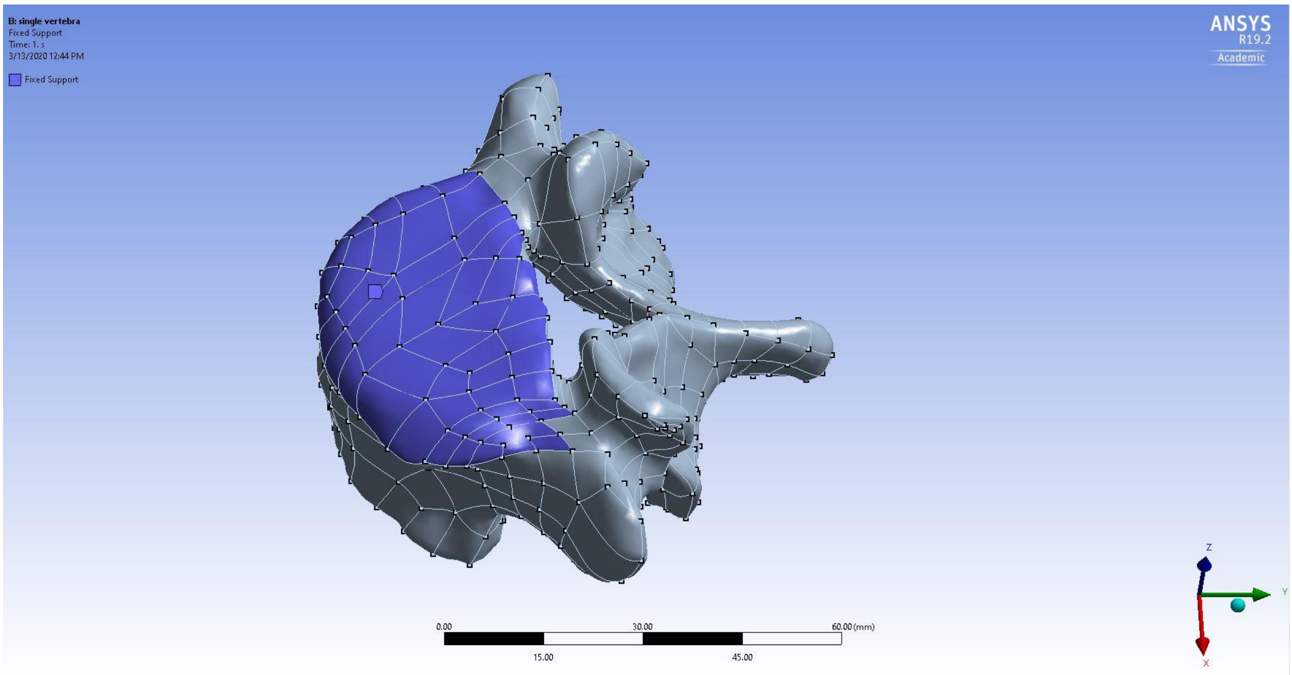

Figure 16: Intact L5 boundary conditions (top view)

Concerning the load, we applied a weight of 500N to the region that is assumed under compression during a possible experiment, as shown in the following Figure:

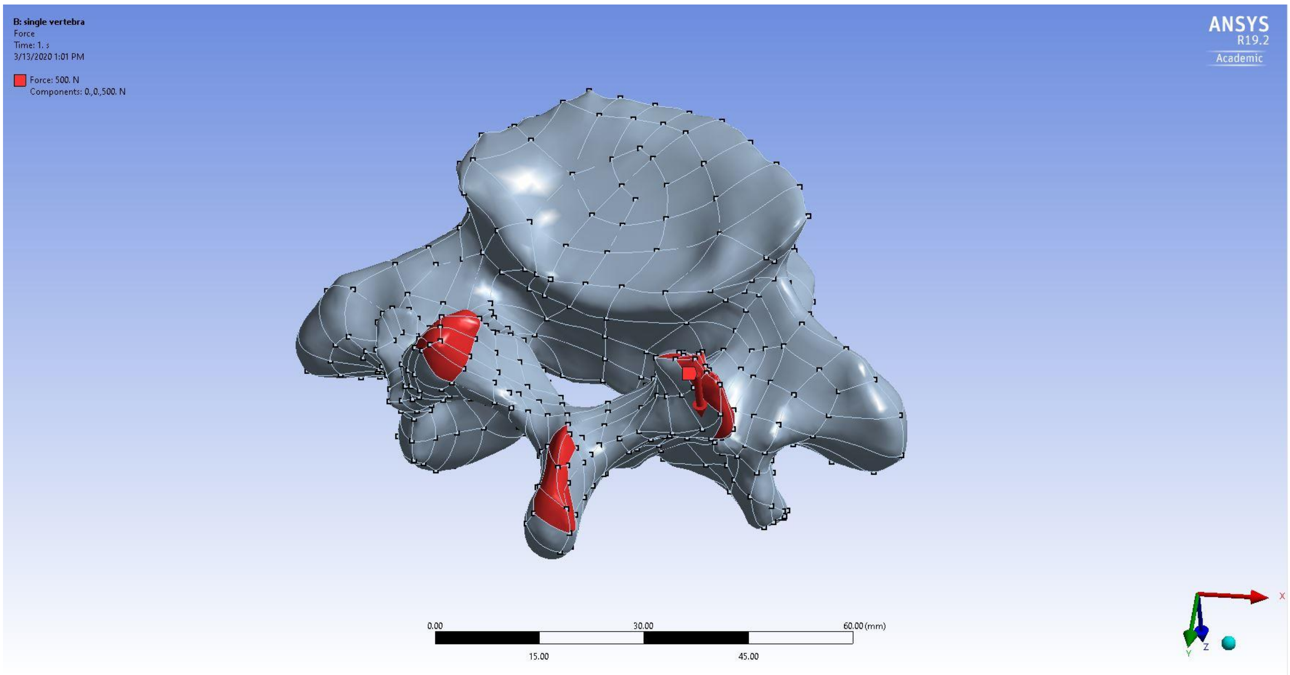

Figure 17: Loading conditions

This particular boundary and loading conditions are well suited for replication in the laboratory environment with a testing machine. These boundary conditions are not meant to simulate an exact physiological movement or condition, but they represent an optimal way to maximise the stresses going directly on the implant and across the fracture. However, the reaction force acting on the L5 level from the S1 at the level of the facets and the spinous process could also mimic, in some way, the direction of the load during an extension movement.

The final model is meshed with 4300 tetrahedron elements and 7933 nodes.

All the following analysis will involve the Equivalent Stress and Strain (i.e. Von Mises) and the deformations. The results are shown in the Figure where the Equivalent Stresses are displayed given in MPa:

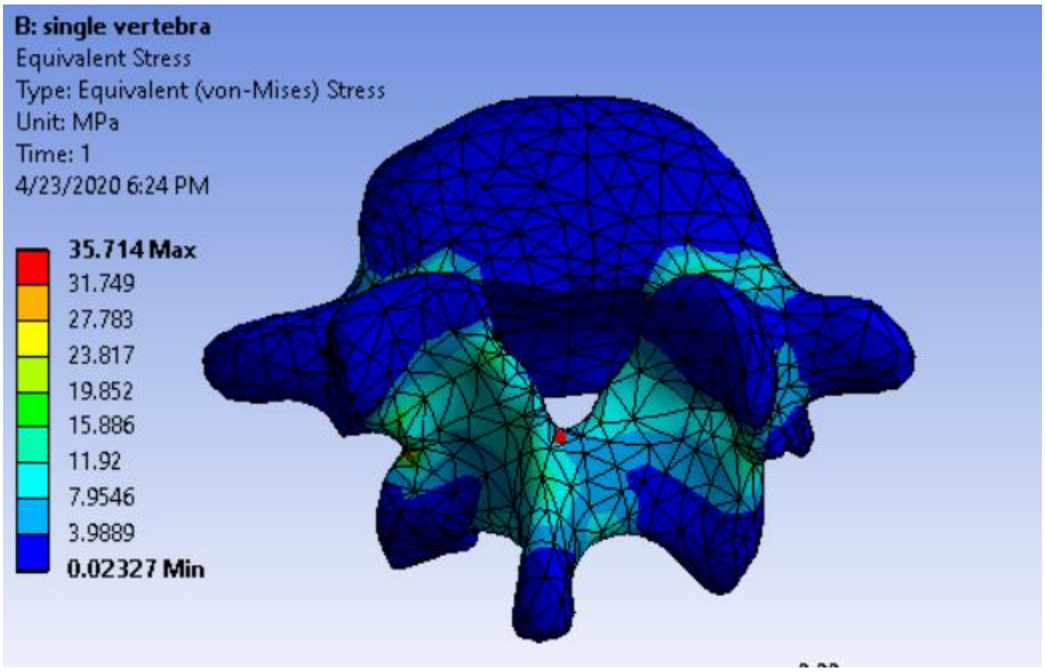

Figure 18: Intact vertebra, stress distribution

As shown, the maximum of 35.71 MPa is reached on the left side of pars interarticularis and we can easily see that that the stresses range from 7-35 MPa.

Regarding the strains, the Figure shows the strain distribution on the intact vertebra, expressed in mm/mm:

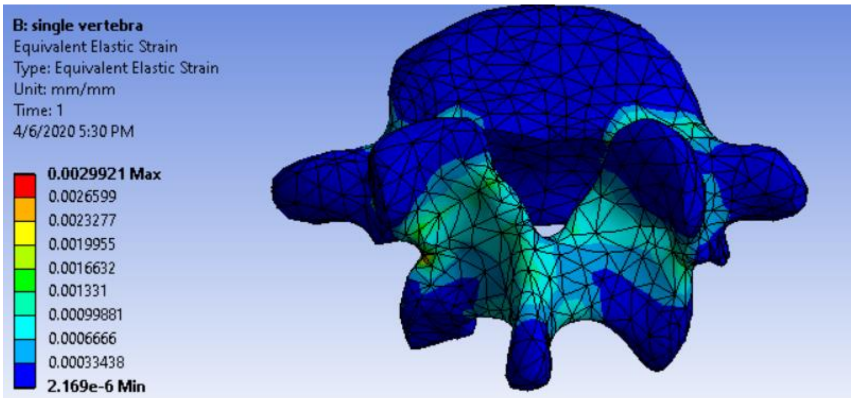

Figure 19: Intact vertebra, strain distribution

The maximum strain is 2.99e-003 reached in the left side of pars interarticularis. The values in the pars range from 7e-004 to 2.99e-003. As show in the the previous pictures, the stress and strain distribution are, as expected, similar.

In the Figure the deformations of the intact vertebra expressed in millimetres (mm):

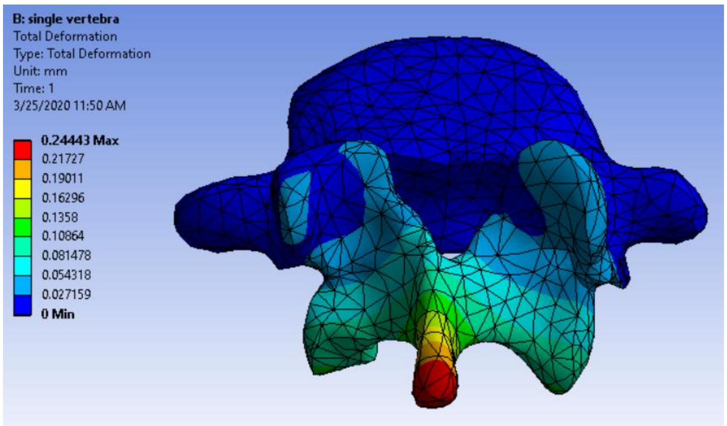

Figure 20: Intact vertebra, deformation distribution

Once we analyse the fractured vertebra, we present a comparative table of the stresses, strains and deformation followed by a discussion on the changings in these parameters produced by the fracture.

Starting from the fractured model of the pars that we previously showed in Figure 18, we imported it in Ansys Workbench to replicate the same simulation as previously performed with the intact vertebra to understand how the fracture influenced the results. Same material properties, boundary and loading conditions were applied. The only and most significant change is defining the contact between the two surfaces that are separated by the fracture. Ansys offers different contact types: bonded, frictional, frictionless, rough and no separation. Since we already know that our surfaces can slide and press with each other, the most precise relation was given by frictional with a friction coefficient of 0.3[59]. We decided to plot the Equivalent Stresses, Strains (Von Mises) and the Total Deformation and see how they changed. Considering the movement imposed by our boundary conditions, it is a sliding movement that would eventually separate the sides of the crack vertically. We also expect the stresses concentration to be in the contralateral pars interarticularis, than the intact one. This is due to the fact that the gap between the two faces of the crack won't allow the stresses to mitigate to the left side of the vertebra (the one with the crack present), hence the stresses will propagate and remain more in the right part of the vertebral arch. The final model is meshed with 4825 tetrahedron elements and 8970 nodes. The two following Figures show the plot of the stresses, strain and the deformations of the vertebra with a crack depicting the fracture:

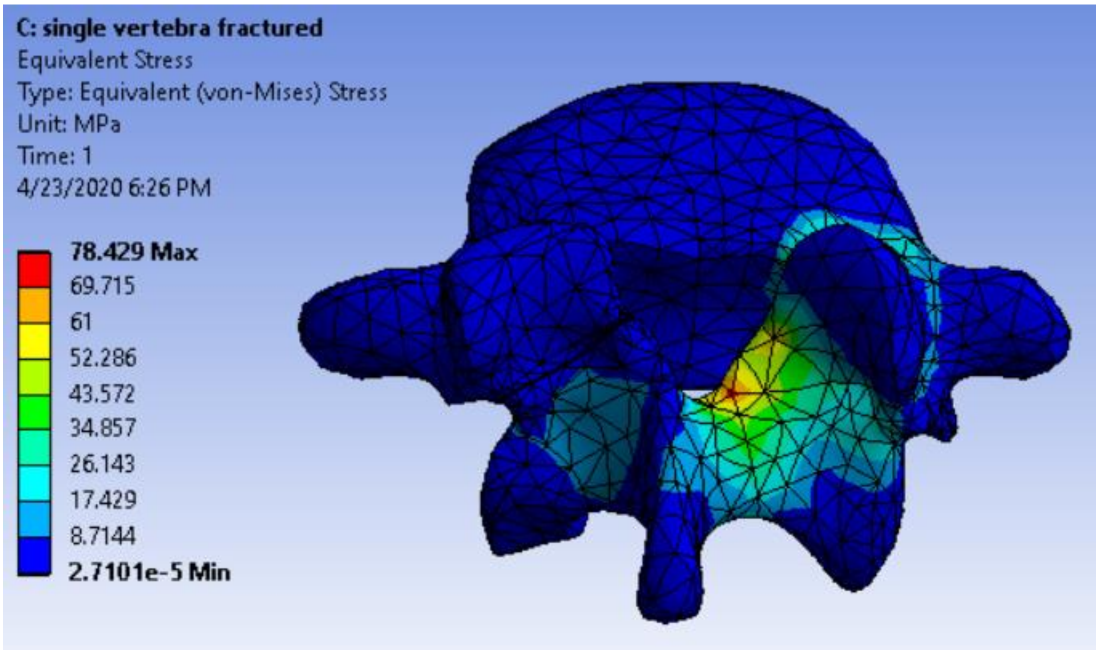

Figure 21:Fractured vertebra, stress distribution

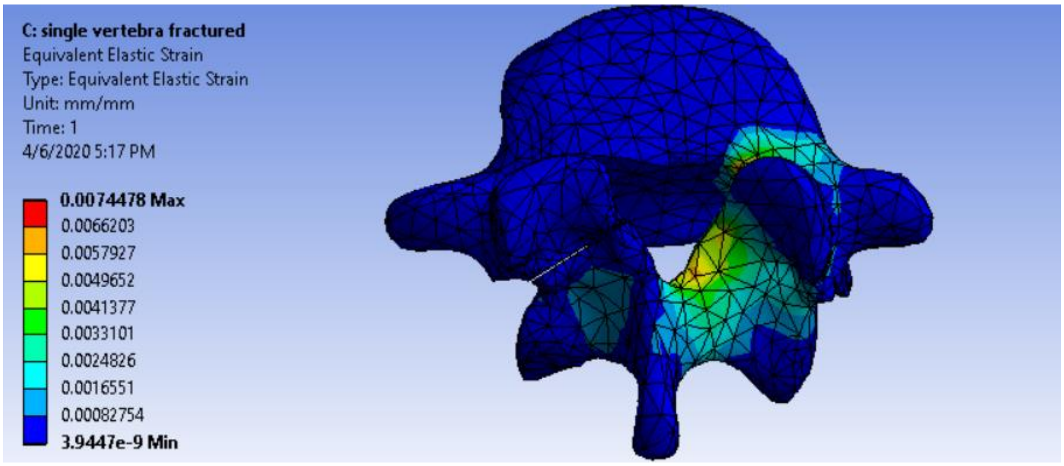

Figure 22: Fractured vertebra, strain distribution

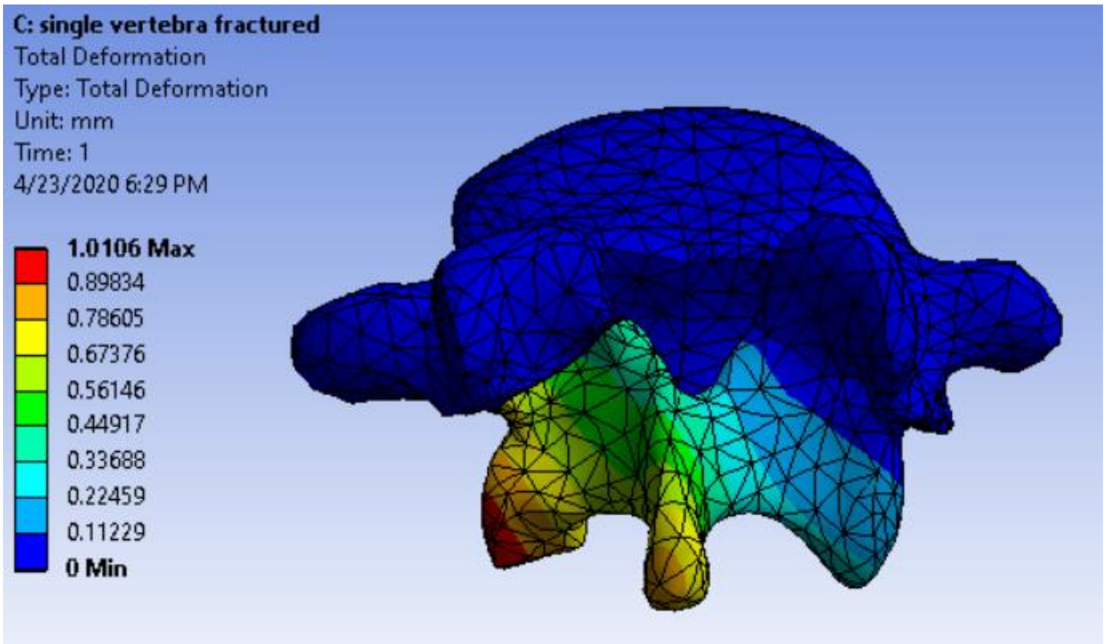

Figure 23: Fractured vertebra, deformation distribution

The images in the Figure show what was predicted before with a new maximum of 78.42 MPa in the right pedicle and a high peak around 75 MPa in the right pars interarticularis. If we try to compare the stresses in the two conditions, we can examine the following images from next the Figure that are used to provide a better distribution of the stresses:

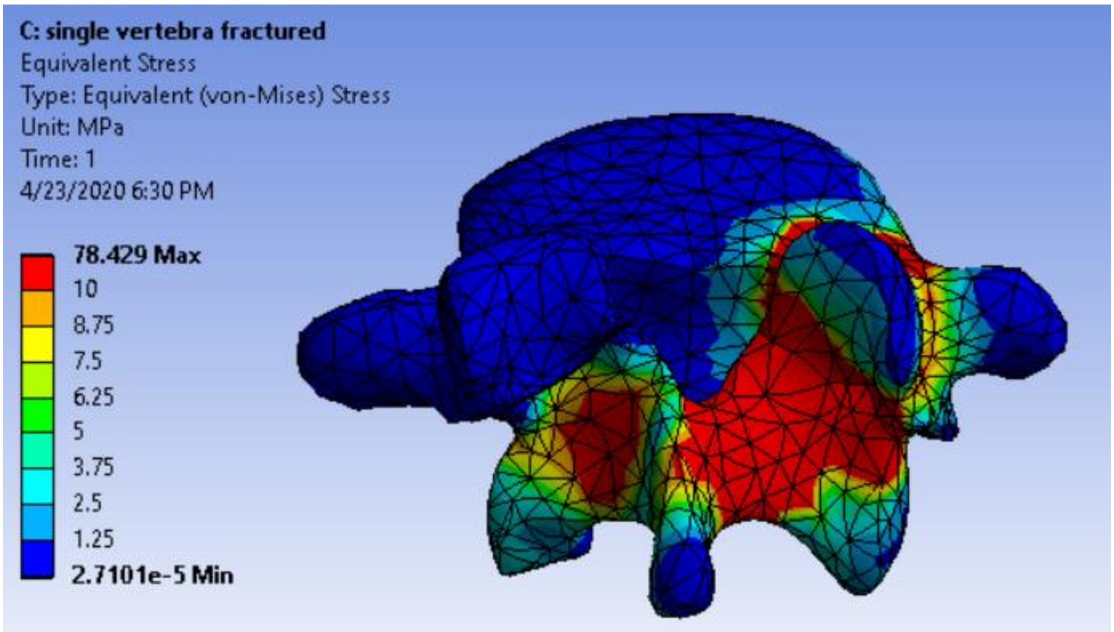

Figure 24: Stress contours of fractured vertebra, threshold at 10 MPa

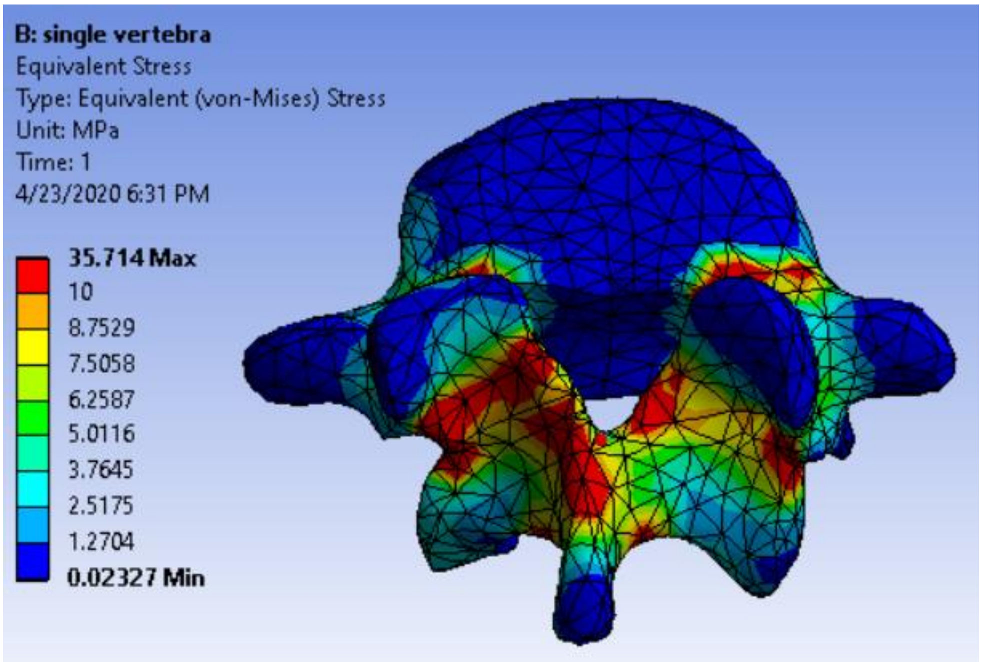

Figure 25: Stress contours of intact vertebra, threshold at 10 MPa

Figure 27 and 28 represent the fractured and intact model respectively, depicting a level of 10 MPa at the red colour interface (i.e. all the red areas are above 10 MPa). With this representation, we can understand how the fracture has visibly increased the stresses overall in the pars interarticularis area and particularly in the contralateral part of the fracture. We also made the following stresses table in order to show the Maximum, Minimum and Average stress value:

	Fractured	Intact	% Decrease
Maximum [MPa]	78.42	35.71	54.46
Average [MPa]	4.54	3.47	23.56

TABLE I: COMPARISON OF THE MAXIMUM AND AVERAGE STRESSES IN THE FRACTURED AND INTACT MODEL, EXPRESSED IN MPA

As shown by Table I, the maximum has increased by 119 % and the mean value by 16 % and thanks to the presence of the fracture. Of course, the presence of increased stress distribution in one single part of the vertebra would eventually lead to fatigue failure over time that will create bilateral spondylolysis. As already explained in the beginning, the bilateral spondylolysis will eventually evolve into spondylolisthesis that will cause slippage to the vertebra (in this specific case L5 over S1) and create other complications to the patients.

We can present a similar comparison with the strain distribution, setting a threshold of 0.0025 mm/mm below the maximum value band colour in the following Figure (i.e. the red colour parts are the one with the strains above the 0.0025):

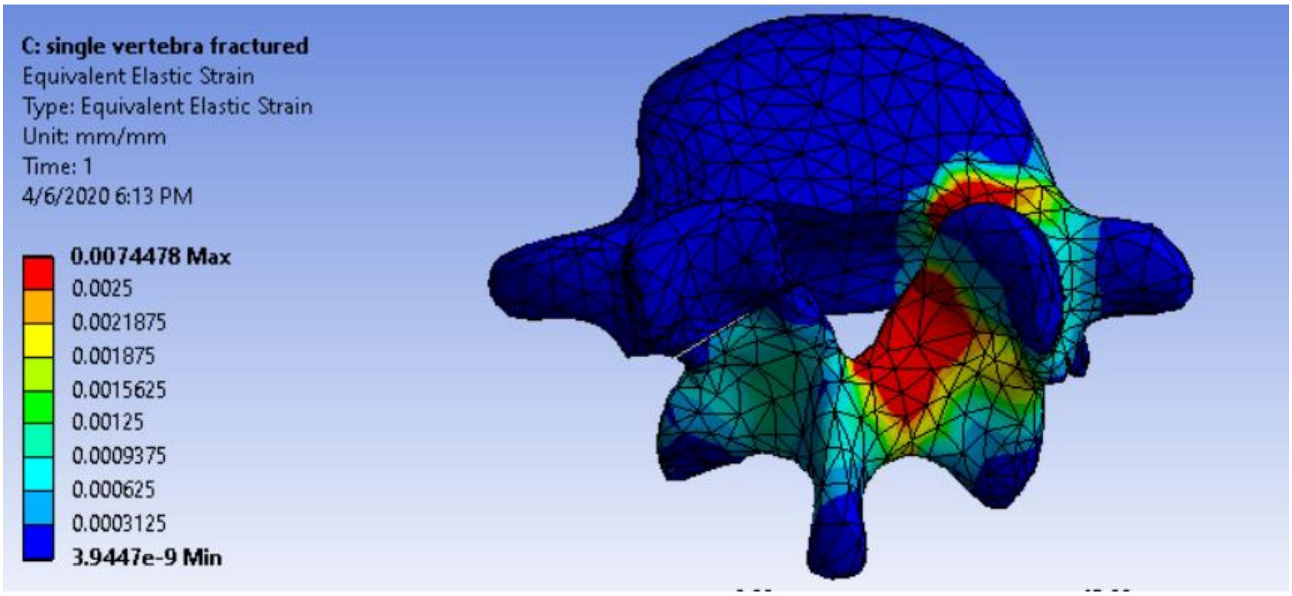

Figure 26: Strain contour of fractured vertebra, threshold at 0.0025 mm/mm

The strains propagate in the contralateral region of the neural arch with respect to the fracture and the strains concentrate mainly in the right pars interarticularis and in the right pedicle, while the left pars and the left pedicle above the fracture do not present any relevant strain value. This was expected since, analogously to the stresses, the gap won't allow the strains to pass through. The next table compares the maximum, minimum and average strain between the intact and the following scenario:

	Fractured	Intact	% Decrease
Maximum [mm/mm]	7.44e-003	2.99e-003	59.81
Average [mm/mm]	4.28e-004	3.21e-004	25

TABLE II: COMPARISON OF THE MAXIMUM AND AVERAGE STRAINS IN THE FRACTURED AND INTACT MODEL, EXPRESSED IN MM/MM

The fracture leads to a significant increase in the strains regarding the maximum and average value since they increase by 1.5 times and 33.33% respectively compared to the intact condition. As we have just written before, the stresses increase as well, but with a different percentage.

Concerning the Total deformation, the following table will compare the maximum, minimum and average deformation expressed in millimetres:

	Fractured	Intact	% Decrease
Maximum (mm)	1.01	0.24	76.23
Average (mm)	0.14	3.01 e-002	78.5

TABLE III: COMPARISON OF THE MAXIMUM AND AVERAGE DEFORMATIONS IN THE FRACTURED AND INTACT MODEL, EXPRESSED IN MM

As expected, the deformations have increased dramatically, more than the stresses in terms of relative percentage. In fact, the maximum has increased by 320% and the average about 351% due to the slippage at the faces of the fracture that was due to the movement prescribed by the boundary conditions and the load direction.

We are also interested in the behaviour of the stresses, strains and deformations just in the proximity of the crack and hence we are going to show, for each scenario, these values probed in the proximity of the two faces of the crack and compare with each other.

Considering the fractured vertebra, the following Figures represent the aforementioned probed values in terms of stresses, strains and deformations respectively:

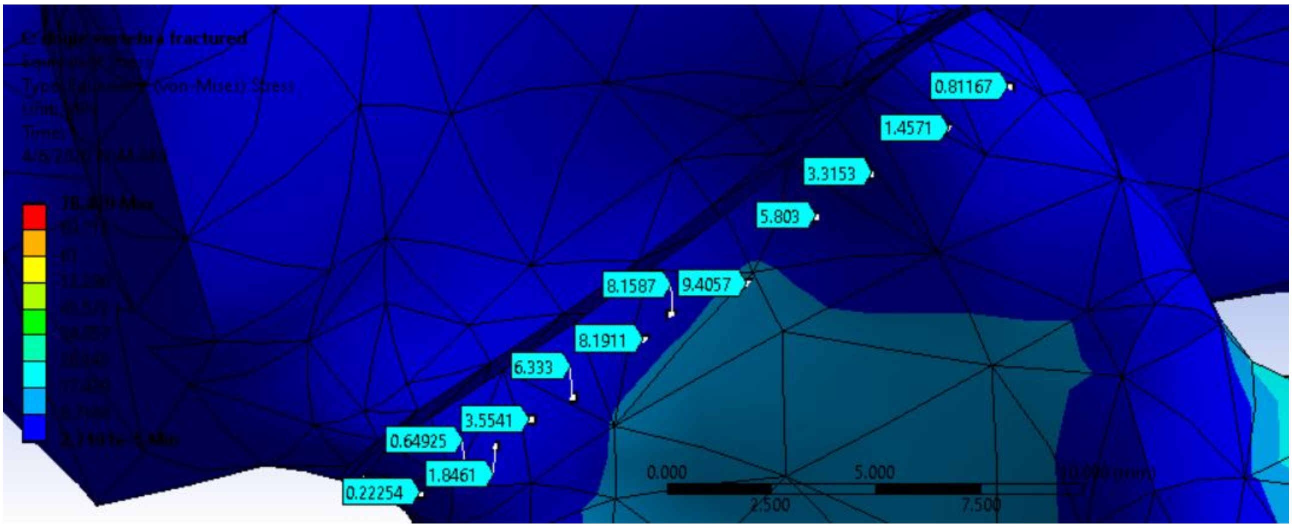

Figure 27: Values of stress in proximity of fracture, fractured vertebra

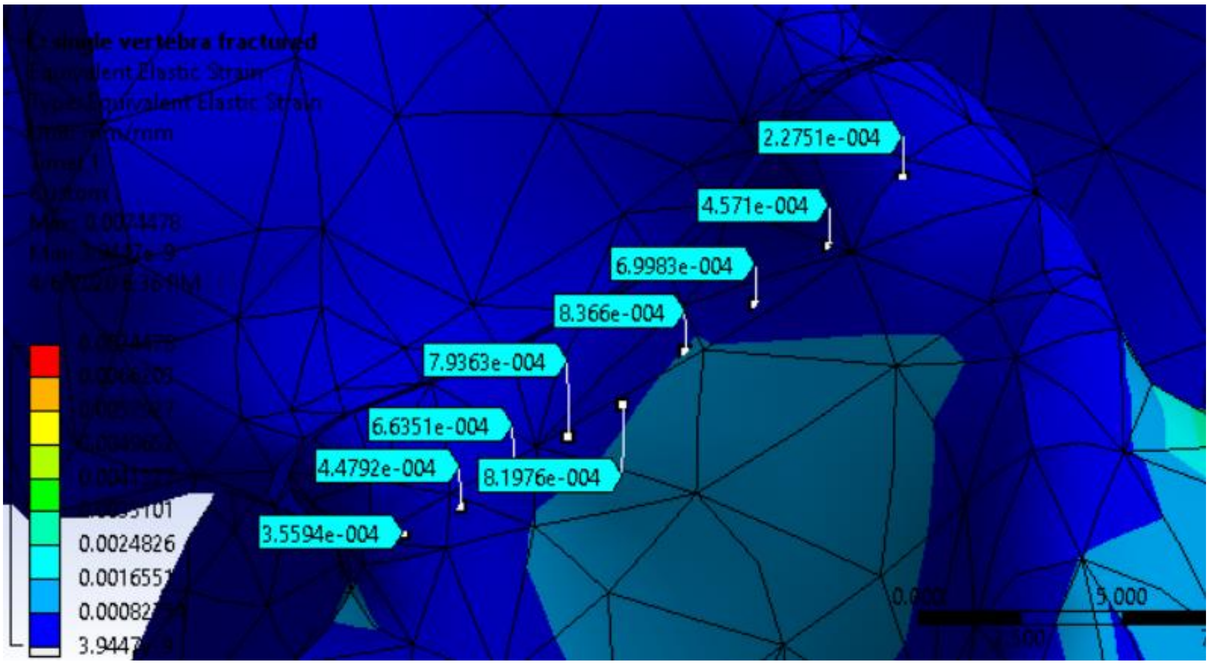

Figure 28:Values of strain in proximity of fracture, fractured vertebra

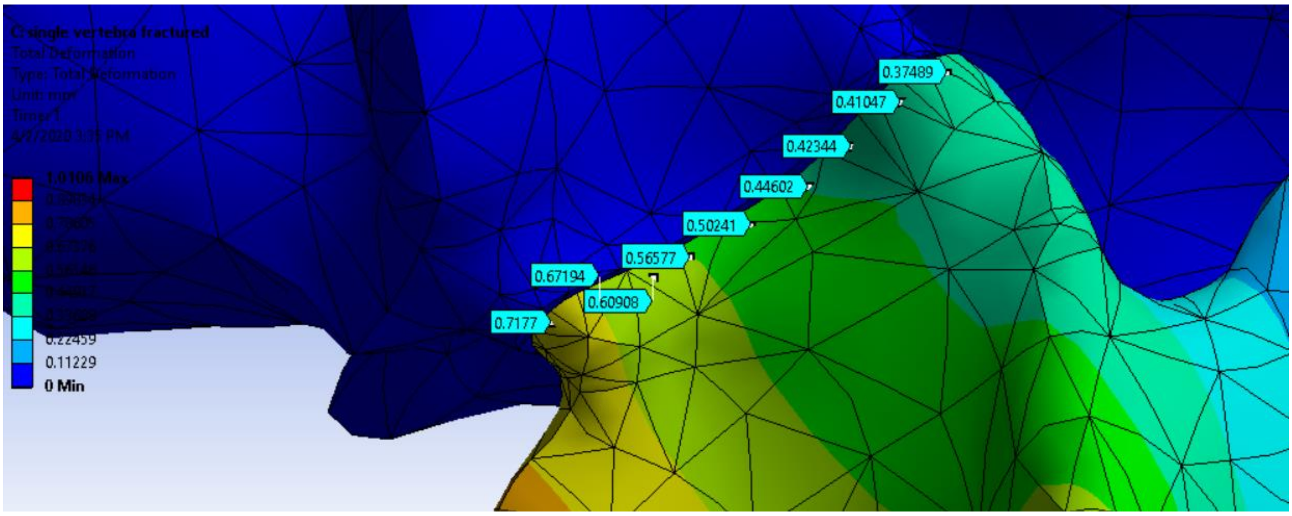

Figure 29: Values of deformation in proximity of fracture, fractured vertebra

The values of stresses, strains and deformations will be probed not only for the fractured vertebra but also for all the scenarios we are going to encounter in the following analysis and see how the medial and the lateral values will change. The stresses values range from 0.81 to 0.22 MPa going from the medial to the lateral side respectively. The strains are extremely low, below the average value in the vertebra and range from 3.55 e-004 to 2.27e-004 mm/mm, increasing in the middle and then decreasing as we proceed to the extremes. As we can see, the values of the deformation range from 0.37 to 0.71 mm from the medial and the lateral side respectively. From the next cases, we are going to compare each scenario with this one and the various scenarios between each other.

CHAPTER 3

FEA COMPARISON OF BUCK AND HOOK-SCREW FRACTURE FIXATION

In this chapter, we are going to compare two clinical solutions to pars using Finite Element Analysis. Essentially, we will model each procedure and assume boundary conditions on each based on available literature. Stress, strain and deformation will be assessed for the same loading conditions

3.1 Buck technique

The Buck technique[33] consists of a screw inserted in the inferior edge of the lamina, few millimetres lateral with respect to the spinous process. The screw will be placed to completely go across the defect in order to avoid the movement of the faces of the fracture. In order to better replicate the exact insertion method, we referred to *Rajasekaran et al* [34] paper that describes brilliantly and with extreme precision the method of insertion of the screw. The point of insertion is identified 10 mm away from the base of the spinous process and the screw crossing the defect should create an angle of 30° with respect to the coronal plane. A graft taken from the iliac crest is placed on the defect in order to increase the healing process. Unfortunately, this graft part cannot be modelled in our CAD but, more importantly, it would not play a significant role in the biomechanics of the implant in the early stages. Hence, this approximation is considered negligible. Overall, the article shows that this technique presents a high outcome of satisfaction between the patients of 78% considering a good and excellent outcome (meaning occasional pain and no pain with no interference at work respectively).

Concerning the designing in SolidWorks environment, we took the fractured vertebra model of 0.5 mm fracture as the starting point of our assembly. We know that the surgeon usually closes the gap of the fracture once the screw is placed. Therefore, we reduced it from 0.5 mm to 0.1 mm which can be considered a negligible gap that could mimic effectively the gap closure procedure. The new vertebra will be coupled with a screw, designed to replicate the Buck screw. The length of the screw was chosen such that the screw would cross the pars defect completely avoiding the perforation of the upper pedicle. Hence, a 30 mm length screw, which corresponds to the standard length used in this technique, was created. The diameter of the screw was chosen to be 4 mm since the articles we reviewed and discussed previously had a diameter ranging from 3.5 mm to 4.5 mm. The next Figure shows the screw design:

Figure 30: Buck screw

Now, in the Assembly module, we combine the vertebra and the screw taking into account the procedure mentioned above. The tool used to perform the combination between the vertebra and the screw once it is positioned properly is called Cavity. This feature present in SolidWorks allows creating a hole that will resemble perfectly the shape of the object inside the main one selected (i.e., in this case, the cavity will have the same shape of the screw). In the following two Figure we are going to show the front view of our assembly:

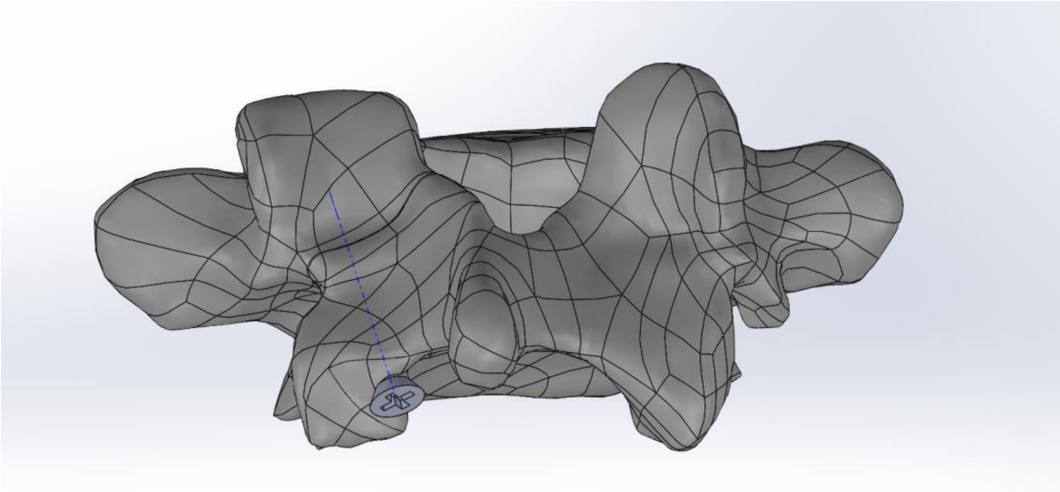

Figure 31: Buck technique assembly front view

This assembly is then imported into Ansys Workbench where, as done in the previous simulations, the same boundary conditions and load conditions where applied at the same faces of the vertebra. The faces of the crack were assigned as frictional contact as in the fractured vertebra previously performed. We decided to put the screw contact with the surrounding vertebra bone as bonded since no separation or slippage is allowed to happen between these two bodies. Considering our new body, the screw, we assigned the material properties as Titanium Medical Grade and in particular a common Titanium Alloy: Ti6Al4V. The Young Modulus was assigned as 114 GPa and the Poisson's Ratio equal to 0.31. The final model is meshed with 11451 tetrahedron elements and 20621 nodes

The output of our analysis will involve, as done before, the Von Mises Stresses, Strains and the Total Deformations that are shown below:

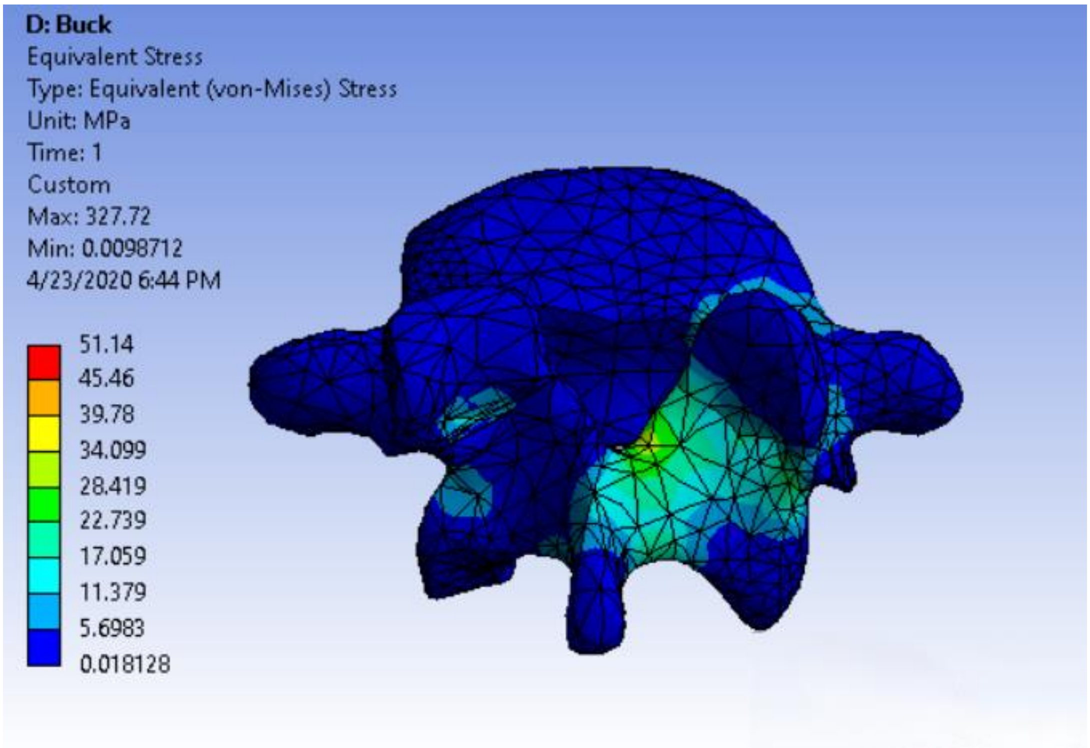

Figure 32: Buck stresses distribution on vertebra

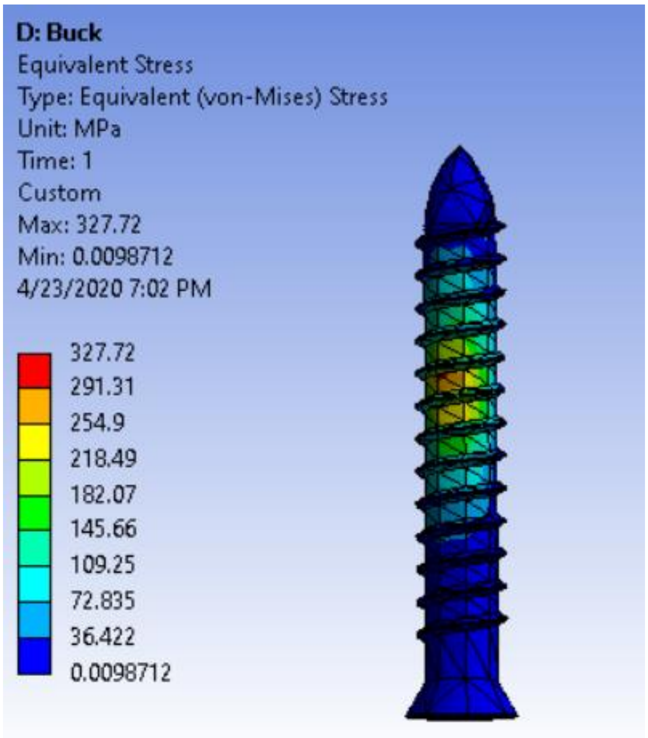

Figure 33: Buck stresses distribution on screw

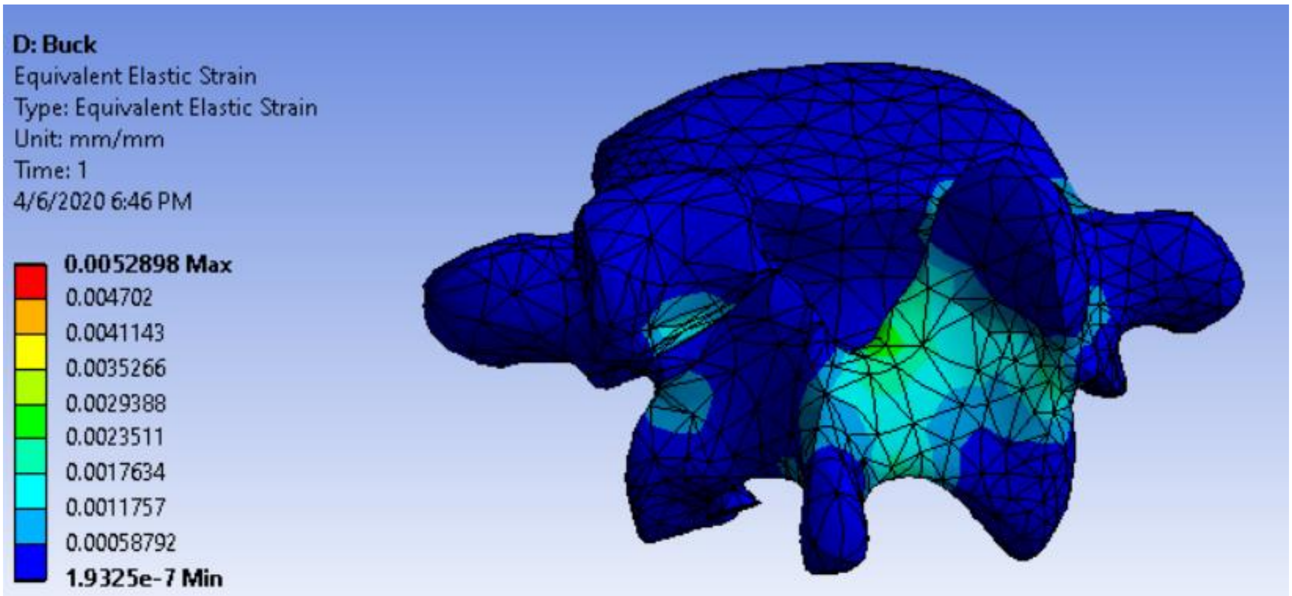

Figure 34: Buck strain distribution on vertebra

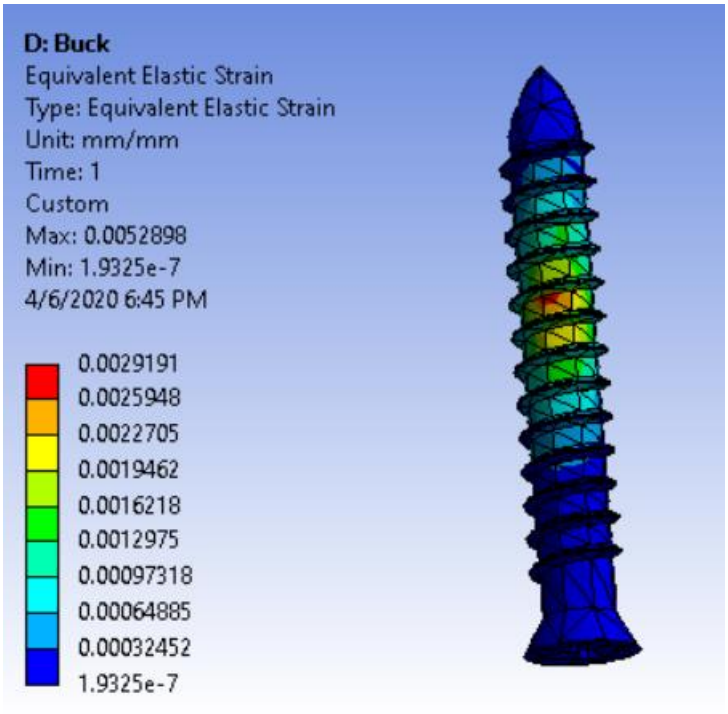

Figure 35: Buck strain distribution on implant

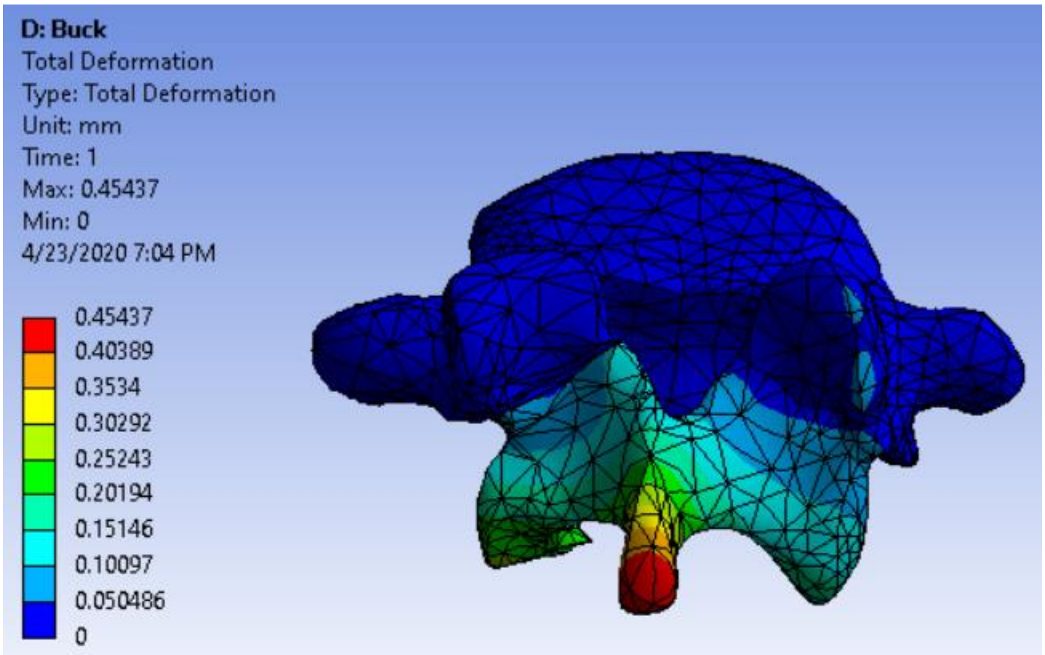

Figure 36: Buck deformation, complete assembly

Regarding the stresses, as we can see from the Figures above, we can see that we split the screw from the vertebra since the stresses on the screw are so high that the one on the vertebra would have been "masked" and resulted as only blue colour. Therefore, we adjusted the stresses hiding the screw and we found the stresses acting on the vertebra only. The stresses on the screw are concentred mainly in the region corresponding to the crack region of the vertebra, this is reasonable since the two faces of the crack will tend to slide to each other and hence the screw will try to contrast this movement. The maximum stresses reached on the screw are 327.72 MPa. For the same rationale, the strain analysis is split into two part, the screw and the vertebra, to understand completely the "real" values acting on each component. Differently, the deformation of the total assembly can be shown in one Figure since they are of the same order. In this case, we can represent the vertebra stresses with the threshold below the red colour as 10 MPa as previously done in order to have a general idea if the stress distribution has changed more similarly compared to the intact one:

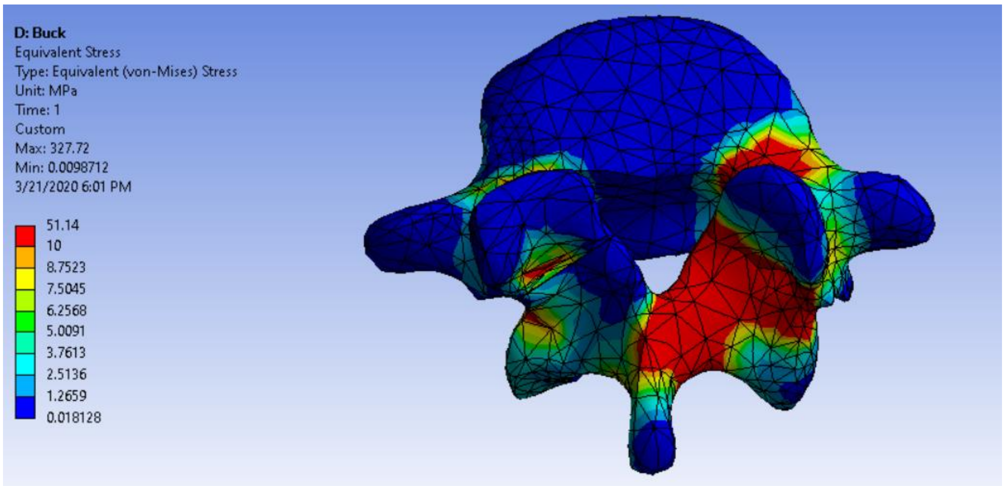

Figure 37: Stress contour of Buck assembly, threshold at 10 MPa

As we can see from the Figure above, it is clear to see that, differently from Figure 27 and similar to Figure 28, we have stresses above 10 MPa on the left pedicle and in the area of the left pars interarticularis, above the fracture and in the area below the fracture where the lower left facet joint starts. Also, other areas around the left pedicle have non-null stresses which are more similar to the intact vertebra case. Another fact worth noticing is that the area with higher stresses on the right pedicle is less wide compared to the one in the fractured vertebra and hence a more physiological stress distribution is obtained. The next table shows the stresses expressed in MPa on the vertebra only:

Maximum [MPa]	51.14
Minimum [MPa]	1.81 e-002

TABLE IV: COMPARISON OF THE MAXIMUM AND MINIMUM STRESSES ON THE VERTEBRA IN THE BUCK TECHNIQUE, EXPRESSED IN MPA

Since the analysis is performed considering also the screw, we cannot obtain the average value of stresses acting on the vertebra only. As expected, the maximum stress acting on the vertebra should decrease since the implant will take part in the stresses and the maximum gets closer to the normal situation of the intact vertebra. Another fact that we should take into account is that the maximum will be found in the canal of the screw inside the vertebra and not on the surface, so the higher stresses are due to the contact between the screw and the vertebra and on the surface we are going to see stresses that won't exceed 35 MPa, which corresponds to the maximum stress registered in the intact vertebra. As done with the fractured vertebra, the next Figure shows the probed values of stresses:

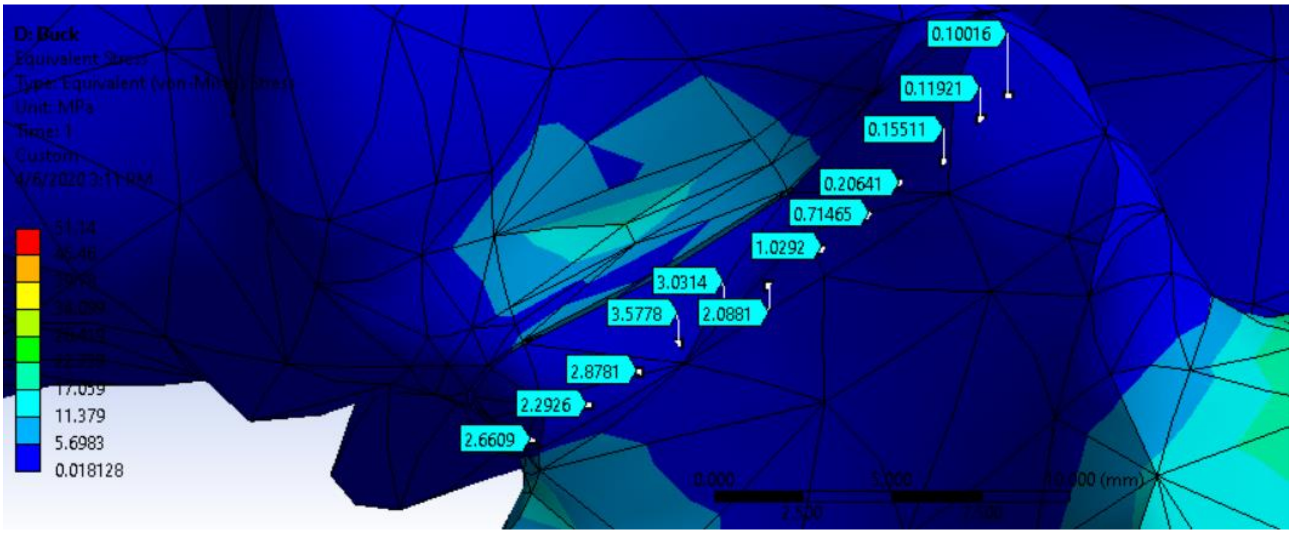

Figure 38: Values of stress in proximity of fracture, Buck technique

The values range from 0.1 to 2.66 MPa going from the medial to the lateral side respectively. As we can see, the values are significantly higher with respect to the fractured situation, since the implant allows the stresses to be transferred to the upper side of the vertebra. In the lateral sides, the value reached is more than ten times higher if compared to the lateral value found in the fractured model. The values of the stresses, differently from the deformations, are almost zero as we get closer to the fracture location. Hence, the surrounding values are influenced and this is the reason why get a value close to zero on the medial side. Another fact worth noticing is that the screw is closer to the lateral compared to the medial side, hence the propagation of stresses will be higher on that side and lower as we go in the centre if we compare to the fractured vertebra. The screw passing through the faces of the crack allows the propagation of the stresses also in the upper part of the crack and hence the values in the middle are lower if compared to the fractured vertebra.

If we analyse the strains, we can see that the values are propagating in the superior left articular facets, thanks to the screw insertion that allows the transmission of the load. The strains on the screw are concentred almost in the same region corresponding to the stress (i.e. the crack region of the vertebra) since the two sides of the crack will tend to slide with respect to each other and hence the screw will try to contrast this movement. The maximum strain reached on the screw is 2.91 e-003 mm/mm. We can represent, as done before, the vertebra strains with the threshold below the red colour as 0.0025 mm/mm as previously done in order to have a general idea if the strains distribution has changed in a more similar way compared to the intact one. The results are shown in the following Figure:

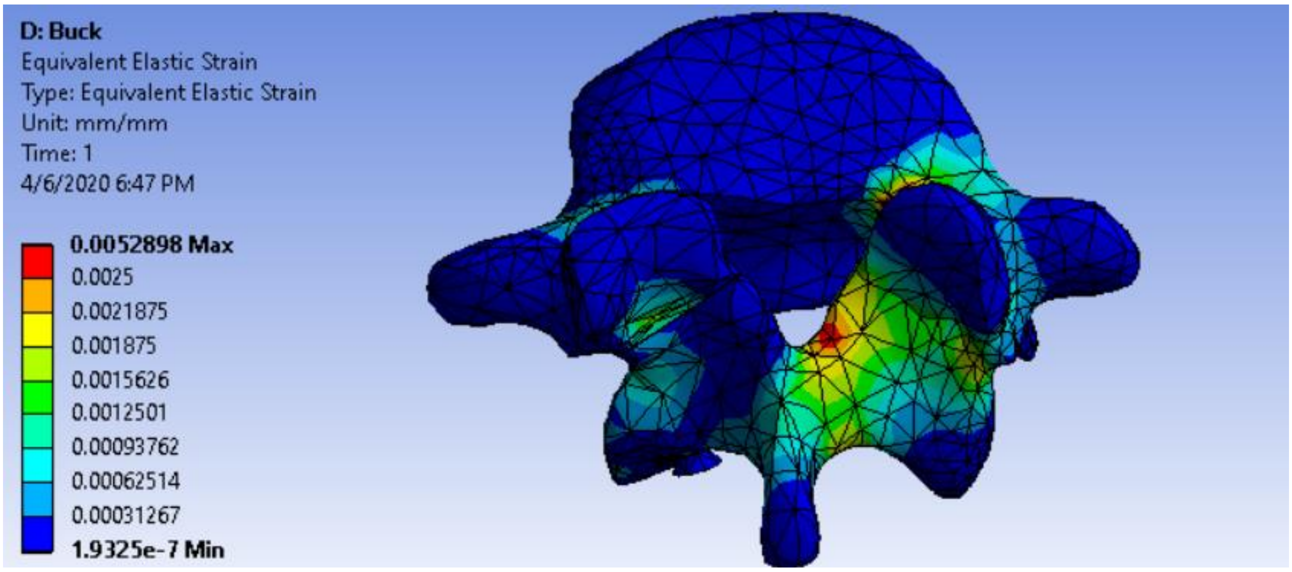

Figure 39: Strain contour of Buck assembly, threshold at 0.0025 mm/mm

The strains reached in the Buck scenario are more similar to the intact vertebra since we have a propagation of stresses also in the area of the left pars interarticularis, the left superior articular process and the lower left part of the lamina. In the Figure is also clearly visible that the strains above the 0.0025 mm/mm are constrained to a limited region in the central lamina and the right pedicle. This represents a significant improvement in the strain distribution compared to fractured vertebra analysis.

The next table shows the strains expressed in MPa on the vertebra only:

Maximum [mm/mm]	5.28e-003
Minimum [mm/mm]	1.93e-007

TABLE V: COMPARISON OF THE MAXIMUM AND MINIMUM STRAINS ON THE VERTEBRA IN THE BUCK TECHNIQUE, EXPRESSED IN MM/MM

Since the analysis is performed considering also the screw, we cannot obtain the average value of strains acting on the vertebra only. As expected, the maximum value of strain acting on the vertebra should decrease since the implant will take part of the strain and the maximum gets closer to the normal situation of the intact vertebra. The strains decreased by about 30% to the fractured scenario and increased by 76.58% to the intact case.

As done with the fractured vertebra, the next Figure shows the probed values of strains:

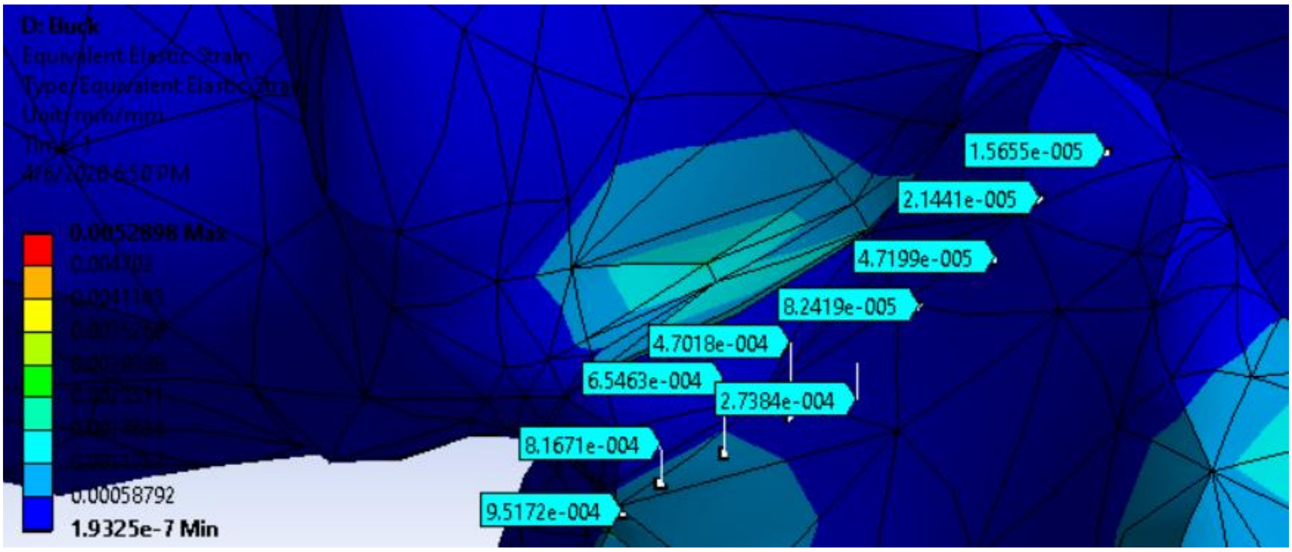

Figure 40: Values of strain in proximity of fracture, Buck technique

The values range from 1.56e-005 to 9.51e-004 mm/mm going from the medial to the lateral side respectively. These values are overall similar in the centre compared to the fractured vertebra, while they are lower on the medial and higher on the lateral side.

Concerning the deformations the next table shows the maximum, minimum and average value expressed in mm

Maximum [mm]	0.45
Minimum [mm]	0
Average [mm]	6.32e-002

TABLE VI: COMPARISON OF THE MAXIMUM, MINIMUM AND AVERAGE DEFORMATIONS IN BUCK MODEL, EXPRESSED IN MM

As we can see from Table VI, the maximum deformation reached is almost twice higher than the intact vertebra value and 55% lower than the fractured one. This was expected since the screw should diminish the deformations of the crack and this results in obtained in a significant way. Regarding the average value, we can still see that the value is still way higher than the one registered in the intact one, slightly more than two times higher. Hence, in terms of deformations, this implant improves the distribution of the values but still is not satisfactory.

As done with the fractured vertebra, here is the Figure with the probed values of deformation in the proximity of the fracture:

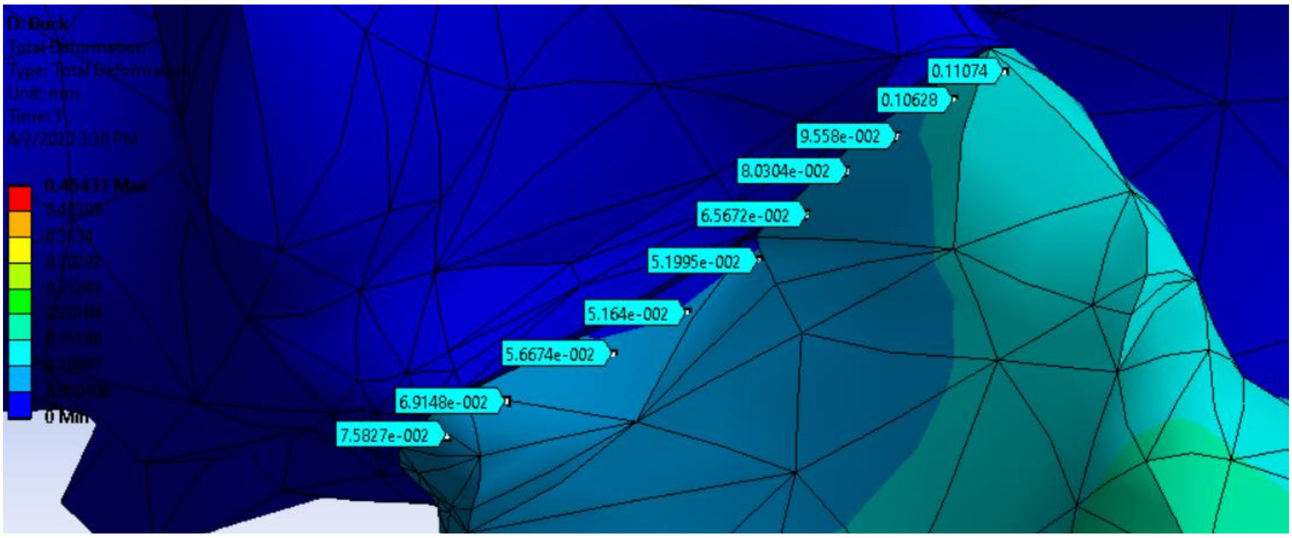

Figure 41: Values of deformation in proximity of fracture, Buck technique

The values range from 0.11 to 7.58e-002 mm going from the medial to the lateral side respectively. As we can see, the values are significantly lower with respect to the fractured situation, since the implant tries to limit the motion of the sides of the fracture.

3.2 Hook-Screw technique

The Morscher technique was first introduced by *Morscher et al*[37] and it consisted in a laminar hook and a screw. The hook would follow the shape of the lower edge of the lamina and anchor the Hook-Screw system to the vertebra. The screw is positioned differently compared to the Buck condition since the screw goes directly inside the base of the superior articular process. This methodology still had some issues, such as facet joint violation and problems associated with patients with a thin lamina. Hence, this method evolved maintaining its principal component, but with a different design [60], [61]. This method represents what now is considered the state of art for this technique: the hook is placed in a similar way compared to the original position, but the screw now is inserted in the ipsilateral pedicle with respect to the pars defect. The screws go in the space between the connection of the transverse process and the superior facet, in order to fit perfectly in the pedicle. A rod connects these two parts. From now on, we are going to refer to this technique as the Hook-Screw technique. The material used for each part is the same used for the screw in the Buck technique (i.e. Ti6Al4V). The advantages of the evolution of this technique rely on the fact that the pedicle screws are easier to be inserted, the failures of the devices decreased and the patient does not require postoperative immobilization[36].

Concerning the design in SolidWorks, we first designed the Hook-Screw system in order to fit perfectly on the vertebra. The rod connecting the screw and the hook has a diameter of 4.5 mm and a length of 41 mm, the screw has a length of 31 mm and a diameter of 4 mm. The length of the screw was made such that it passes through the entire pedicle to guarantee the best support and attachment. We made the hook trying to mimic the literature examples[60], [61], but most importantly to fit the shape of our vertebra and guarantee a proper anchorage on the lamina. The final Hook-Screw hardware has the following shape:

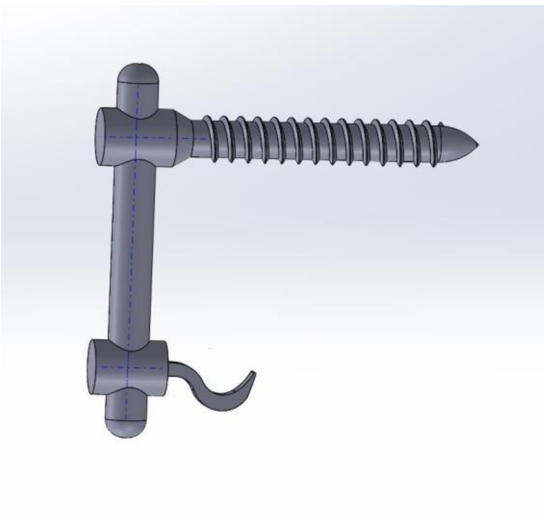

Figure 42: Hook-Screw hardware, lateral view

In the Assembly module, we finally assembled the Hook-Screw hardware and the vertebra to obtain the final assembly showed in the next Figure:

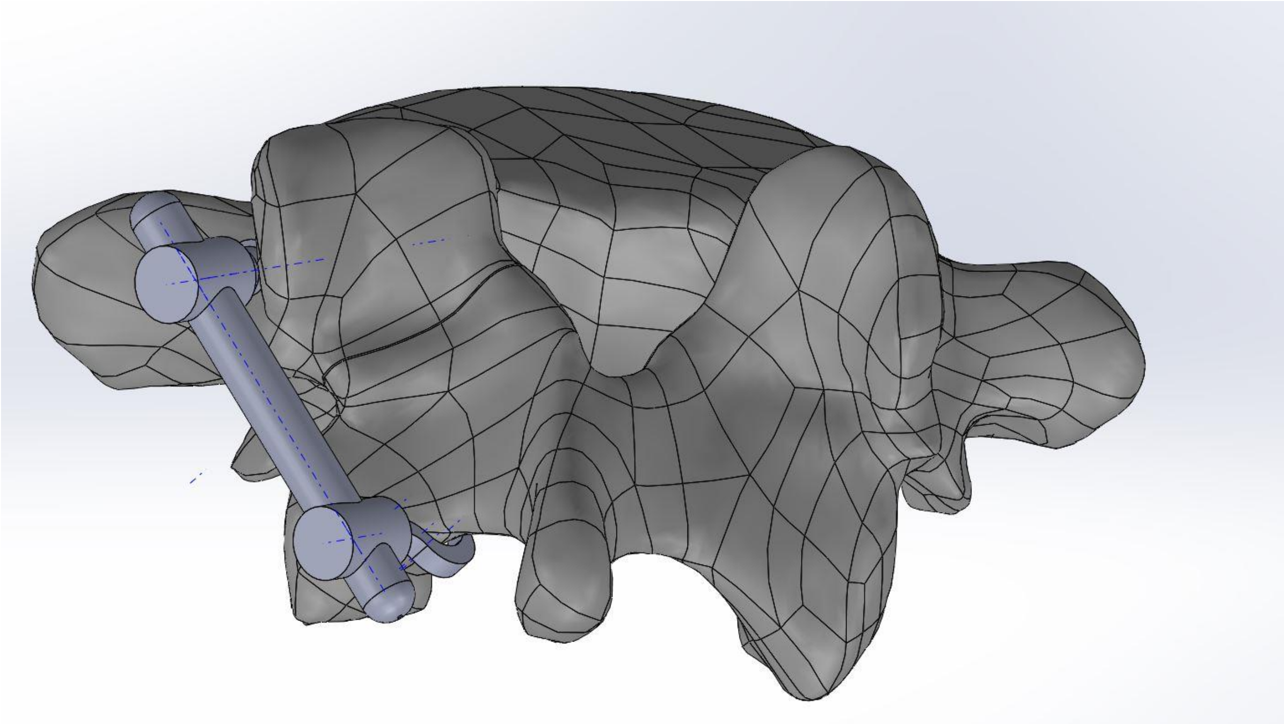

Figure 43: Hook-Screw-vertebra assembly, front view

As performed with the other methods, the crack has been reduced from 0.5 mm to 0.1 mm in order to simulate what the surgeon performs in reality. As already stated previously, the material assigned for the Hook-Screw hardware are the same of the buck screw and they were imported in Ansys Workbench. The contact boundaries were similar compared to the Buck technique since the rod connecting the screw and the hook had a bound condition to simulate the fact that both the screw and the hook could not detach from the rod. The faces of the crack that could come into contact were treated as frictional. The hook and the screw were simulated as bonded since they are both not supposed to separate or slide with respect to their original position. The boundary conditions are the same as the previous simulations with the lower and upper surface of the vertebral body fixed rigidly without the possibility of rotation or translation and the force of 500N was applied in the vertical direction (z-direction) as showed in Figure 20. The final model is meshed with 15832 tetrahedron elements and 26896 nodes. Thus, the Equivalent Stresses, Strain and Total Deformation were requested as the output of our static analysis. The following Figures represent the equivalent stresses and strains acting on the vertebra, on the Hook-Screw implant and the total deformation on the total assembly (i.e. Hook-Screw implant + vertebra):

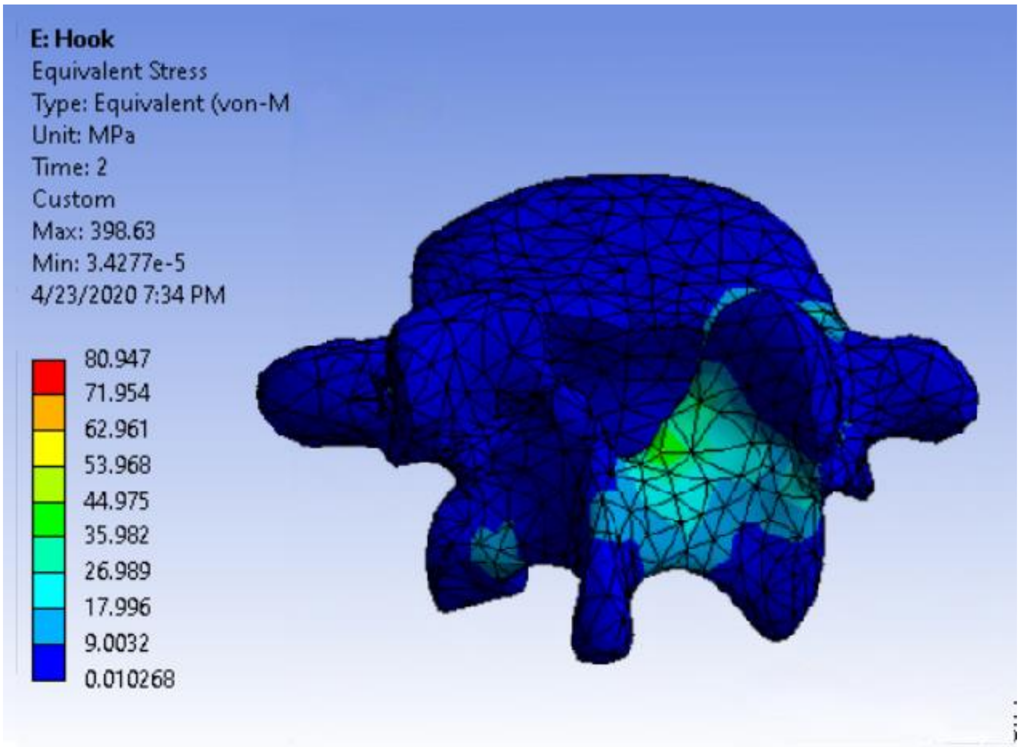

Figure 44: Hook-Screw system stresses distribution on vertebra

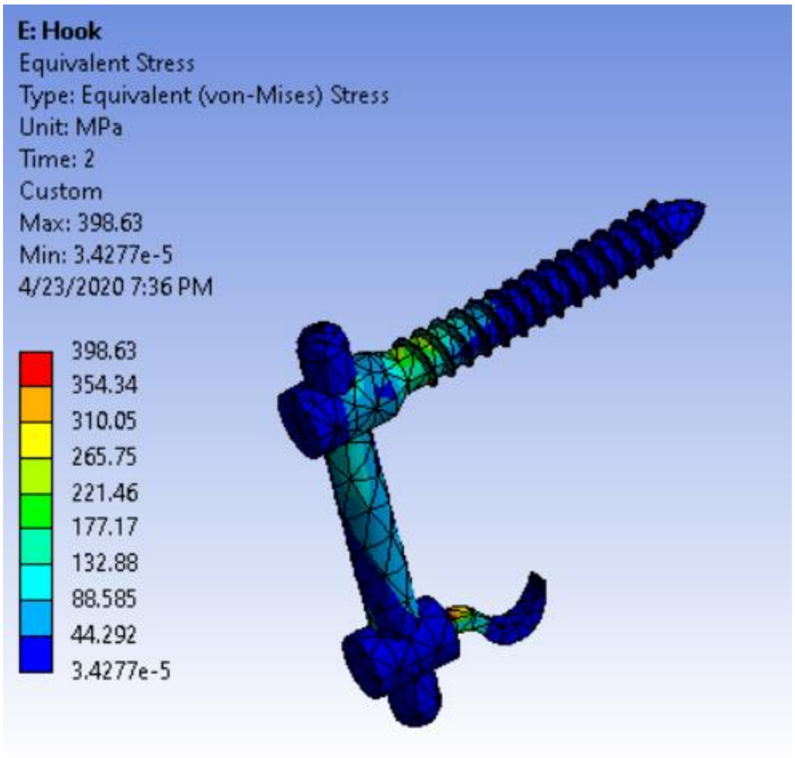

Figure 45: Hook-Screw system stresses distribution on implant

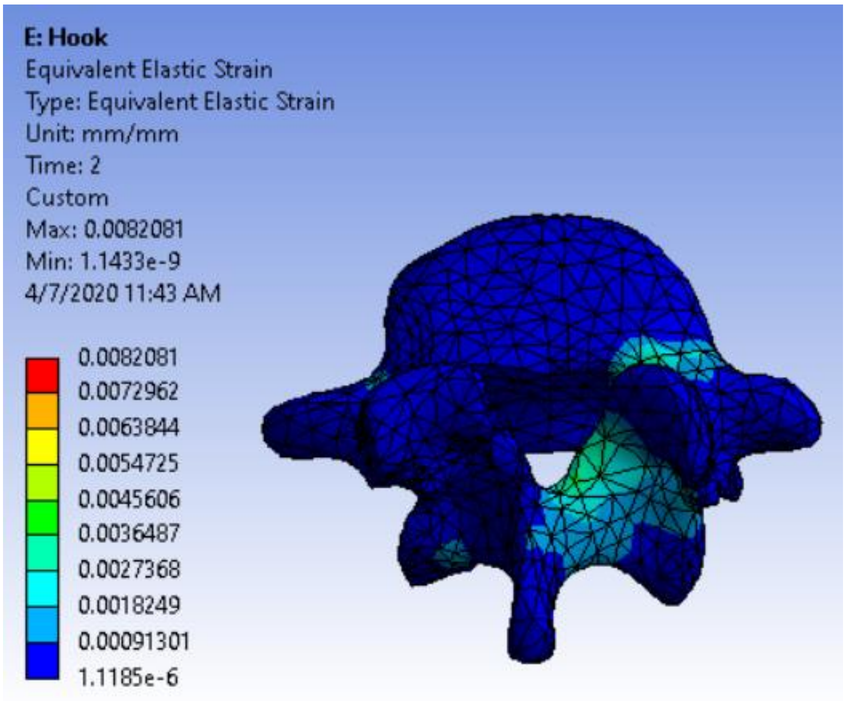

Figure 46: Hook-Screw system strains distribution on vertebra

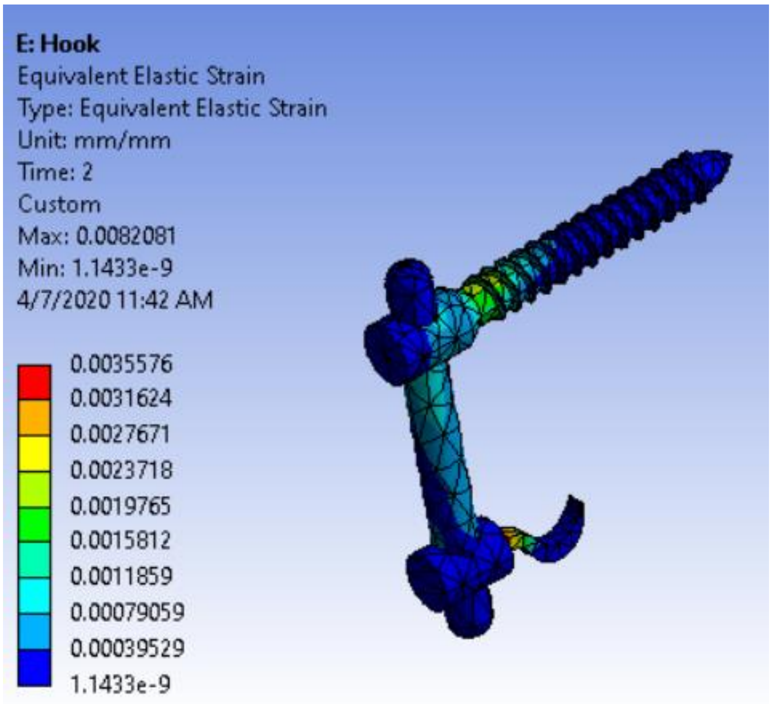

Figure 47: Hook-Screw system strains distribution on implant

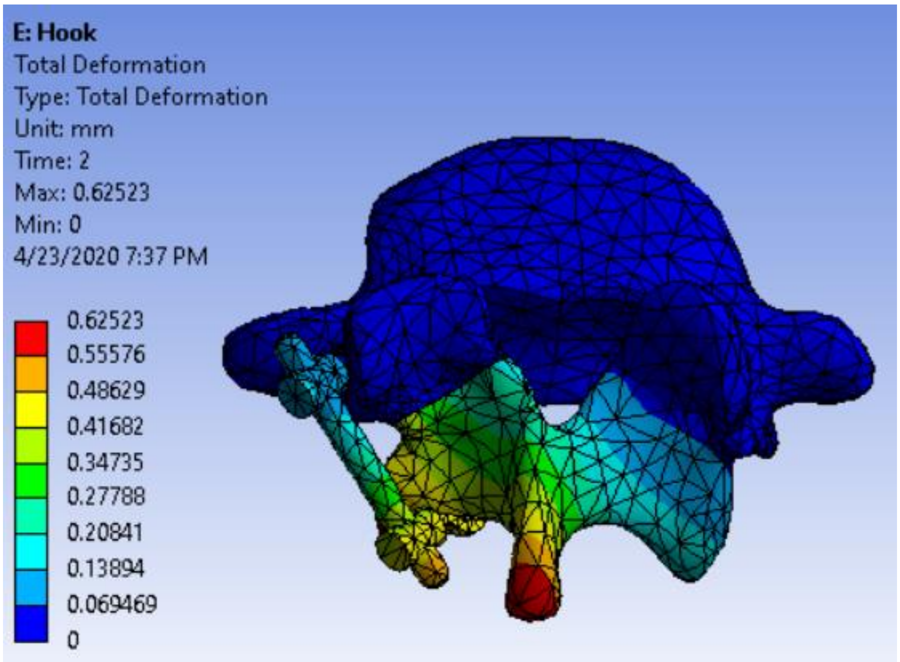

Figure 48: Hook-Screw system deformations

As we can see from the Figures above, we chose to separate the vertebra from the implant in order to have a better understanding of the stresses acting on the vertebra. This time the stresses on the implant concentrate mainly on the hook base and the screw base. This result is coherent with the fact that these are the parts that press on the hole of the vertebra and the base of the lamina when the force is applied. The stresses reached by the implant are 398.63 MPa at the base of the hook, where it is connected to the rod.

As done in the other cases, we can represent the vertebra stresses with the threshold below the red colour as 10 MPa in order to have a general idea if the stress distribution has changed more correspondingly compared to the intact one:

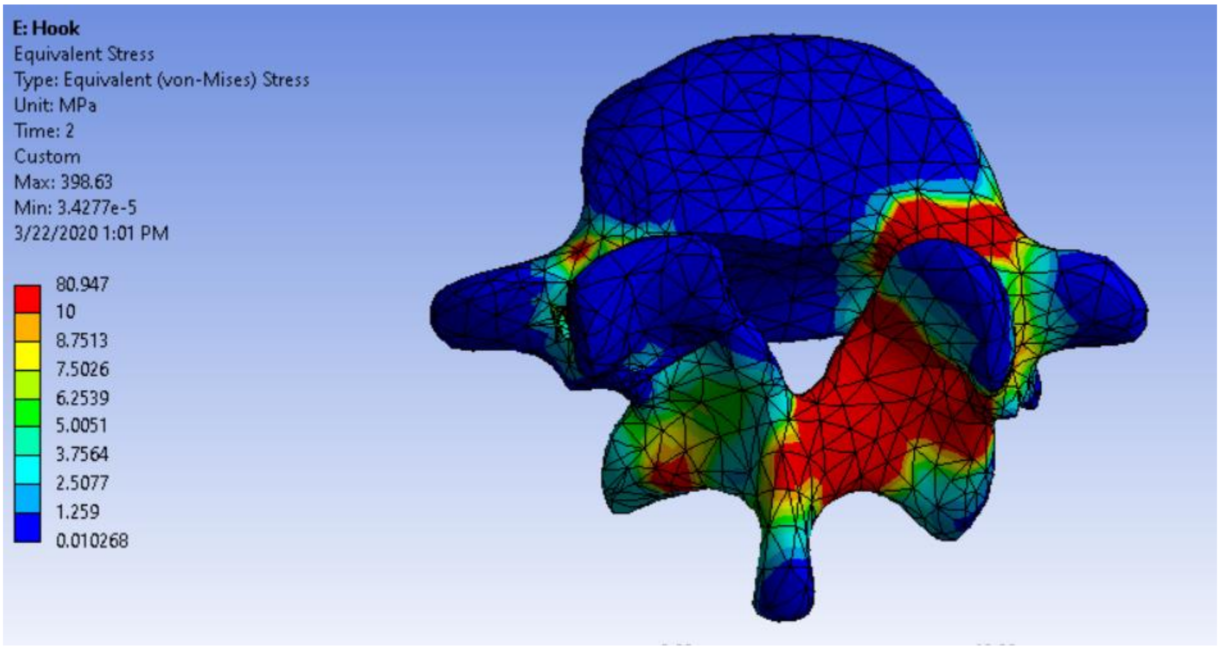

Figure 49: Stress contour of Hook-Screw assembly, threshold at 10 MPa

Figure 52 shows that the stresses distribution of the hook propagates in both pedicles, with a higher propagation in the right one, and propagation in the lower edge of the lamina due to the hook contact that propagates towards the crack of the pars interarticularis. This situation is still similar to a stress distribution to the intact vertebra, but the stresses reached are higher compared to the Buck method and intact vertebra. The next table shows the stresses expressed in MPa on the vertebra only:

Maximum [MPa]	80.94
Minimum [MPa]	1.02 e-002

TABLE VII: COMPARISON OF THE MAXIMUM AND MINIMUM STRESSES ON THE VERTEBRA IN THE HOOK-SCREW TECHNIQUE, EXPRESSED IN MPA

Since the analysis is performed considering also the Hook-Screw hardware, we cannot obtain the average value of stresses acting on the vertebra only. As expected, the maximum stress acting on the vertebra should decrease since the implant will take part in the stresses and the maximum gets closer to the normal situation of the intact vertebra. Another fact that we should take into account is that the maximum will be found in the canal of the screw inside the vertebra. Another remarkable difference in the stress distribution compared to the intact and the Buck case vertebra is that if we plot the stresses with a 35 MPa threshold, which was the maximum registered in the intact vertebra, differently from Buck where the stresses were only in the screw canal, the stresses reach values above 35 MPa in the counter lateral pars interarticularis. The next Figure represents visually what we described in the latest analysis:

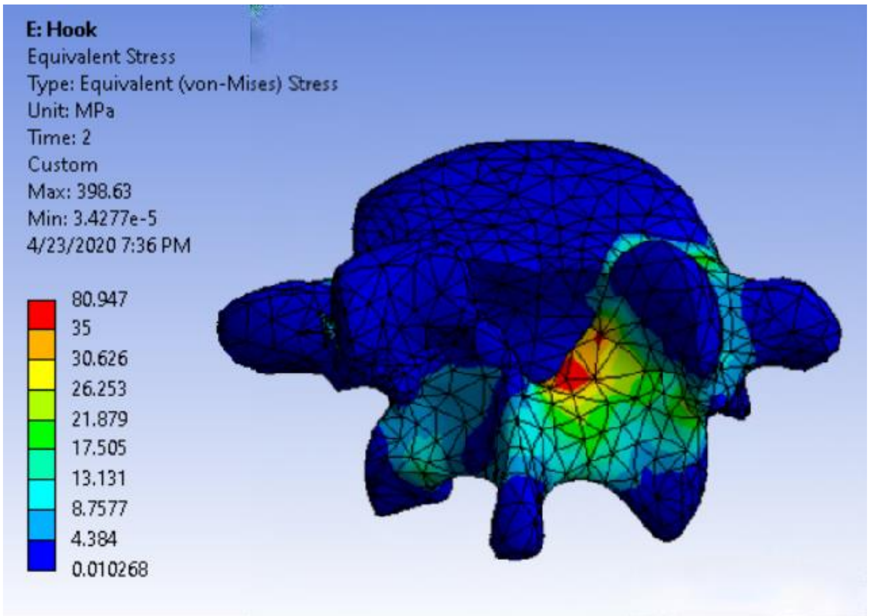

Figure 50: Stress contour of Hook-Screw assembly, threshold at 35 MPa

Hence, from a stress point of view, taken into account all the hypothesis and the limitations of our analysis, it seems that the Buck technique would have a better stress distribution since the stresses spread in other areas, with a distribution more similar to the intact part of the vertebra and the maximum reached is lower compared to the Hook-Screw technique with maximum reached only in the area in contact with the screw. A higher concentration of stresses would inevitably lead to a higher probability, over time, to generate an initiation of another fracture in the remaining intact pars. Another fact worth noticing is that the stresses considering the implant are way higher in the Hook-Screw method compared to the Buck technique, about 22% more. This could create an excessive decrease of stresses on bone, leading to his resorption and hence, increasing the stresses in the implant more and not healing the fracture properly.

The values of stresses probed in proximity of the crack are showed in the following Figure:

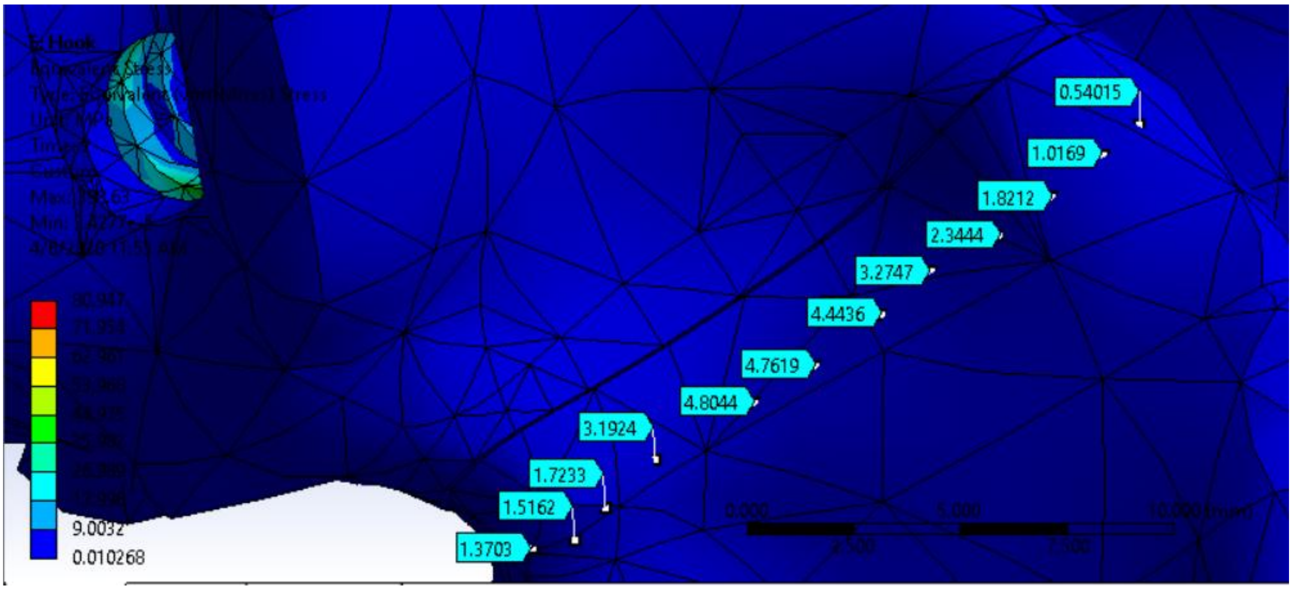

Figure 51: Values of stress in proximity of fracture, Hook-Screw technique

The values of the stresses reach a value of 1.37 and 0.54 MPa on the lateral and medial side respectively. This could be explained knowing that the stresses are not able to propagate on the other side of the crack, as done in the Buck case. However, in the central part, the stresses on the vertebra seem to be higher compared to Buck and hence this results in better stimulation of the bone in the area around the crack.

Differently from the Buck scenario and more similar to the fractured vertebra, the strains are concentrated mainly in the right pars interarticularis and right pedicle. We can see that the strains in the implant are found, similarly to the stresses, on the base of the hook and where the screw is inserted in the pedicle. The maximum value of strain reached in the implant is 3.55e-003 mm/mm, almost 22% higher compared to the Buck implant. The next Figure shows the strain representation with a threshold of 0.0025 mm/mm to see and understand how the strain distribution has changed:

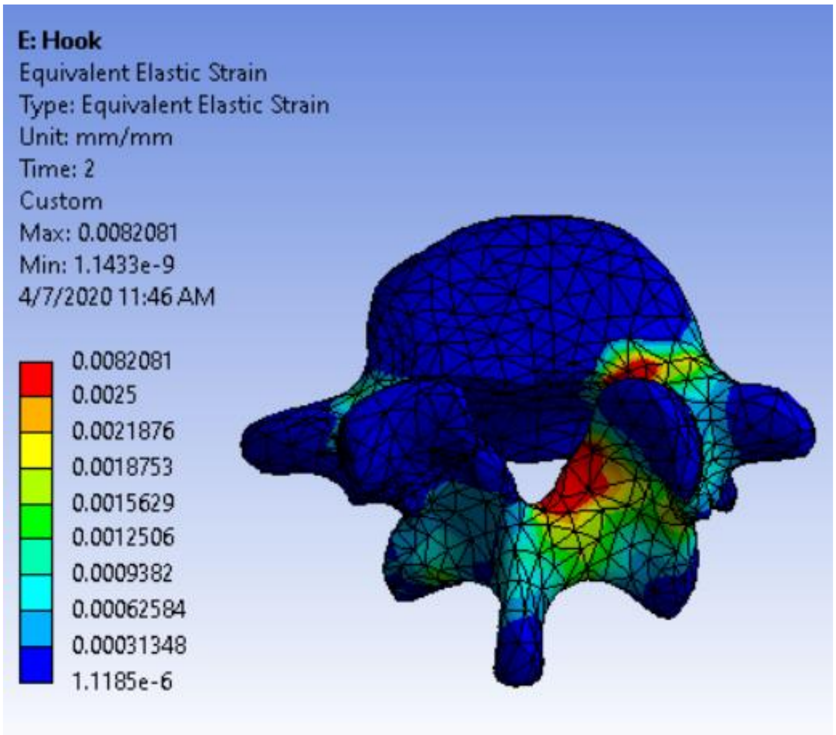

Figure 52: Strain contour of Hook-Screw assembly, threshold at 0.0025 mm/mm

Compared to the Buck technique, the strain area that exceeds the threshold is wider. We can see that it goes from the base of the spinous process to the part of the lamina where it merges with the superior articular facets. Most importantly, the region of the upper left articular process has strains close to zero, while the Buck technique, in the same area, has higher strains. Looking at the vertebra in the Hook-Screw technique, we can see that it is similar in terms of strain distribution to the fractured vertebra without implant in Figure 30.

The next table shows the strains expressed in mm/mm on the vertebra only:

Maximum [mm/mm]	8.20e-003
Minimum [mm/mm]	1.11e-006

TABLE VIII:COMPARISON OF THE MAXIMUM AND MINIMUM STRAINS ON THE VERTEBRA IN THE HOOK-SCREW TECHNIQUE, EXPRESSED IN MM/MM

If we compare the above values with the one found in the previous analysis, we can see that the maximum strain reached is the highest found so far. This behaviour was also found in the stresses comparison. The maximum value is 55% higher with respect to the previous technique and 10% if compared to the fractured vertebra without an implant.

As done before, the next Figure shows the probed values of strains:

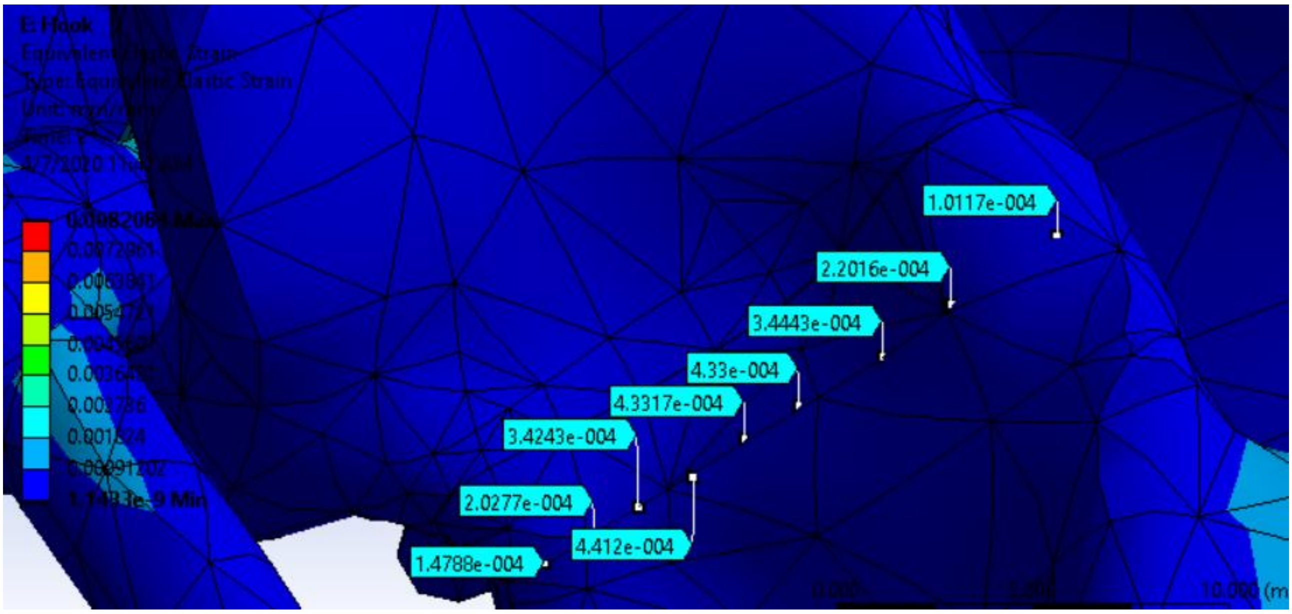

Figure 53: Values of strain in proximity of fracture, Hook-Screw technique

The values range from 1.01e-004 to 1.47e-004 mm/mm going from the medial to the lateral side respectively. These values are overall lower compared to Buck and the fractured scenario, going from medial to lateral. This could be due to the fact that, compared to the Buck technique, the implant does not pass through the faces of the crack directly and this does not allow the stresses and the strains to propagate. However, the value on the medial side is similar if compared to the previous technique, while they are lower on the lateral one.

Concerning the deformations, the following table shows the maximum, minimum and average value expressed in mm in the Hook-Screw model:

Maximum [mm]	0.62
Minimum [mm]	0
Average [mm]	5.08e-002

TABLE IX: COMPARISON OF THE MAXIMUM, MINIMUM AND AVERAGE DEFORMATIONS IN THE FRACTURED HOOK-SCREW MODEL, EXPRESSED IN MM

The maximum value reached by this technique is more than 2.5 times with respect to the one compared to the intact vertebra. Nevertheless, we know from the previous Figures of the deformations that this maximum is present in the area of the spinous process and hence due to the condition and direction of the loading, distant from the fracture line. Concerning the average value, we can see a reduction compared to the Buck technique and hence this method allows to get closer to the deformation behaviour we can find in the intact vertebra.

Considering the values in the proximity of the faces of the crack, the following Figures show the results obtained:

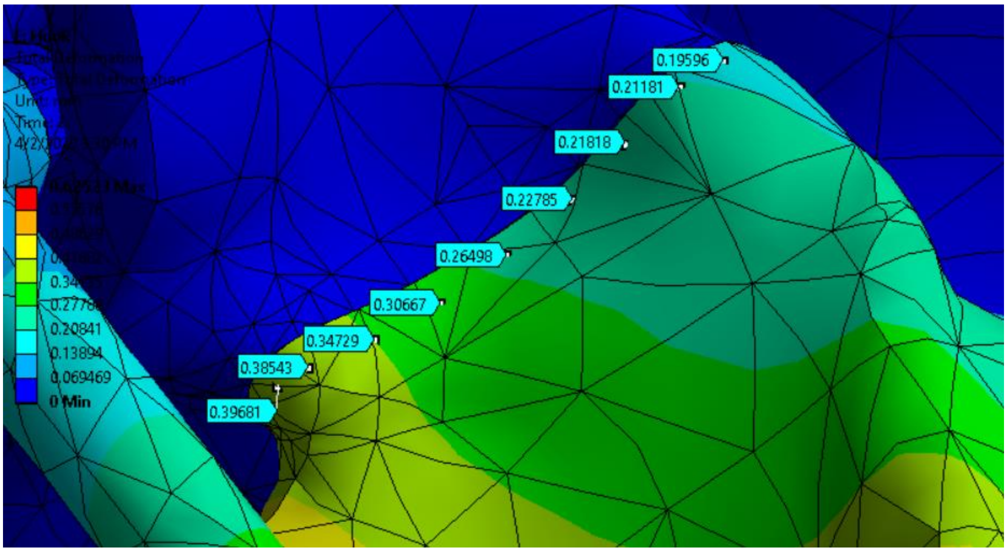

Figure 54: Values of deformation in proximity of fracture, Hook-Screw technique

The results obtained are almost half, both on the medial and the lateral side, compared to the fractured case without the implant. Nevertheless, even though the medial side values are somehow similar to what the Buck technique, 0.19 compared to 0.11 mm, the lateral side of the Hook-Screw technique is way higher compared to the Buck case, 0.39 compared to 7.58e-002 mm. We can hence assess that the Buck technique has better value in the proximity of the fracture for this particular analysis.

It is important to understand that the complex evaluation of an implant goes way beyond a stresses, strains and deformations analysis of the two implants because both methods are currently used commonly in the state of the art and several studies are underlying the pros and cons of each one. Most of the times, it is up to the surgeon’s choice to decide one method to another, based on the patient’s anatomy

CHAPTER 4

NEW DESIGN: ANALYSIS AND COMPARISON WITH EXISTING IMPLANTS

4.1 Implants design

The design concept was conceived and proposed in the UIC Biomechanics Research Laboratory by Professor Farid Amirouche. Starting from the previous results, the main idea was to keep the two entry points of the previous methods, respectively the lower point of entry from the Buck technique and the upper entry point form the Hook-Screw technique, and a plate was used to connect them. This plate idea has not been used before nor there is anything similar in use. To realize this innovative idea, we decided to design two similar plates with different curvature and see how the results are affected, not only with respect to each other but with the other two previous methods in general.

In SolidWorks environment, to connect the two screws, by first creating a rectangular section of 1.5 mm in width and then using the Boundary Boss feature we create a solid from the contours we have defined. The screw holes in the proposed plate were done in the aforementioned points since the curvature of the plate won't allow for additional holes that might contribute to the stability of the plate. The first plate was designed to be more curved and follow more the geometry and shape of the vertebra in order to avoid contact with many surrounding muscles or tendons. The second plate has a similar shape compared to the previous one, but the curvature is reduced. The choice of reducing the curvature relies on the possibility to try a different design and understand that an increase in the curvature would inevitably complicate the manufacturing processes that will be used to manufacture the implant in the future. The two following Figures below are used to show the two proposed plates designs with the screws already inserted, the lower screw will be used to go through the faces of the defect in order to immobilise the fracture and the upper screw will fix the implant with a pedicle cavity.

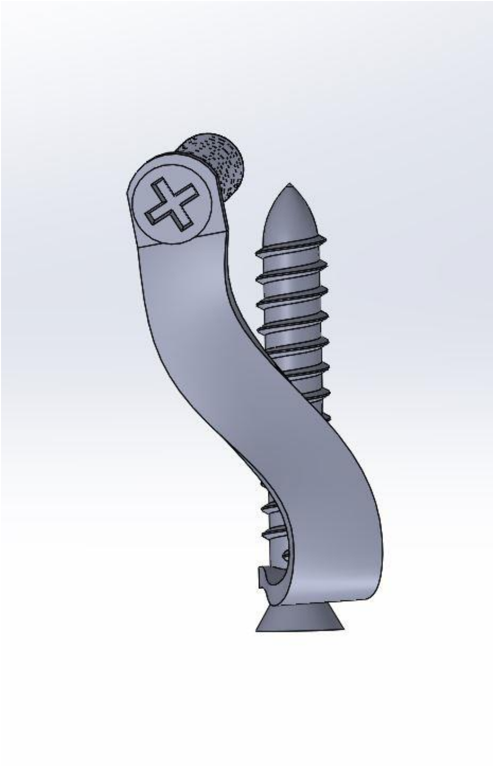

Figure 55: Plate 1 design, front view

Figure 56: Plate 2 design, front view

The two screws are shown on the L5 vertebra replicating the same positions obtained with the Buck and Hook-Screw with their respective screw position. As done in the previous cases, the screw shape inside the vertebra is performed through the Cavity feature. The fracture distance is reduced to 0.1 mm as the previous cases. The following Figures show the final assembly for Implant 1 and 2 respectively.

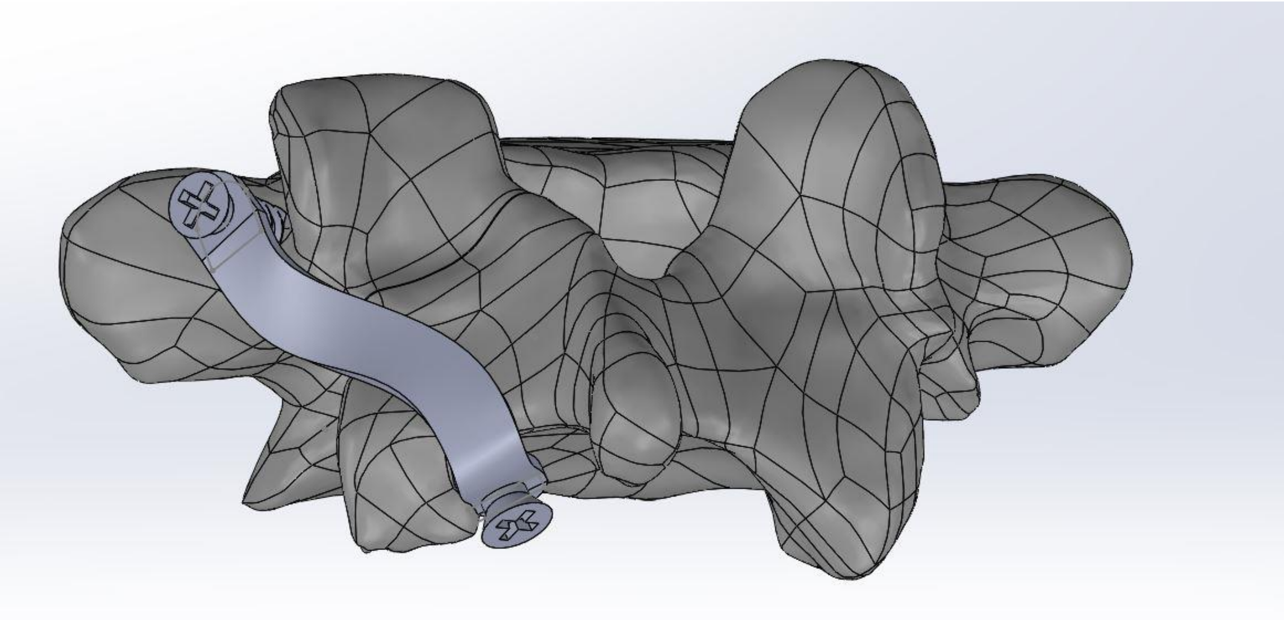

Figure 57: Implant 1 final assembly, front view

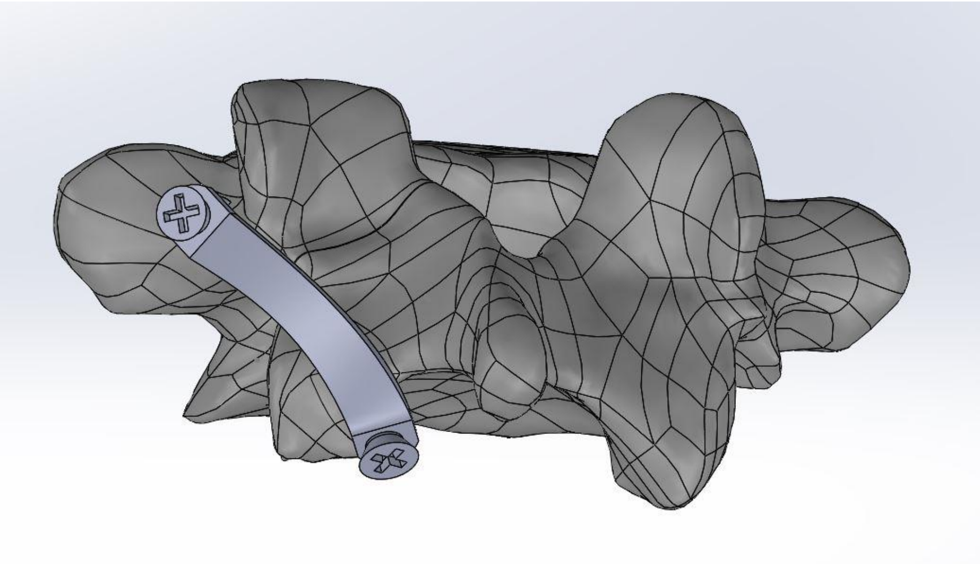

Figure 58: Implant 2 final assembly, front view

4.2 Implants simulation

Concerning the simulations in Ansys Workbench, the implant has the same material properties of the screws and all the other metallic components. The connection between the screws is the same used in their previous models respectively (upper screw Hook-Screw and lower screw Buck screw) since both screws are bonded to their surrounding bone. The connection between the screw and the plate is of course bonded since the screws are supposed to be fixed with no relative motion allowed. The same boundary and load conditions are used for each plate for the analysis.

The following Figures represent the stresses and strains acting on the vertebra with the implant 1 along with the deformations on the assembly Implant 1 + vertebra where the final model is meshed with 20581 tetrahedron elements and 37188 nodes:

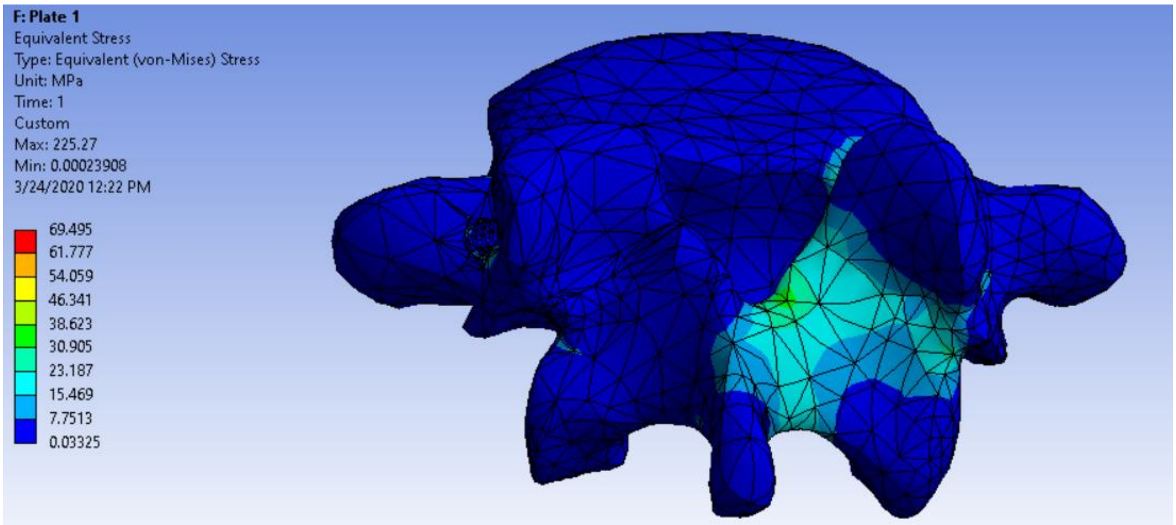

Figure 59: Implant 1 assembly stresses distribution on vertebra

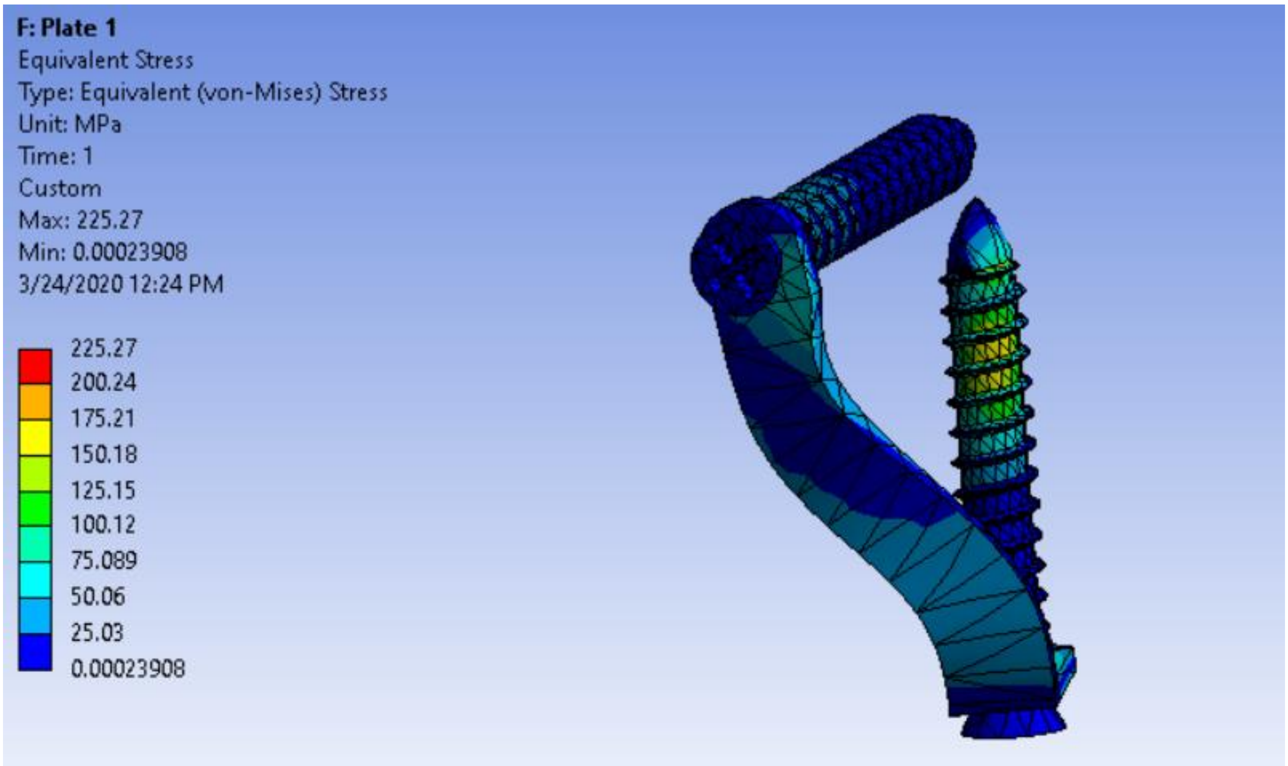

Figure 60: Implant 1 assembly stresses distribution on implant

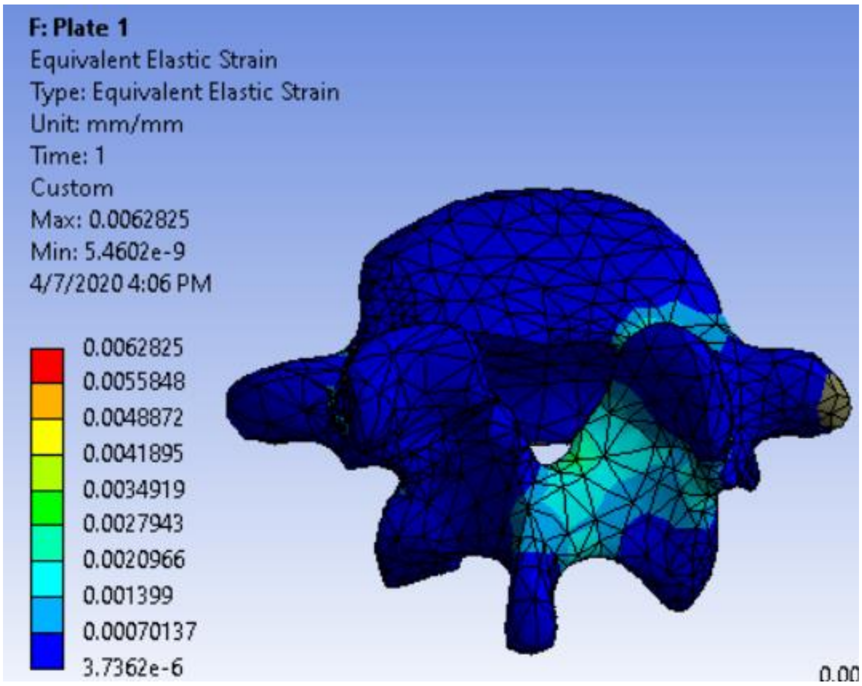

Figure 61: Implant 1 assembly strains distribution on vertebra

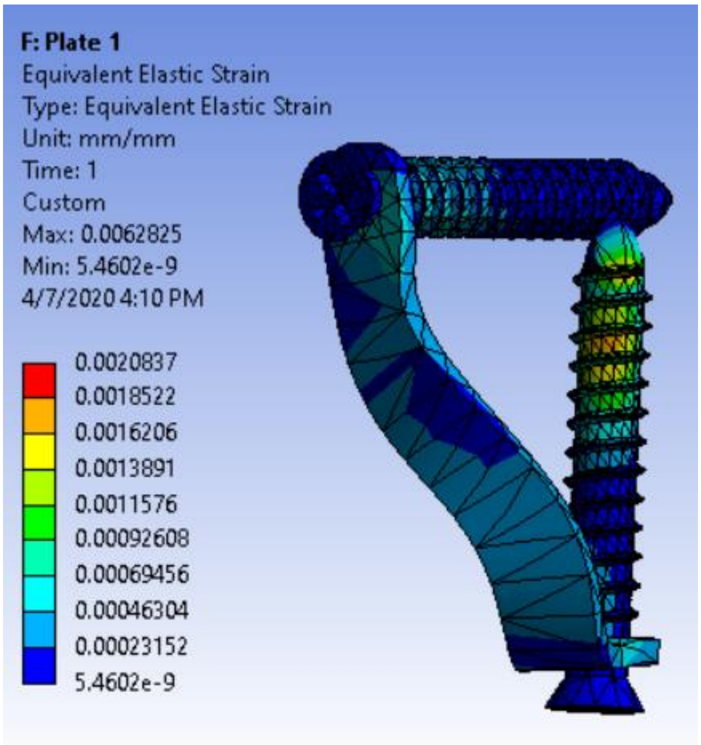

Figure 62: Implant 1 assembly strains distribution on implant

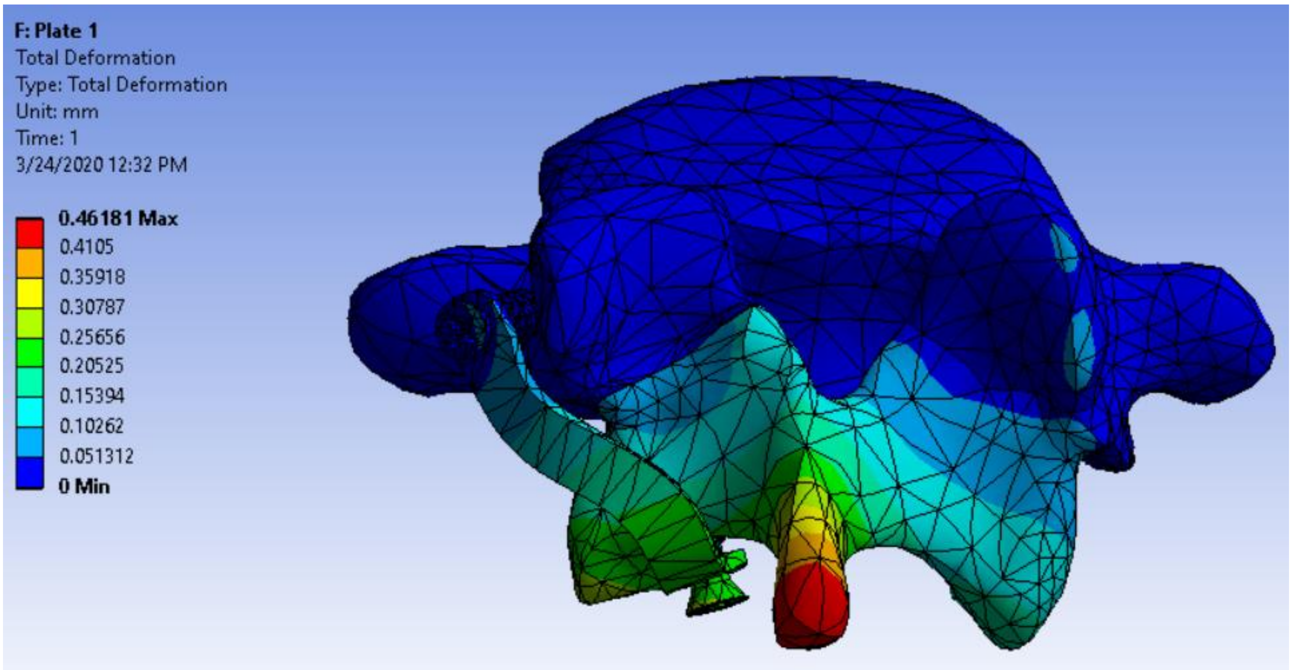

Figure 63: Implant 1 assembly deformations

As previously shown, we separate the vertebra from the implant to have a better understanding of the stresses acting on the first. As we can see, the stress concentration on the implant is on the lower screw, which keeps the two faces of the crack together. This result makes sense since we already saw a similar response in the Buck model. The stresses reached are 225.27 MPa in the aforementioned region of the implant.

As done in the other cases, we can represent the vertebra stresses with the threshold below the red colour as 10 MPa to have a general idea if the stress distribution has changed more similarly compared to the intact one:

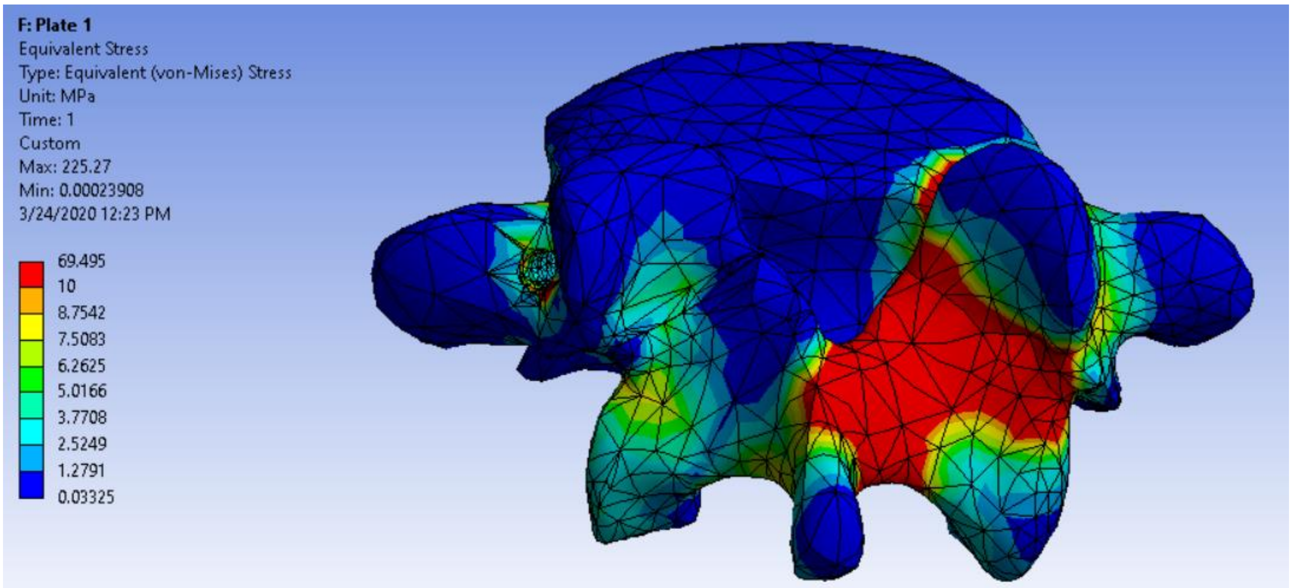

Figure 64: Stress contour of Implant 1 assembly, threshold at 10 MPa

Figure 65 shows that the stresses propagate smoothly in the left pars interarticularis both above and below the fracture. This stress distribution is similar to the one of the intact vertebra when all the areas of the lamina are under some stress in the pars interarticularis. We still can see a major part of the right lamina under stress above 10 MPa, but overall the stress distribution seems more similar to the intact vertebra.

The peak stresses reached by the vertebra are higher compared to the Buck method and intact vertebra, but lower if compared to the Hook-Screw method. The next table shows the stresses expressed in MPa on the vertebra only:

Maximum [MPa]	69.49
Minimum [MPa]	3.32 e-002

TABLE X: COMPARISON OF THE MAXIMUM AND MINIMUM STRESSES ON THE VERTEBRA IN THE IMPLANT 1 DESIGN, EXPRESSED IN MPA

Overall, the peak value is 36 % times higher than the Buck technique and 14% lower if compared to the Hook-Screw technique. The maximum value of stress is in the cavity created by the lower screw, where the two faces of the crack tend to slide.

If we show the stresses with a threshold at 35 MPa for the red colour interface, we obtain the following Figure:

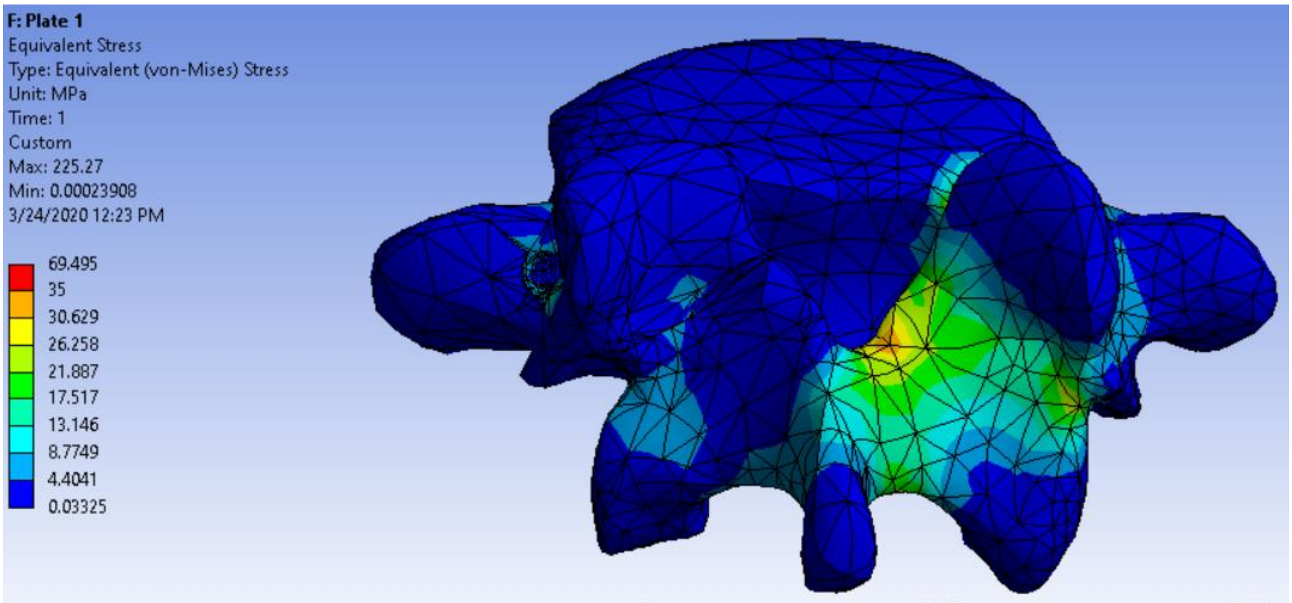

Figure 65: Stress contour of Implant 1 assembly, threshold at 35 MPa

As shown, we have no peaks above the set threshold on the surface of the vertebra, similarly to Buck scenario. The Hook-Screw, as previously shown, had a small area of stresses above 35 MPa at the base of the spinous process. Hence, we can see that this Implant solution has a better stress distribution compared to the Hook-Screw method.

Regarding the maximum stresses reached by the implant, the peak value of stresses is 45% and 77% lower compared to the Buck and Hook-Screw respectively. Since the stresses acting on the implant decreased with respect to the classical surgical technique, the probability of implant failure due to high stress concentration will decrease as well. On the other hand, the stresses on the bone increase, allowing bone growth and healing on the fracture site.

If we consider the values of stress in the proximity of the fracture, we can represent them as done before in the following Figure:

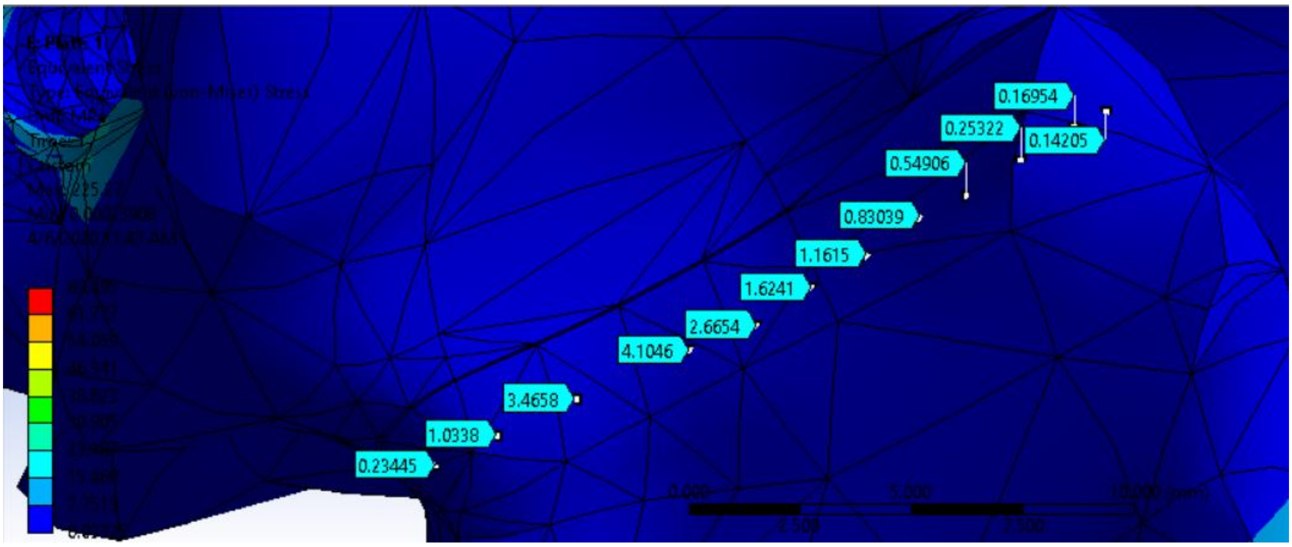

Figure 66: Values of stress in proximity of fracture, Implant1

The stresses value range from 0.23 to 0.14 MPa from the lateral to the medial side respectively. Compared to the Hook-Screw technique, the values reached are lower not only at the extremes but also in the middle. They are more similar to the Buck technique, particularly on the medial side.

Still, the values are not as higher as the fractured vertebra since the stresses can distribute more smoothly thanks to the screw that goes inside the crack faces.

The maximum value of strain reached in the implant is 2.08e-003 mm/mm, almost 28.5% and 41% lower compared to the Buck and the Hook-Screw implant respectively. To compare the results obtained in this technique with the Buck and Hook-Screw techniques, we need to represent the strains with a threshold of 0.0025 mm/mm:

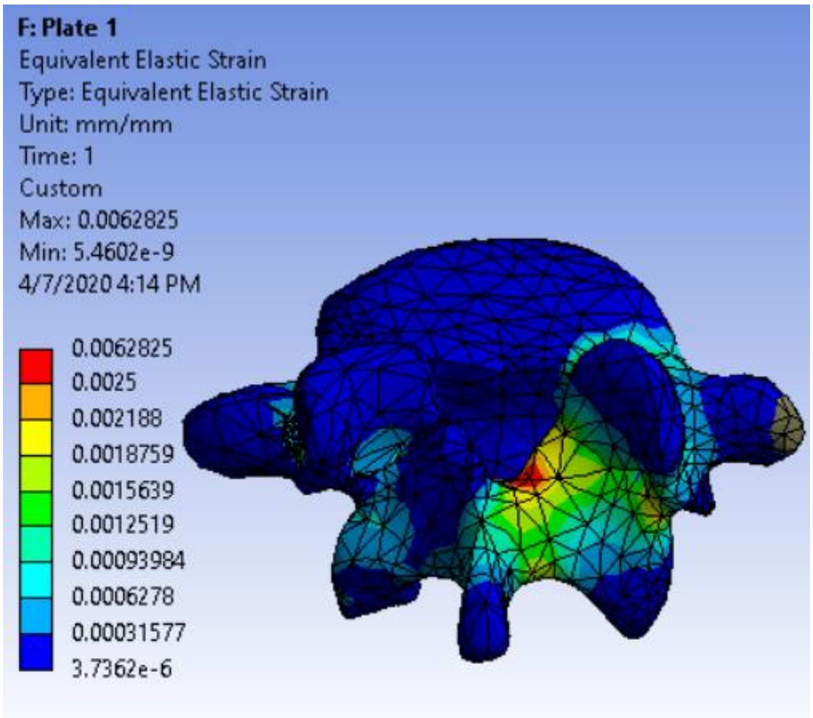

Figure 67: Strain contour of Implant1 assembly, threshold at 0.0025 mm/mm

As expected, the strains propagate in the upper left facet joint similar to the Buck technique and, hence, more similar to the intact vertebra than the fractured without an implant. The area above the selected threshold is restriced to a small region of the lamina, where it joins with the spinous process. The next table shows the maximum and minimum strain value expressed in mm/mm on the vertebra only:

Maximum [mm/mm]	6.28e-003
Minimum [mm/mm]	3.73e-006

TABLE XI: COMPARISON OF THE MAXIMUM AND MINIMUM STRAINS ON THE VERTEBRA IN THE IMPLANT 1 TECHNIQUE, EXPRESSED IN MM/MM

If we want to compare the strain values to the other techniques described before, the maximum value is 19% higher than the Buck technique and, most importantly, 23% and 15.5% lower than the Hook-Screw technique and the fractured vertebra respectively.

The next Figure shows the probed values of strains:

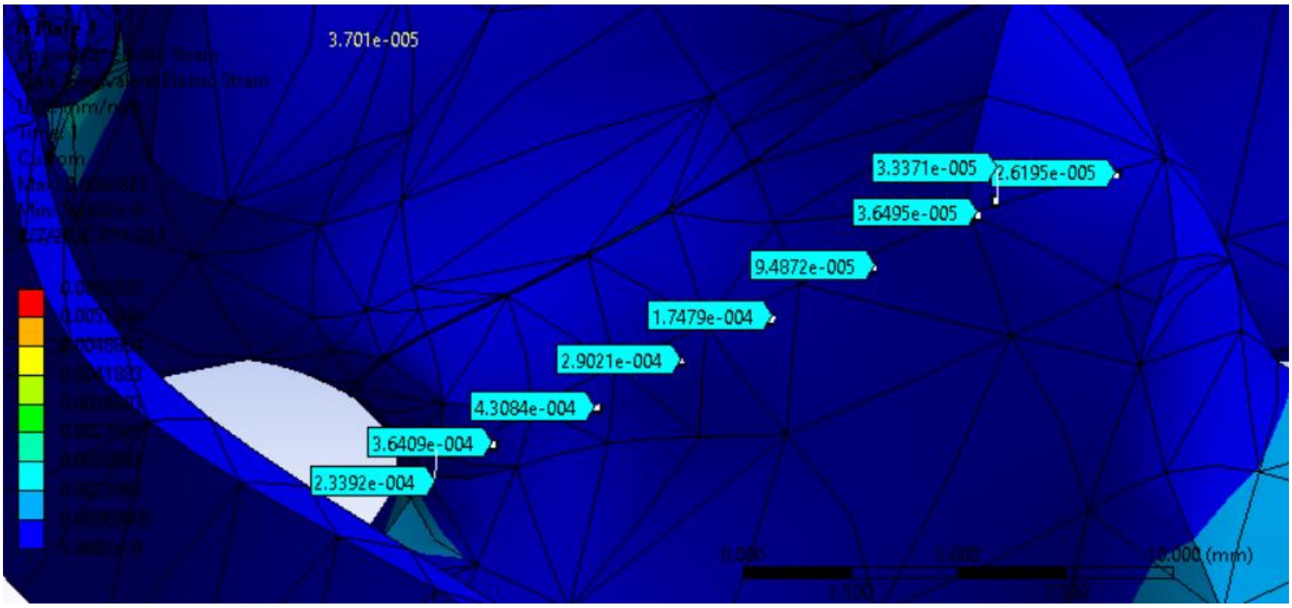

Figure 68: Values of strain in proximity of fracture, Implant1

The values range from 2.61 e-005 to 2.33 e-004 mm/mm going from the medial to the lateral side respectively. These values are higher on the lateral side if compared to Hook-Screw technique since there is the presence of the screw, but lower to Buck. Regarding the medial side, they are lower with respect to the fractured vertebra and the Hook-Screw technique while they are higher if compared to Buck. In the central part, we can see that the values are more similar to the Buck technique and lower with respect to the Hook-Screw technique.

The next table represents the maximum, minimum and average deformation on the Implant 1 assembly:

Maximum [mm]	0.46
Minimum [mm]	0
Average [mm]	5.07e-002

TABLE XII: COMPARISON OF THE MAXIMUM, MINIMUM AND AVERAGE DEFORMATIONS IN THE FRACTURED IMPLANT 1 MODEL, EXPRESSED IN MM

The maximum reached by the Implant 1 is similar with respect to the one seen in the Buck scenario, but lower if compared with the Hook-Screw technique. However, the average value is lower than the Buck technique and almost equal to the Hook-Screw technique. Hence, regarding the deformation analysis, this technique seems to be the best option compared to the previous techniques.

If we analyse the values of deformation nearby the fracture, we can see the following:

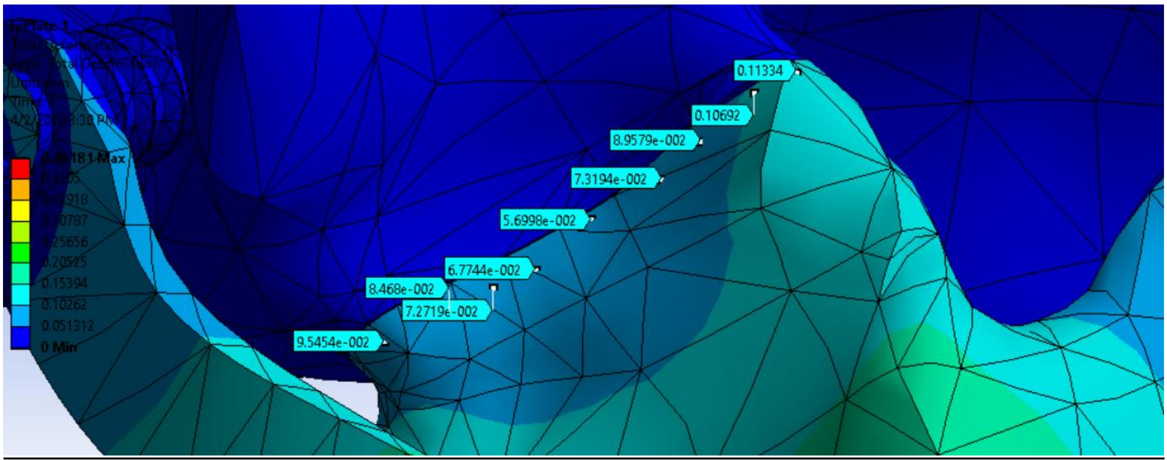

Figure 69: Values of deformation in proximity of fracture, Implant1

The values range from 0.11 to 9.54e-002 mm from medial to lateral side respectively. As shown in Figure they are very similar to the Buck technique, but on the lateral side they slightly higher. Since the difference is negligible, we can assess that this implant design represents almost an identical alternative to the Buck technique in terms of deformations in the proximity of the crack.

The following Figures represent the stresses and strains acting on the vertebra and the implant 2 separately and then the deformation on the assembly implant 2 + vertebra where the final model is meshed with 21923 tetrahedron elements and 39239 nodes:

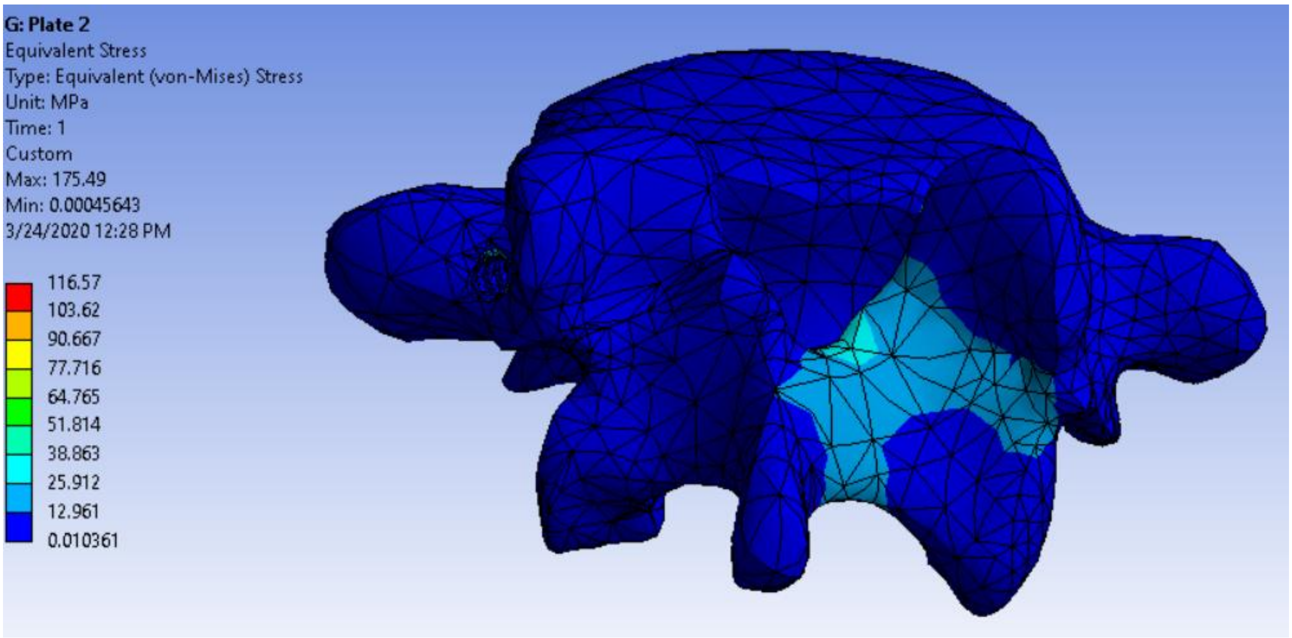

Figure 70: Implant 2 assembly stresses distribution on vertebra

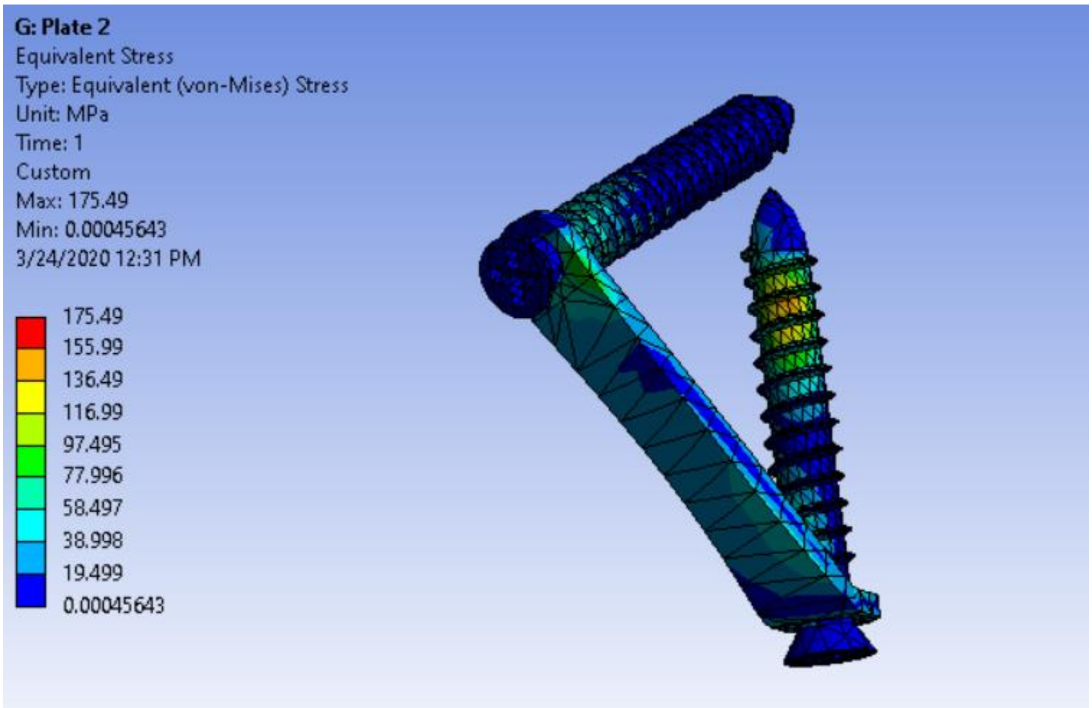

Figure 71: Implant 2 assembly stresses distribution on implant

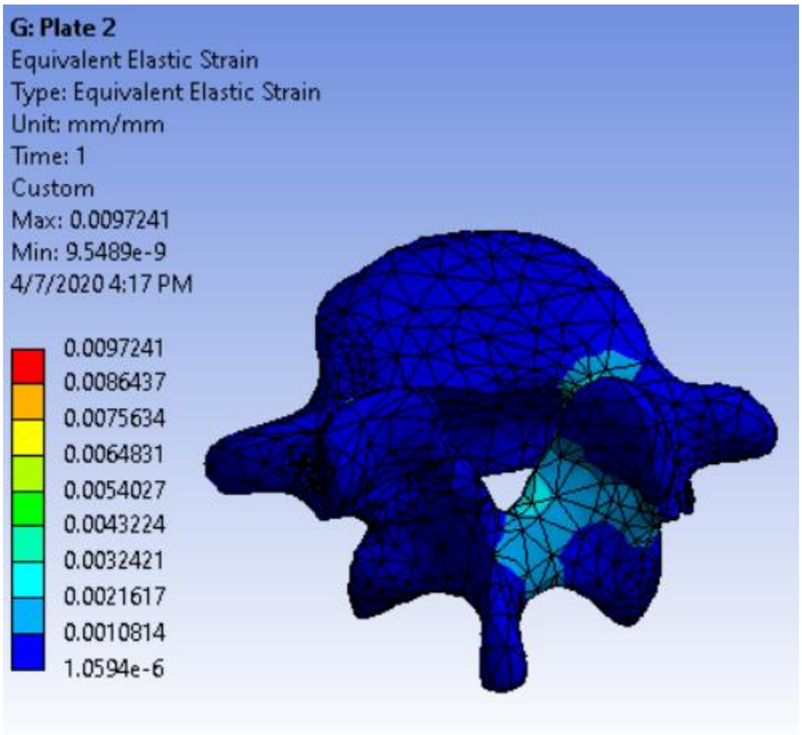

Figure 72: Implant 2 assembly strains distribution on vertebra

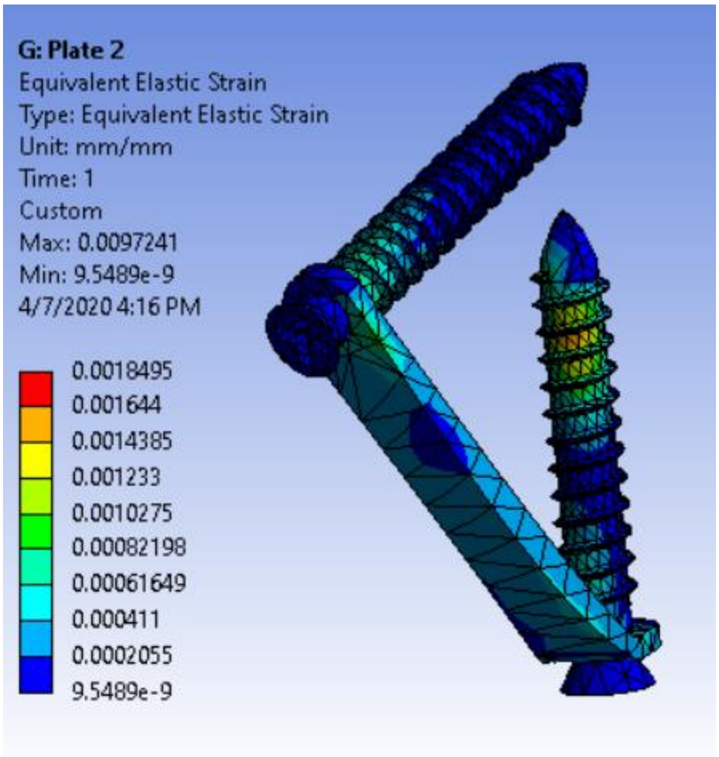

Figure 73: Implant 2 assembly strains distribution on implant

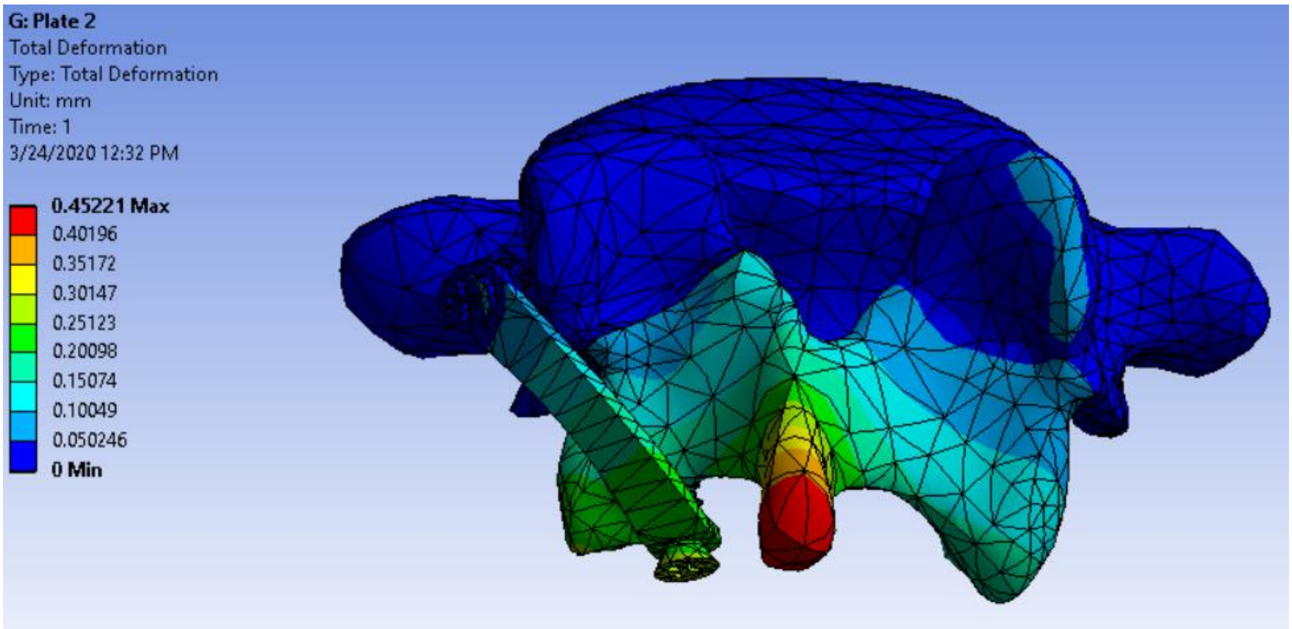

Figure 74: Implant 2 assembly deformations

The stresses concentrate on the implant in the lower screw, in the part that keeps the two faces of the crack united. This result follows the behaviour of stresses previously seen in Implant 1. The stresses reached by the implant are 175.49 MPa in the cavity where the lower screw is supposed to keep together the two faces of the crack.

As in the other cases, we can represent the vertebra stresses with the threshold below the red colour as 10 MPa to have a general idea if the stress distribution has changed more similarly compared to the intact one:

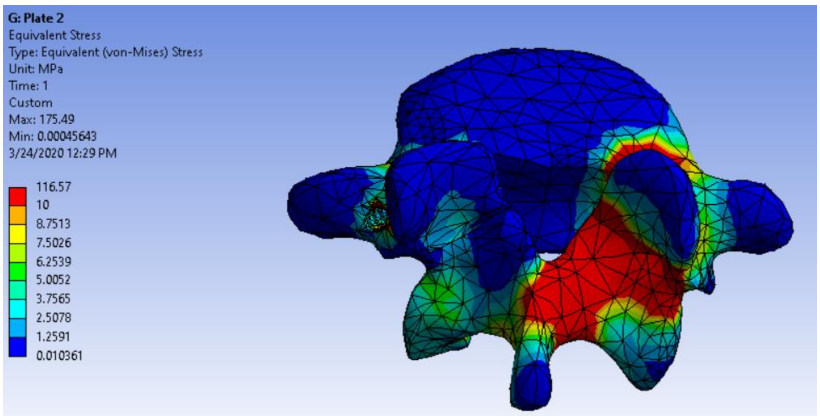

Figure 75: Stress contour of Implant 2 assembly, threshold at 10 MPa

This stress distribution is the closest to the intact vertebra since all the area of the left pedicle and left articular processes undergo a stress distribution thanks to both the screws. However, we can still see that a major part of the right lamina is above stresses above 10 MPa.

The peak stresses reached by the vertebra in the Implant 2 scenario are the highest values reached by any implant analysed as shown in the next Table:

Maximum [MPa]	116.57
Minimum [MPa]	1.03 e-002

TABLE XIII: COMPARISON OF THE MAXIMUM AND MINIMUM STRESSES ON THE VERTEBRA IN THE IMPLANT 2 DESIGN, EXPRESSED IN MPA

The peak value is 128% times higher than the Buck technique and 1.5 times higher compared to Hook-Screw technique. Similarly to Implant 1, the maximum will be found in the screw canal of the vertebra, where the two faces of the crack try to separate.

If we decide, as done in the previous cases, to plot the stresses setting a threshold of 35 MPa, we obtain the following Figure:

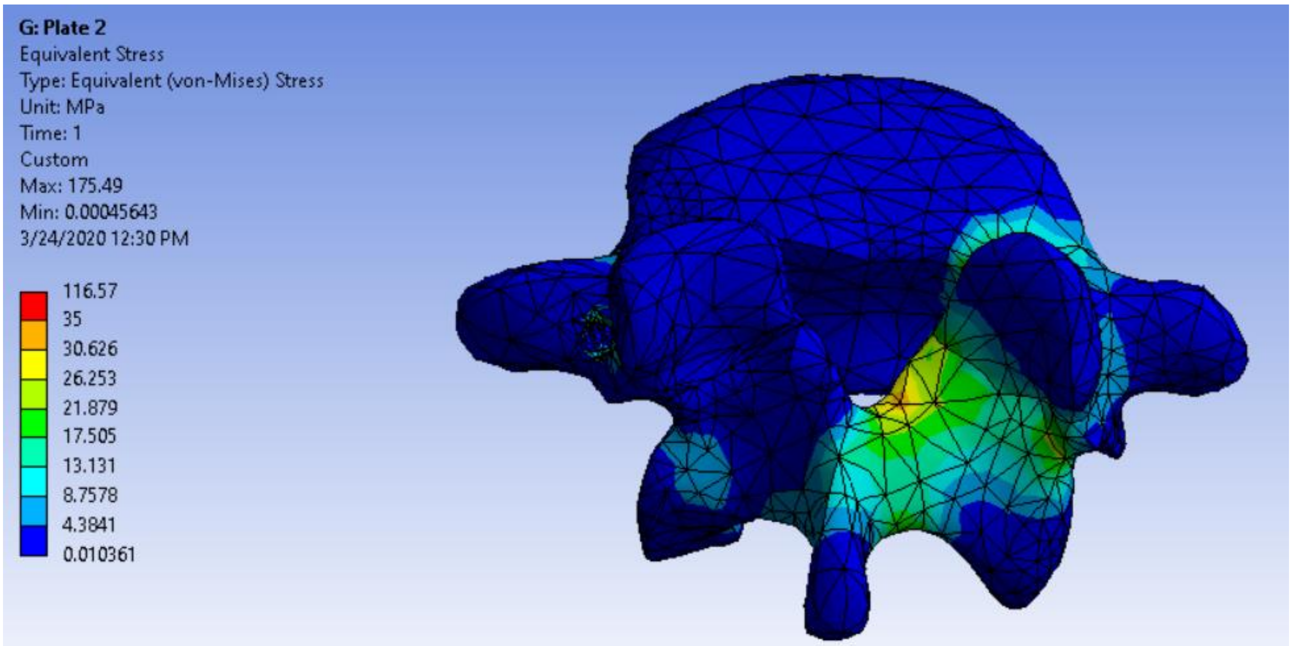

Figure 76: Stress contour of Implant 2 assembly, threshold at 35 MPa

We have no peaks in the external surface of the vertebra and this confirms that considering only the stress distribution on the vertebra, this method is better than the Hook-Screw.

The stresses reached by the implant are lower compared to Buck technique and Hook-Screw technique and 22% lower compared to the previous implant design.

If we decide to plot the values of stress near the fracture, we obtain the values showed in the next Figure:

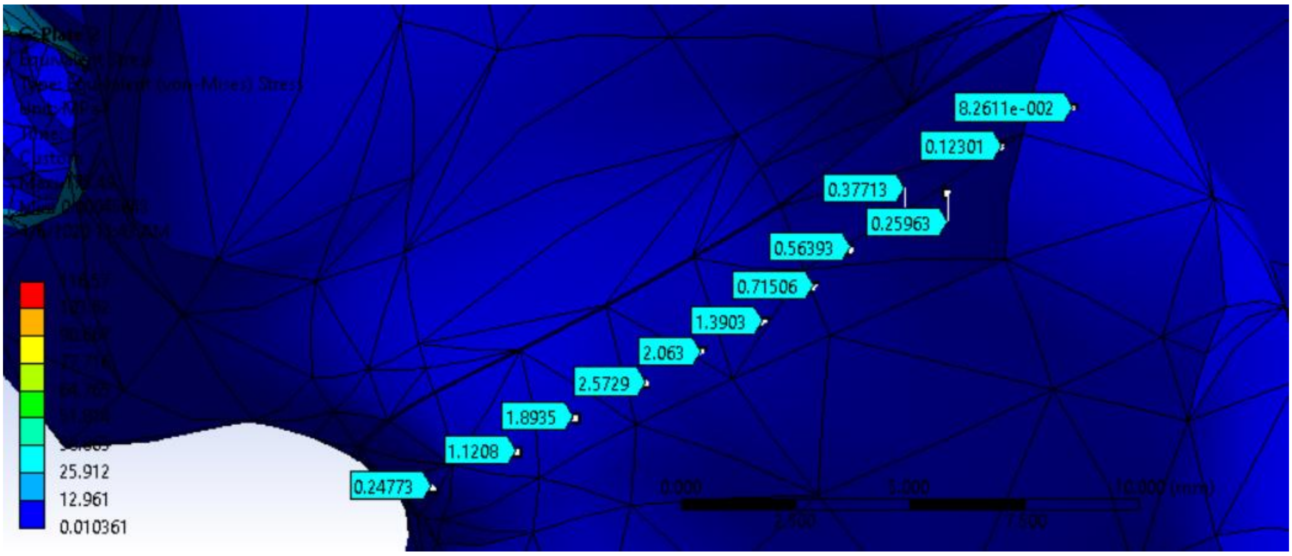

Figure 77: Values of stress in proximity of fracture, Implant2

The stresses value range from 0.24 to 8.26e-002 MPa from the lateral to the medial side respectively. The values and the corresponding discussion is similar to the Implant 1 technique. Overall, analysing the behaviour of the stresses close to the fracture, we found that the Hook-Screw technique still maintains the stresses high in the centre and on the medial side, while the Buck technique shows the best results on the lateral side.

Regarding the strain analysis on Implant 2, the maximum value of strain reached in the implant is 1.84 e-003 mm/mm, the lowest value found in any implant. Compared to the previous design, the maximum value is 11.5% lower but it is in the same location. To compare the results obtained in this technique with the two previous ones, we need to represent the strain with a threshold of 0.0025 mm/mm:

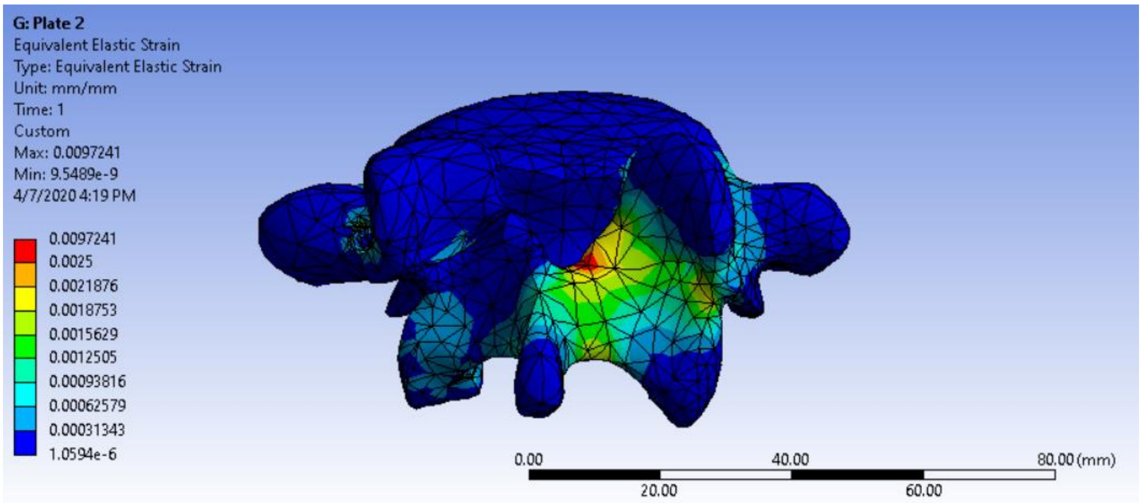

Figure 78: Strain contour of Implant2 assembly, threshold at 0.0025 mm/mm

The behaviour of the strains distribution is similar to the previous design since we can see the strains propagating in the area of the upper facet joint. The values above 0.0025 mm/mm are present just in the same spot seen both in the Buck technique and the Implant1. The next table shows the maximum and minimum strain value expressed in mm/mm on the vertebra only:

Maximum [mm/mm]	9.72e-003
Minimum [mm/mm]	1.05e-006

TABLE XIV: COMPARISON OF THE MAXIMUM AND MINIMUM STRAINS ON THE VERTEBRA IN THE IMPLANT2 TECHNIQUE, EXPRESSED IN MM/MM

The maximum strain reached is the highest among all the techniques, similarly as the stresses. The maximum value is 18.5% times higher with respect to the Hook-Screw technique and 54.77% higher with respect to the Implant 1 and the fractured vertebra.

As done before, the next Figure shows the probed values of strains:

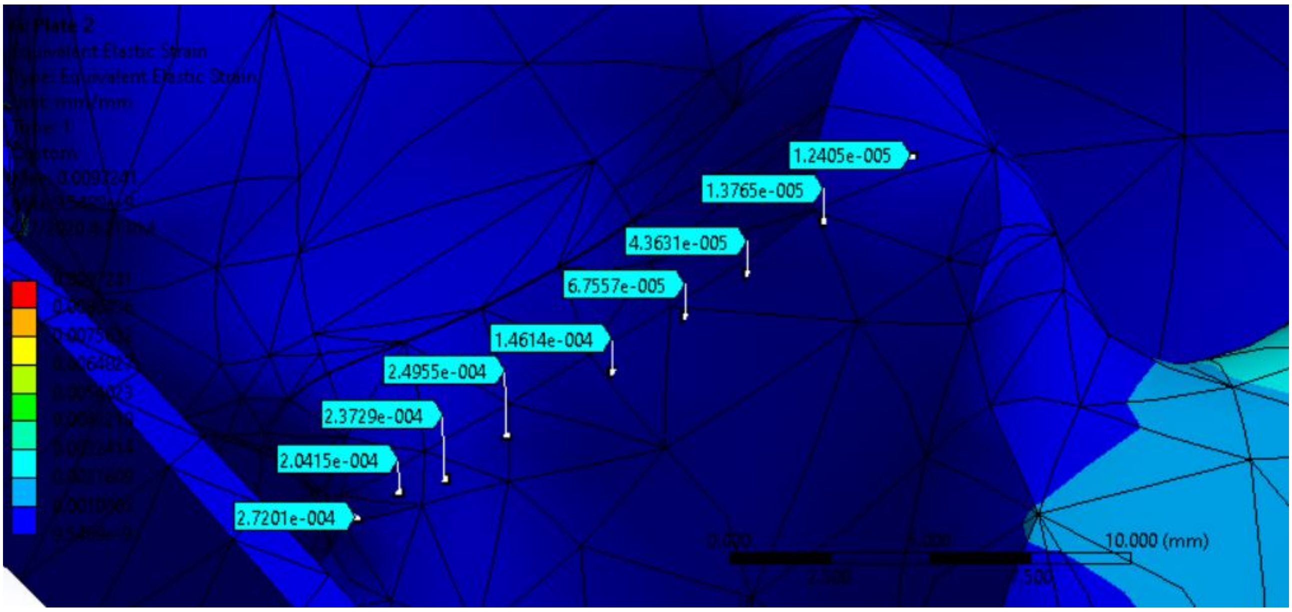

Figure 79: Values of strain in proximity of fracture, Implant2

The values range from 1.24 e-005 to 2.72 e-004 mm/mm going from the medial to the lateral side respectively. These values are similar to the previous design and hence the same rationale can be used here.

Regarding the deformations, the next table represents the maximum, minimum and average deformation on the Implant 1 assembly:

Maximum [mm]	0.45
Minimum [mm]	0
Average [mm]	5.33e-002

TABLE XV: COMPARISON OF THE MAXIMUM, MINIMUM AND AVERAGE DEFORMATIONS IN THE FRACTURED IMPLANT 2 MODEL, EXPRESSED IN MM

Implant 2 has a similar value of peak defomrations of Implant 1 but the average value is 5% higher. Hence, the two implants can be considered similar in terms of deformation distribution.

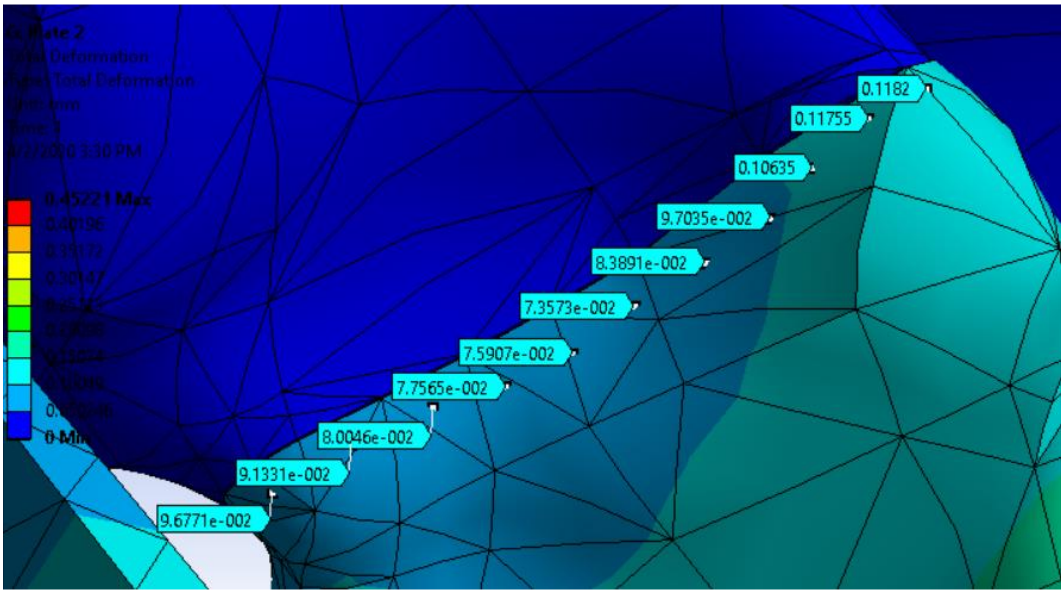

Figure 80: Values of deformation in proximity of fracture, Implant2

The values range from 0.11 to 9.67e-002 mm from medial to lateral side respectively and they are similar when compared to the previous Implant 1 design and the Buck technique. Overall, we would assert that the behaviour of deformations in the proximity of the fracture is comparable for all the techniques seen in this analysis, except for the Hook-Screw technique that shows the higher values for the deformation.

CHAPTER 5

CONCLUSION

The spondylolysis fracture is a defect in the neural arch that is estimated to affect 6% of the global population[1] and could develop into spondylolysis if not treated properly. The surgical techniques used to fix this kind of fracture are described in the previous chapter. Our thesis aimed to find a new solution and provide the analysis of a new plate designed in the Biomechanics Research Laboratory by our Professor. These designs proposed are compared with existing techniques and the final comparison on stresses, strains and deformations will be used to evaluate their effectiveness.

The following tables compare the maximum stresses, strains and the deformations (maximum and average) of two techniques and the new designs in the presence of the fracture:

	Maximum [MPa]
Intact	35.71
Buck	51.14
Implant 1	69.49
Fractured	78.42
Hook-Screw	80.94
Implant 2	116.57

TABLE XVI: FINAL COMPARISON, STRESSES ON VERTEBRA [MPA]

	Maximum [mm/mm]
Intact	2.99e-003
Buck	5.28 e-003
Implant 1	6.28 e-003
Fractured	7.44 e-003
Hook-Screw	8.20 e-003
Implant 2	9.72 e-003

TABLE XVII: FINAL COMPARISON, STRAINS ON VERTEBRA [MM/MM]

	Maximum [mm]	Average [mm]
Intact	0.24	3.01 e-002
Implant 1	0.46	5.07 e-002
Implant 2	0.45	5.33 e-002
Buck	0.45	6.32 e-002
Hook-Screw	0.62	5.08 e-002
Fractured	1.01	0.14

TABLE XVIII: FINAL COMPARISON, DEFORMATIONS [MM]

The tables are created to have an instant clue to compare the various techniques compared to the intact and fractured which should represent the best and the worst case respectively in terms of stresses, strains and deformations.

The only techniques where the stresses on the vertebra are lower than the fractured vertebra without fixation are the Buck and the Implant 1 designs. The Hook-Screw method is comparable to the fractured vertebra while the Implant 2 reaches the highest value of stress. Hence, considering the Von-Mises stresses, the Buck technique and Implant 1 represents the best fixation solutions in our analysis.

As we should expect, the strains reflect the same behaviour of the stresses. Therefore, Buck technique and Implant 1 have the closest value of stress compared to the intact vertebra. The maximum stress is found in the region where the to faces of the crack tend to separate. On the other hand, the Hook-Screw technique and Implant 2 design present a stress peak above the fractured vertebra. Similarly to the stress analysis, the Buck technique and Implant 1 should are the best design in terms of strain distribution.

Regarding the analysis of the deformation, the two new implants seem to be the best designs compared to the classic techniques. The average deformation is significantly lower in the two new designs compared to the Buck technique and the Hook-Screw technique.

Concerning the limitations of our model, we used to model both the bone and the implants as isotropic with a constant Young Modulus. Secondly, the boundary conditions are suited for specific test validation which does not simulate a physiological movement. Unfortunately, due to the COVID-19 emergency, we didn't manage to print and test the implants on sawbones to validate our results. This could be an important evolution of this project in the near future. A possible changing and improvement in the designs of the proposed implants would be on the shape of the plates since the points of insertion are fixed. A new approach could consider the insertion of additional points of entry and screws, but we should take into account that the lamina in the pars is extremely thin and this would create significant damage to the vertebral bone. Regarding the surgical compatibility, we think that the implant would not increase the overall difficulty of the surgery and that the eventual learning curve should be comparable to the other methods since the same points of entry are maintained. Overall, regarding the anatomical compatibility, the implants do not interfere or cross with the ligaments surrounding the vertebra since the points of insertion do not coincide with the insertion of the ligament on the bone. All the soft tissues, ligaments excluded, would have been removed by the surgeons in any type of surgical intervention on the spine and hence we can assess that the implants satisfy also the anatomical constraint.

Thus, taking into consideration all the aforementioned considerations, the new designs could be a promising start for a new way of approaching the fixation of this fracture and, hopefully, increase the chances of success during surgery.

CITED LITERATURE

[1] C. A. M. McTimoney and L. J. Micheli, “Current evaluation and management of spondylolysis and spondylolisthesis.,” *Current sports medicine reports*. 2003.

[2] S. S. Hu, C. B. Tribus, M. Diab, and A. J. Ghanayem, “Spondylolisthesis and spondylolysis.,” *Instructional course lectures*. 2008.

[3] G. D. Cramer, “General Characteristics of the Spine,” in *Clinical Anatomy of the Spine, Spinal Cord, and ANS*, 2013.

[4] M. Rathore, M. B. Sinha, S. Trivedi, and D. K. Sharma, “A Focused Review – Thoracolumbar Spine : Anatomy , Biomechanics and Clinical Significance,” *Indian J. Clin. Anat. Physiol.*, 2014.

[5] N. K. Mahato, “Anatomy of Lumbar Interspinous Ligaments: Attachment, Thickness, Fibre Orientation and Biomechanical Importance,” *Int. J. Morphol.*, 2013.

[6] K. A. Gillespie and J. P. Dickey, “Biomechanical role of lumbar spine ligaments in flexion and extension: Determination using a parallel linkage robot and a porcine model,” *Spine (Phila. Pa. 1976).*, 2004.

[7] E. Syrmou, P. P. Tsitsopoulos, D. Marinopoulos, C. Tsonidis, I. Anagnostopoulos, and P. D. Tsitsopoulos, “Spondylolysis: A review and reappraisal,” *Hippokratia*. 2010.

[8] L. L. Wiltse, P. H. Newman, and I. Macnab, “Classification of spondylolisis and spondylolisthesis.,” *Clin. Orthop. Relat. Res.*, 1976.

[9] C. C. Hasler, “Back pain during growth,” *Swiss Med. Wkly.*, 2013.

[10] R. Wynne-Davies and J. H. S. Scott, “Inheritance and spondylolisthesis. A radiographic family survey,” *J. Bone Jt. Surg. - Ser. B*, 1979.

[11] M. Albanese and P. D. Pizzutillo, “Family study of spondylolysis and spondylolisthesis,” *J. Pediatr. Orthop.*, 1982.

[12] R. S. and W. M., “Suspecting lumbar spondylolysis in adolescent low back pain,” *Clinical Pediatrics*. 1998.

[13] C. J. Standaert and S. A. Herring, “Spondylolysis: A critical review,” *British Journal of Sports Medicine*. 2000.

[14] M. Sato, Y. Mase, and K. Sairyo, “Active stretching for lower extremity muscle tightness in pediatric patients with lumbar spondylolysis,” *J. Med. Investig.*, 2017.

[15] J. A. E. Dutton, S. P. F. Hughes, and A. M. Peters, “SPECT in the management of patients with back pain and spondylolysis,” *Clin. Nucl. Med.*, 2000.

[16] S. Brotzman and R. Manske, *Clinical Orthopaedic Rehabilitation: An Evidence-Based Approach*. 2011.

[17] J. J.G. and D. R.A., “Diagnostic evaluation of low back pain with emphasis on imaging,” *Annals of Internal Medicine*. 2002.

[18] J. G. Scavone, R. F. Latshaw, and W. A. Weidner, “Anteroposterior and lateral radiographs: An adequate lumbar spine examination,” *Am. J. Roentgenol.*, 1981.

[19] E. Libson, R. A. Bloom, and G. Dinari, “Symptomatic and asymptomatic spondylolysis and spondylolisthesis in young adults,” *Int. Orthop.*, 1983.

[20] A. Saifuddin, J. White, and S. Tucker, “Orientation of lumbar pars defects: implications for radiological detection and surgical management,” *Radiology*, 1998.

[21] J. Lowe, E. Schachner, E. Hirschberg, Y. Shapiro, and E. Libson, “Significance of bone scintigraphy in symptomatic spondylolysis,” *Spine (Phila. Pa. 1976).*, 1984.

[22] S. Elliott, M. A. Hutson, and M. L. Wastie, “Bone scintigraphy in the assessment of spondylolysis in patients attending a sports injury clinic,” *Clin. Radiol.*, 1988.

[23] R. S. D. Campbell, A. J. Grainger, I. G. Hide, S. Papastefanou, and C. G. Greenough, “Juvenile spondylolysis: A comparative analysis of CT, SPECT and MRI,” *Skeletal Radiol.*, 2005.

[24] J. Congeni, J. McCulloch, and K. Swanson, “Lumbar spondylolysis. A study of natural progression in athletes,” *Am. J. Sports Med.*, 1997.

[25] J. Iwamoto, T. Takeda, and K. Wakano, “Returning athletes with severe low back pain and spondylolysis to original sporting activities with conservative treatment,” *Scand. J. Med. Sci. Sport.*, 2004.

[26] R. Cavalier, M. J. Herman, E. V. Cheung, and P. D. Pizzutillo, “Spondylolysis and spondylolisthesis in children and adolescents: I. Diagnosis, natural history, and nonsurgical management,” *Journal of the American Academy of Orthopaedic Surgeons*. 2006.

[27] P. B. O’Sullivan, L. T. Twomey, and G. T. Allison, “Evaluation of specific stabilizing exercise in the treatment of chronic low back pain with radiologic diagnosis of spondylolysis of spondylolisthesis,” *Spine (Phila. Pa. 1976).*, 1997.

[28] J. Iwamoto, Y. Sato, T. Takeda, and H. Matsumoto, “Return to sports activity by athletes after treatment of spondylolysis,” *World J. Orthop.*, 2010.

[29] M. E. Steiner and L. J. Micheli, “Treatment of symptomatic spondylolysis and

spondylolisthesis with the modified boston brace," *Spine (Phila. Pa. 1976).*, 1985.

[30] J. Gibson and G. Waddell, "Surgery for degenerative lumbar spondylosis," in *Cochrane Database of Systematic Reviews,* 2005.

[31] P. Rasoulinejad, S. D. McLachlin, S. I. Bailey, K. R. Gurr, C. S. Bailey, and C. E. Dunning, "The importance of the posterior osteoligamentous complex to subaxial cervical spine stability in relation to a unilateral facet injury," *Spine J.*, 2012.

[32] K. Haddadi and H. R. Ganjeh Qazvini, "Outcome after Surgery of Lumbar Spinal Stenosis: A Randomized Comparison of Bilateral Laminotomy, Trumpet Laminectomy, and Conventional Laminectomy," *Front. Surg.*, 2016.

[33] J. E. Buck, "Direct repair of the defect in spondylolisthesis. Preliminary report.," *J. Bone Jt. Surg. - Ser. B*, 1970.

[34] S. Rajasekaran, M. Subbiah, and A. Shetty, "Direct repair of lumbar spondylolysis by Buck′s technique," *Indian J. Orthop.*, 2011.

[35] R. O. Nicol and J. H. Scott, "Lytic spondylolysis: Repair by wiring," *Spine (Phila. Pa. 1976).*, 1986.

[36] M. Deguchi, A. J. Rapoff, and T. A. Zdeblick, "Biomechanical comparison of spondylolysis fixation techniques," *Spine (Phila. Pa. 1976).*, 1999.

[37] E. Morscher, B. Gerber, and J. Fase, "Surgical treatment of spondylolisthesis by bone grafting and direct stabilization of spondylolysis by means of a hook screw," *Arch. Orthop. Trauma. Surg.*, 1984.

[38] P. Gillet and M. Petit, "Direct repair of spondylolysis without spondylolisthesis, using a rod- screw construct and bone grafting of the pars defect," *Spine (Phila. Pa. 1976).*, 1999.

[39] N. Mohammed *et al.*, “A comparison of the techniques of direct pars interarticularis repairs for spondylolysis and low-grade spondylolisthesis: A meta-analysis,” *Neurosurg. Focus*, 2018.

[40] F. Altaf *et al.*, “Repair of spondylolysis using compression with a modular link and screws,” *J. Bone Jt. Surg. - Ser. B*, 2011.

[41] Z. Askar, D. Wardlaw, and M. Koti, “Scott wiring for direct repair of lumbar spondylolysis,” *Spine (Phila. Pa. 1976).*, 2003.

[42] K. Ishida *et al.*, “Spondylolysis repair using a pedicle screw hook or claw-hook system. ―a comparison of bone fusion rates―,” *Spine Surg. Relat. Res.*, 2018.

[43] M. E. Launey, M. J. Buehler, and R. O. Ritchie, *On the Mechanistic Origins of Toughness in Bone*, vol. 40, no. 1. 2010.

[44] F. A. Sabet, A. R. Najafi, E. Hamed, and I. Jasiuk, “Modelling of bone fracture and strength at different length scales: A review,” *Interface Focus*, vol. 6, no. 1, pp. 20–30, 2016.

[45] E. A. Zimmermann, B. Busse, and R. O. Ritchie, “The fracture mechanics of human bone: influence of disease and treatment,” *Bonekey Rep.*, 2015.

[46] R. K. Nalla, J. S. Stölken, J. H. Kinney, and R. O. Ritchie, “Fracture in human cortical bone: Local fracture criteria and toughening mechanisms,” *J. Biomech.*, vol. 38, no. 7, pp. 1517–1525, 2005.

[47] E. A. Zimmermann, M. E. Launey, H. D. Barth, and R. O. Ritchie, “Mixed-mode fracture of human cortical bone,” *Biomaterials*, 2009.

[48] R. K. Nalla, J. H. Kinney, and R. O. Ritchie, “Mechanistic fracture criteria for the failure

of human cortical bone," *Nature Materials*. 2003.

[49] R. Eberlein, G. A. Holzapfel, and M. Fröhlich, "Multi-segment FEA of the human lumbar spine including the heterogeneity of the annulus fibrosus," *Comput. Mech.*, 2004.

[50] J. Chazal *et al.*, "Biomechanical properties of spinal ligaments and a histological study of the supraspinal ligament in traction," *J. Biomech.*, 1985.

[51] D. J. Heylings, "Supraspinous and interspinous ligaments of the human lumbar spine.," *J. Anat.*, 1978.

[52] N. Bogduk, "Clinical Anatomy of the Lumbar Spine & Sacrum (4th Ed.)," *LAVOISIER S.A.S.*, 2005. .

[53] F. A. Pintar, N. Yoganandan, T. Myers, A. Elhagediab, and A. Sances, "Biomechanical properties of human lumbar spine ligaments," *J. Biomech.*, 1992.

[54] Z. Sant, M. Cauchi, and M. Spiteri, "Analysis of stress-strain distribution within a spinal segment," *J. Mech. Mater. Struct.*, 2012.

[55] W. M. Park, C. H. Kim, Y. H. Kim, C. K. Chung, and T. A. Jahng, "The change of sagittal alignment of the lumbar spine after dynesys stabilization and proposal of a refinement," *J. Korean Neurosurg. Soc.*, 2015.

[56] M. A. Tyndyk, V. Barron, P. E. McHugh, and D. O'Mahoney, "Generation of a finite element model of the thoracolumbar spine," *Acta Bioeng. Biomech.*, 2007.

[57] K. Sairyo *et al.*, "Athletes with unilateral spondylolysis are at risk of stress fracture at the contralateral pedicle and pars interarticularis: A clinical and biomechanical study," *Am. J. Sports Med.*, 2005.

[58] K. Sairyo, V. K. Goel, A. Faizan, S. Vadapalli, S. Biyani, and N. Ebraheim, "Buck's

direct repair of lumbar spondylolysis restores disc stresses at the involved and adjacent levels," *Clin. Biomech.*, 2006.

[59] Y. Kim, "Prediction of mechanical behaviors at interfaces between bone and two interbody cages of lumbar spine segments," *Spine (Phila. Pa. 1976).*, 2001.

[60] M. Kakiuchi, "Repair of the defect in spondylolysis. Durable fixation with pedicle screws and laminar hooks," *J. Bone Jt. Surg. - Ser. A*, 1997.

[61] F. Debusscher and S. Troussel, "Direct repair of defects in lumbar spondylolysis with a new pedicle screw hook fixation: Clinical, functional and Ct-assessed study," *Eur. Spine J.*, 2007.

VITA

NAME:	Niccolò Galdini
EDUCATION:	Scientific High School Diploma (2010-2015), Liceo G.B. Grassi, Lecco, Italy
	Bachelor of Science in Biomedical Engineering (2015-2018), Politecnico di Milano, Milan, Italy
	Master of Science in Biomedical Engineering (2018-present), Politecnico di Milano, Milan, Italy
	Master of Science in Bioengineering (2019-present), University of Illinois at Chicago, Chicago, USA
WORK EXPERIENCE:	Graduate Hourly Assistant (2020-present) for Biomechanics Research Laboratory, University of Illinois at Chicago, Chicago, USA